

This dissertation has been 65-5643
microfilmed exactly as received

HAZLEBECK, David Eppler, 1934-
TRANSPORT OF ADSORBABLE GAS
THROUGH MICROPOROUS MEDIA.

The Ohio State University, Ph.D., 1964
Engineering, chemical

University Microfilms, Inc., Ann Arbor, Michigan

TRANSPORT OF ADSORBABLE GAS
THROUGH MICROPOROUS MEDIA

DISSERTATION

Presented in Partial Fulfillment of the Requirements for
the Degree Doctor of Philosophy in the Graduate
School of The Ohio State University

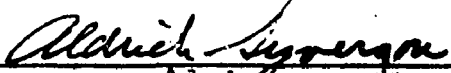
By

David Eppler Hazlebeck, B.Ch.E., M.Sc.

* * * * *

The Ohio State University
1964

Approved by


Adviser
Department of Chemical
Engineering

PLEASE NOTE:

Figure pages are not original copy.
They tend to "curl". Filmed in the
best possible way.

University Microfilms, Inc.

ACKNOWLEDGMENTS

The author is grateful to Professor A. Syverson for his encouragement and timely, helpful discussions, and for allowing the author much freedom in formulating and performing this research.

Mr. K. Svank's invaluable aid in the construction and operation of the x-ray and flow equipment and Dr. J. W. Lacksonen's measurement of the porous media surface area are very much appreciated.

The Welding Engineering Department, the Ohio State University, was extremely cooperative in allowing the use of their x-ray equipment for a preliminary experiment. Mr. Merle L. Rhoten and Mr. Frank J. Sattler were very helpful by making suggestions on x-ray technology and by taking the x-ray pictures in a preliminary experiment.

The author is grateful to Dr. E. E. Smith for his help in using his gas-liquid chromatograph for testing gas samples and to Dr. W. B. Kay for many helpful suggestions on the vacuum system and the use of his calibrated thermometers for thermocouple calibration. Dr. R. S. Brodkey loaned his volt recorder for use as the detector position recorder and gave several helpful suggestions.

This work was accomplished with the aid of fellowships from the Procter and Gamble and Linde Companies. Equipment was purchased through contributions by the E. I. du Pont de Nemours and Hercules Powder Companies and the Chemical Engineering Development Fund of the Ohio State University. This financial assistance, without which this work could not have been accomplished, is greatly appreciated.

VITA

June 19, 1934 Born - Portsmouth, Ohio

1957. B.Ch.E., University of Cincinnati,
Cincinnati, Ohio

1957-1960 . . Research Engineer, Monsanto Chemical
Company, Dayton, Ohio

1961. M.Sc., Ohio State University,
Columbus, Ohio

1961-1962 . . University Fellow, Ohio State University,
Columbus, Ohio

1962-1963 . . Proctor & Gamble Fellow, Ohio State
University, Columbus, Ohio

1963-1964 . . Linde Fellow, Ohio State University,
Columbus, Ohio

PUBLICATIONS

"Axial Dispersion in a Spray-Type Extraction Tower,"
Ind. Eng. Chem. Fundamentals, 2, 310, Nov. (1963).

FIELDS OF STUDY

Major Field: Engineering

Studies in Gas Transport in Porous Media. Professor
Aldrich Syverson.

Studies in Extraction Column Axial Mixing. Professor
Christie J. Geankoplis.

CONTENTS

	Page
TABLES	vii
FIGURES	ix
Chapter	
I. INTRODUCTION	1
II. RELATED LITERATURE	4
III. EXPERIMENTAL MATERIALS	18
IV. EXPERIMENTAL EQUIPMENT	20
General Design	20
Gas Loading System	22
Flow Metering and Inlet Pressure Control System	22
Porous Plug System	24
Exit Pressure Control and Flow Measurement System	25
Vacuum System	27
Constant Temperature Baths	27
X-ray Analytical System	29
Porous Vycor Plug Characterization	35
Operation of Experimental Equipment	36
V. RESULTS	37
Original Data	37
Porous Vycor Plug Physical Data	37
Thermocouple Calibration	38
Manometer Scale Calibration	39
Syringe Feeder Calibration	39
System Volume Measurement	39
Differential Pressure Controller	40
X-ray System Calibration	40
Adsorption Isotherm	46
Helium Permeability	49
Steady State CH ₃ Br Permeability	49
Concentration Profiles of CH ₃ Br Runs	53

CONTENTS--continued

Chapter	Page
VI. DISCUSSION OF RESULTS	72
Adsorption Isotherm	72
Helium Permeabilities	77
Methyl Bromide Permeabilities	79
Black Box Treatment	80
Literature Correlations	83
Steady State Concentration Profiles	93
End Effect	104
Unsteady State Concentration Profiles	106
Time Lag	115
Qualitative Discussion of Excess Flow Theory.	116
VII. CONCLUSIONS	119
VIII. RECOMMENDATIONS	121
Appendix	
A. NOMENCLATURE	124
B. EQUIPMENT DETAILS	129
C. X-RAY SYSTEM VARIABLES AND EQUATIONS	138
D. OPERATING PROCEDURES	150
E. ORIGINAL DATA TABULATION	167
F. CALCULATED QUANTITIES	215
REFERENCES	234

TABLES

Table	Page
1. Physical Properties of Gases Used	19
2. System Volumes	40
3. Physical Parameters of Vycor Plugs Used for Helium Permeabilities by Other Investigators	51
4. Specific Surface Areas	75
5. Data for Black Box Type Correlations	82
6. Summary of Diffusion Coefficient Calculations Based on Over-all Flow Data	86
7. Data for Testing Theoretical Equations Based on Measured Flow	89
8. Data for Testing Theoretical Equations Based on Experimental Profiles for Runs 6 and 7	98
9. D_S Values from the Concentration Profile of Run II	100
10. Thermocouple Calibration Data	167
11. Manometer Scale Calibration Data	168
12. Syringe Feeder Calibration Data	169
13. Calibration Data for System Volume	170
14. Steady State Helium Permeability at 40°C	172
15. Helium Original Flow Data at 40°C.	173
16. Steady State CH ₃ Br Permeability at 40°C.	176
17. Methyl Bromide Original Flow Data at 40°C.	177
18. Exit Pressure Data for Runs 6, 7, and 13	183

TABLES--continued

Table	Page
19. Adsorption Isotherm Data at 40°C	184
20. Summarized Experimental Adsorption Isotherm Data	186
21. Calculated Adsorption Isotherm Data	186
22. X-ray Detector Position Calibration for X-ray Calibration Profiles	187
23. X-ray Calibration Profiles	189
24. X-ray Detector Position Calibration for CH ₃ Br Profiles	194
25. Steady State Concentration Profiles for CH ₃ Br Runs	197
26. Unsteady State Concentration Profiles for CH ₃ Br Runs	201
27. X-ray Intensity Variation with KV Changes	214

FIGURES

Figure	Page
1. Gas Flow System	21
2. Flow Metering and Upstream Pressure Control System	23
3. Exit Pressure Control Circuit	26
4. X-ray Analytical System	30
5. X-ray Scanning Device	32
6. Base Line X-ray Scan	42
7. Attenuation Factor Versus Axial Distance	44
8. Attenuation Factor Versus Equilibrium Pressure	45
9. Attenuation Factor Versus Volume Adsorbed	47
10. Adsorption Isotherm for CH ₃ Br on Porous Vycor at 40°C	48
11. Helium Permeability for Porous Vycor	50
12. Steady State CH ₃ Br Permeability at 40°C	52
13. X-ray Detector Position Calibration for Run 1	55
14. Run 1 Steady State Concentration Profile	56
15. Run 2 Steady State Concentration Profile	57
16. Run 3 Steady State Concentration Profile	58
17. Run 4 Steady State Concentration Profile	59
18. Run 5 Steady State Concentration Profile	60
19. Runs 6 and 7 Steady State Concentration Profile	61
20. Run 11 Steady State Concentration Profile	62

FIGURES--continued

Figure	Page
21. Run 6 Unsteady State Concentration Profiles . . .	65
22. Run 7 Unsteady State Concentration Profiles . . .	66
23. Radiographs of Run 13 Concentration Profile Development	69
24. Run 12 Desorption Concentration Profile	70
25. B.E.T. Plot for CH ₃ Br on Porous Vycor at 40°C . . .	74
26. Total Flow Versus Pressure Difference	81
27. D _s Versus \bar{C}_s based on CH ₃ Br permeability Runs . .	87
28. N _s versus $\int (C_s^2/P)dP$	90
29. Metzner and Smith Type Plot	92
30. Comparison of Experimental with Assumed Concentration Profiles for Run 1	94
31. Comparison of Experimental with Assumed Concentration Profiles for Runs 6 and 7	95
32. D _{sm} Based on Steady State Profiles	101
33. D _T versus C _s	108
34. Reduced Unsteady State Plot For D _T Form A	109
35. Reduced Unsteady State Plot for D _T Form B	111
36. Steady State Profiles Predicted from Unsteady State Profiles	113
37. Plug Clamping Assembly	130
38. Teflon Disc Removal Tool	133

FIGURES--continued

Figure	Page
39. Pin Hole Mold	134
40. Main Electrical Circuit	136
41. Scanner Position Indicator Circuit	137
42. Variation of (μ/ρ) CH_3Br with KV	146

FIGURES--continued

Figure	Page
39. Pin Hole Mold	134
40. Main Electrical Circuit	136
41. Scanner Position Indicator Circuit	137
42. Variation of (μ/ρ) CH ₃ Br with KV	146

CHAPTER I

INTRODUCTION

Transport of gases in porous materials is essential to many industrial processes. These include heterogeneous catalysis, gas separations by adsorption or by porous barriers, and fuel cells.

The literature abounds with studies which apparently establish satisfactory techniques for correlating the flow data for nonadsorbable gases in porous materials. In the Knudsen range, i.e., the region where the molecular mean free path is at least ten times the average pore diameter, one can predict the flow rate of any nonadsorbable gas through a porous material based on the experimental measurement of the flow rate of one nonadsorbable gas through the same material.

However, when this same technique is applied to predict the flow of an adsorbable gas, it is found experimentally that the flow rate is higher than the predicted rate. Further, the influence of the adsorption is more prominent in large surface area, microporous materials. This enhanced flow has been attributed to movement of the adsorbed phase parallel to the gas phase movement.

Most of the early experimental studies were concerned with demonstrating the existence of surface movement (1-5). The more recent studies have involved the measurement of flow rates for adsorbable gases together with attempts to derive equations which will correlate this flow data. None of this has led to a satisfactory understanding of the effect of adsorption on flow through porous material.

Although external flow measurements have provided useful information, this type of study cannot give direct experimental evidence of the surface effect. Measurement of the concentration profile within the porous material while the adsorbed layer is developing and in steady state might provide some additional insight into how the adsorption influences the over-all flow.

Based on this new approach, i.e., measuring the concentration profiles in addition to the flow rates, the general objectives of this work were--

1. To design and build a system for measuring the flow of pure gases through a porous plug with provision for simultaneously measuring the concentration profile within the porous plug for both steady and unsteady state operation.

2. To select a suitable gas-solid system such that the feasibility of x-ray absorption for quantitative measurement of concentration profiles could be demonstrated.

3. To develop a better qualitative understanding of the nature of transport of adsorbable gases to indicate the direction for further research in this area.

4. If possible, to develop a mathematical model which would adequately correlate the results.

For this initial attempt at the measurement of concentration profiles within the porous material, the use of x-ray absorption measurements was selected. X-ray absorption for qualitative measurement was shown to be feasible by Timofeev and Voskresenskii (6).

It was desirable to have as simple an experimental system as possible for this initial study. Consequently, a constant pressure, isothermal flow system employing only a one component gas was chosen. To further simplify the analysis of the data a porous material with a narrow range of pore size such that operation in the Knudsen type flow region was sought.

The porous material selected was porous Vycor glass since this material had been used in many previous adsorbable gas transport studies and it had a narrow pore size distribution in the 40-60⁰Å diameter range.

Methyl bromide was chosen for the gas since it was gaseous at room temperatures, adsorbed appreciably on Vycor glass, and the bromine atoms would absorb x-rays sufficiently.

CHAPTER II

RELATED LITERATURE

Porous Vycor glass

The porous plug material used in this investigation was porous Vycor glass. The properties and method of production have been given by Nordberg (7). In summary, porous Vycor has a surface area in the range of 80 to 220 m.²/gm., an average pore radius of 20 to 30 Å, and a porosity of 28 to 32%.

Porous Vycor is produced by leaching a boro-silicate glass with a hot acid solution. This results in a 96% silica glass having a fine pore structure. Lyon and co-workers (8) give pore size distributions for some samples of porous Vycor which indicate a very narrow pore size range.

Barrer and Barrie (9) report a tortuosity factor for Vycor glass of 2.56.

Methyl bromide--Vycor glass system

The system methyl bromide and porous Vycor has been used in only two previous studies. Yates and co-workers (10) studied the infrared spectra of methyl bromide adsorbed on porous Vycor and Lacksonen (11) studied the transient adsorption of methyl bromide and the binary system methyl bromide-

carbon dioxide on porous Vycor glass. In the former publication, Yates and co-workers report a methyl bromide monolayer capacity of 24.5 cc. (S.T.P.)/gm. at 0°C for a sample of porous Vycor having B.E.T. nitrogen surface area of 180 m.²/gm. They also present two adsorption isotherm points at 20°C along with the methyl bromide B.E.T. surface area of 145 m.²/gm. and a molecular area of 22.1 Å².

Lacksonen (11) gave three points on the adsorption isotherm for methyl bromide on a porous Vycor sample having a B.E.T. nitrogen surface area of 126.7 m.²/gm. at 26°C. More will be said about this study later in this chapter.

Transport of physically adsorbed gases

Much experimental and theoretical work has been published on the anomalously high flow of physically adsorbed gases through porous materials. Most of this work has been well summarized by Carman (12), Russell (13), Timofeev (14), and Field, Watts, and Weller (15). Consequently, we will merely mention the theoretical approaches, comment on papers published since the previously mentioned reviews, and concentrate on the more pertinent points presented in past publications.

By analogy with gas diffusion processes, many workers (9, 16-27) have treated the excess flow over that which is

expected by Knudsen flow as a surface diffusion process and applied Fick's law:

$$J_S = -D_S \frac{dC_S^!}{dL} \quad (1)$$

J_S = surface phase flux

D_S = surface diffusion coefficient

$C_S^!$ = surface phase concentration

L = length in the direction of flow

They evaluated D_S as a function of C_S by using a small $\Delta C_S^!/\Delta L$ and obtain J_S by solving the equation:

$$J_T = J_g - J_S \quad (2)$$

J_g = predicted Knudsen type flux based on helium permeability measurements

J_T = total flux measured experimentally

This assumes no net gas phase--adsorbed phase flux interchange. This type of treatment gives a D_S which increases with increasing C_S up to near monolayer coverage. This region is followed by a region of fairly constant D_S , with some systems indicating a small maximum and minimum in D_S . As $C_S^!$, increases toward the capillary condensation region, D_S increases rapidly. The idea of a diffusion process seems questionable outside of the low pressure region.

A mechanistic picture of the assumed surface diffusion process was proposed as early as 1930 by Clausing (29). In this picture a two-dimensional mean free path and a mean velocity of the molecules governed the diffusion. A very

similar picture which postulated a hopping mechanism for surface diffusion, in which the hopping distance between sites and the lingering time between hops governed the diffusion, was presented by Kruyer (30). Both pictures are presented and discussed by de Boer (31). It should be noted that these pictures actually only apply for very low pressures where the adsorbed gas is by analogy a two-dimensional Knudsen gas, i.e., they consider only gas-solid interaction.

For this same low pressure region, Metzner and Smith (32) recently proposed an equation for surface transport based on absolute rate theory and a hopping mechanism reminiscent of that proposed by Kruyer (29) combined with a two-dimensional type Knudsen flow derivation similar to that in Loeb (33) for three dimensions. They postulate that the activation free energy for the migration process is determined primarily by a partial desorption step. However, in reducing their equations they treat the migrating molecules as if they were completely desorbed. As pointed out by Lacksonen (34), this seems to make the partial desorption idea rather fictitious. Further, their choice of an average jumping distance seems rather arbitrary. However, they claim the experimental data fits their one constant equation. Their data itself is given only in a graphical test. They also show a graphical test of equation 3 (to be presented in the next paragraph) which indicates no correlation. Again the data used for the test are not presented.

Babbitt (35,36) and Gilliland and co-workers (37,38) have treated surface transport as a hydrodynamic process and assumed that the driving force for surface flow is a two-dimensional spreading pressure analogous to the three dimensional pressure driving force in gaseous flow. By means of a two-dimensional force balance and the assumptions that the resistance to surface flow is proportional to C_s and that the gas and surface phases are in thermodynamic equilibrium at all points, Gilliland and co-workers (37) obtain the equation

$$J_s = \frac{RT\rho_{app.}}{22,400 k^2 C_R S_s L_p} \int_{P_0}^{P_1} \left(\frac{C_s^2}{P} \right) dP \quad (3)$$

R = the gas constant

T = the absolute temperature

$\rho_{app.}$ = the bulk density of the porous plug

k = tortuosity

C_R = coefficient of resistance

S_s = specific surface area of the porous plug

L_p = length of porous plug

P = gas phase pressure

The authors point out that to evaluate J_s by using equation 2, the ratio of surface to gas phase flux must be relatively high to ensure no net flux interchange. Since at present there is no good way of separating the two fluxes, the ratio of the two fluxes is difficult to calculate without some simplifying assumption. They assumed that the

gas phase flux could be predicted by the Knudsen equation. Field et al. (14) question this assumption. However, equation 3 was adequate for correlating much experimental excess flow data when small pressure drops were used experimentally. As also pointed out by the authors, equation 3 did not correlate the flow data well in the low pressure range. The degree of fit also seems questionable in the higher pressure range when they applied it to literature data.

It should also be noted, as pointed out by Rothfeld (39), that Flood and co-workers (40) obtained an equation which can be extended to obtain the same form as equation 3. They obtained their equation by treating the excess flow as a hydrodynamical flow of fluid adsorbate and assuming a radial density profile.

Barrer (41) recently applied the irreversible thermodynamics approach to transport of adsorbable gases through porous media. In this approach the chemical potential is the driving force. Theoretical equations are derived involving phenomenological coefficients. As the author states, the evaluation of these coefficients with experimental data is very difficult. Barrer and Ash (42) extended this type of treatment to include the effect of a temperature gradient.

One of the more recent publications is that of Barrer, Ash, and Pope (43). They studied the flow of pure component

and binary gases through a high surface area ($\sim 370 \text{ m}^2/\text{gm.}$), porous carbon.

They used their pure component steady state data to test equation 3, proposed by Gilliland and co-workers. Their data did not support equation 3 except in some cases for small pressure-difference operation. Although they did not comment, this might be construed as significant since as Gilliland and co-workers stated, they did not adequately test the effect of pressure difference.

They also used empirical-diffusions coefficients, based on their pure component steady state flow data, to calculate the time lag using the method of Frisch (46). The time lag is the average time for a molecule to pass through a porous material under steady state flow conditions (45,46). They found that this estimated value did not agree with their experimentally measured value. This discrepancy was attributed to dead end pores.

The authors pointed out a very important point pertaining to the nature of the excess flow observed over that to be expected by Knudsen flow. They state that the excess flow itself may have gas and surface phase components.

The second part of Barrer and co-workers' paper (43) deals with the simultaneous flow of relatively non-adsorbable and adsorbable gases. They essentially study the effect of the adsorbable gas on the flow of the non-adsorbable gas. However, most of their analysis is based on the statement

that the flow of the adsorbable gas was not affected by the non-adsorbable gas. Based on the data they presented, this statement may have been an assumption rather than an experimentally observed fact. If they showed this statement to be true, experimentally, then their analysis is very enlightening since they were able to estimate the steady state pressure profile using this basis to separate the gas and surface fluxes. One reason for questioning this statement is their previous point that some of the excess flow, over that predicted by the Knudsen relationship, might be in the gas phase. If there is extra flow in the gas phase, then the Knudsen flow conditions may not be present. Hence there might be some effect of the nonadsorbed gas on the adsorbable gas flow.

One further observation on this paper pertains to their discussion of the blockage of non-adsorbable gas flow by the presence of an adsorbed phase. This blockage can be given as a blockage factor, B, which is the ratio of the permeability with an adsorbed layer to the permeability without an adsorbed layer. Their interpretation of the blockage factor suggested by Gilliland and co-workers (37) seems to be in error. Gilliland and co-workers (37) proposed:

$$B = \left(1 - \left(\frac{\rho_{app.} M C_s}{22,400 \rho_L \epsilon} \right) \right)^{1.5} \quad (4)$$

where ρ_L = density of the adsorbed phase
 ϵ = porosity of plug

Barrer and co-workers (43) appear to have left out the power 1.5 in equation 4. However, they subsequently show that to make a similar blockage factor equation fit their data, for the system SO_2 , He, and carbon, the power 1.456 must be used:

$$B = \left(1 - \alpha \left(\frac{\rho_{\text{app.}} M C_s}{22,400 \rho_L \epsilon} \right) \right)^{1.456} \quad (5)$$

where α = empirical constant.

Jones (47) introduced the idea that only part of the adsorbed phase was mobile. He derived an equation in a similar manner to the way the Knudsen equation is derived only in two dimensions. He obtained the mean speed of the surface molecules by use of partition functions. He then modified this equation by adding a factor to express the fraction of the total molecules in the adsorbed phase which are mobile. He related the fraction of adsorbed molecules which are mobile to the fraction of molecules having sufficient energy for lateral movement based on the Maxwellian distribution of energies of the molecules. His equation gives a surprisingly good prediction of the flow data of Tomlinson and Flood (48) over a limited range. As the author states, his equation does not, however, take into consideration the change in the depth of the potential wells with concentration and hence assumes a constant activation energy for lateral motion. In addition, the method of calculation is relatively complicated and has only been solved for cases where Langmuir's adsorption isotherm applies.

The author also shows that for some cases all of the adsorbed phase appears to be mobile and that differences between his predicted flows and the experimental flows are in the direction predicted by qualitative consideration of the variation in the depth of the potential wells with concentration.

Although he reported only one set of measurements, Lacksonen (11), through a transient step-function desorption method, seems to have indicated qualitatively that not all of the methyl bromide adsorbed on porous Vycor has the same mobility.

The idea of relatively mobile and immobile adsorbed phase is supported by some unpublished work by Macarus (49) on the high temperature transient adsorption and desorption of acetic acid and hexene on activated bauxite.

In 1958, at a symposium held at the University of Bristol, there was a very interesting discussion of various aspects of surface flow. This discussion was reported by Everett and Stone (50) in their book which is really the Proceedings of the Tenth Symposium of the Colston Research Society. Professor E. Rideal points out that molecules will have different lengths of travel in a free path depending on their original activation energy. This appears to be another way of saying different adsorbed molecules will have different mobilities, and does not rule out the possibility that some molecules have relatively little surface mobility.

Two other very important ideas were suggested during this discussion. Professor R. M. Barrer suggested that in some cases of surface transport in porous media, with essentially a vacuum downstream, there might be a problem with the desorption step at the plug exit. At the exit the molecules would have to acquire an activation energy equivalent to the heat of adsorption. As Professor Barrer says, "It is quite possible to visualize a situation where this process acts as a kind of barrier to the release of molecules on the exit side--what we call an evaporation barrier." As he further states, the true driving force for flow would not be the over-all ΔP but would have to be corrected for this end effect. Professor J. R. Dacey stated that he had also worried about a possible end effect but had concluded that as long as he avoided having a vacuum downstream, the end effects should not be a problem.

The other interesting idea was brought up by Professor J. R. Dacey. He suggested that the concentration profile is not a straight line. In talking about this concentration gradient, he says, "It must be some sort of curve where as you get towards the output end the concentration gradient is steeper." Professors Barrer and Dacey discussed this idea. Professor Barrer pointed out that if there is a non-linear surface concentration gradient, then there might also be a non-linear pressure gradient which would invalidate the use

of nonadsorbed gas permeabilities for predicting the gas phase flux of an adsorbable gas. He rejected this idea on the basis of facts available at that time. Dr. R. K. Schofield suggested that self-diffusion studies with a radioactive tracer might throw some light on the problems of end effects and non-linear concentration profiles. Professor Dacey said that he would consider using this idea but to our knowledge has not done so.

Along the line of seeing what is happening inside a porous material when surface flow occurs, Timofeev and Voskresenskii (6) employed low energy x-ray absorption in an attempt to study surface transport. They attempted to separate the gas and surface phase components of diffusion of the adsorbable gas ethyl bromide through a granulated wood charcoal counter current to the nonadsorbable gas nitrogen. Their idea was to block the gas phase flow of the adsorbable component with the countercurrent flow of nonadsorbable gas. Then they would follow the surface phase adsorption front movement using x-ray pictures made with 30KV (10 ma) x-rays from a copper target tube. In this way, if most of the transport were on the surface, the countercurrent gas would have little effect on the rate of advance of the adsorption front, but if most of the transport were in the gas phase the reverse would be true.

As the authors state, the idea of gas phase blockage with a countercurrent stream only applies to larger pores (in their material average radius $> 10^{-5}$ cm.) where Knudsen flow conditions do not exist. They found that most of the flow was in the gas phase in the larger pores which could be blocked by the countercurrent stream. This is not too surprising since surface transport phenomena is generally only significant in much smaller pores. They did show through some desorption experiments that transfer of adsorbed phase into the gas phase and reversal of movement by the countercurrent stream did not occur since the desorption rate was too slow. Regardless of the results, the idea of observing the adsorbed phase within a porous material by means of x-ray absorption was excellent.

To summarize the related literature, there have been two main approaches to surface transport. These are activated diffusion with a surface concentration driving force and hydrodynamic flow with a spreading pressure driving force. The first has been most useful well below monolayer coverage and the second for intermediate and higher surface coverages. However, both have been satisfactory only for limited systems, ranges, and experiments, and no general theory has proved adequate. Many complicating factors need much more experimental study. Among these are the quantitative distribution of the adsorbable gas flux between the

gas and surface phases, the fraction of the adsorbed phase which is mobile, the concentration dependence of the resistance to movement of this mobile material, the shape of the concentration profiles, and the possibility of end effects.

CHAPTER III

EXPERIMENTAL MATERIALS

The porous glass (Vycor No. 7930) used in this work was purchased from the Corning Glass Works, Corning, New York. The glass was obtained in 1/4 inch nominal diameter rod form. The porous plug for flow measurements was made by breaking short segments from the long rod, using great care not to contaminate the ends of the short segments. One short segment with nearly flat ends was selected for the flow measurements. The surface area of the glass was determined using the material from one side of the selected plug and is given in the Results section.

The plug was embedded in Epocast epoxy resin as described in the Appendix section on the Experimental Equipment.

The physical properties and sources of the gases used in this work are reported in Table 1.

TABLE 1
PHYSICAL PROPERTIES OF GASES USED

Gas	Molecular Weight	Source	Purity ^a	Critical ^a Temp., °C	Vapor ^b Pressure at 40°C mm. Hg
CH ₃ Br	94.95	Matheson	99.5	191	2600
He	4.00	Matheson	99.99	-267.9	---

^aFrom "Matheson Gas Data Book," The Matheson Company, Inc., Joliet, Ill., 1961.

^bT. E. Jordan, "Vapor Pressure of Organic Compounds," Interscience Publishers, Inc., New York (1954).

CHAPTER IV

EXPERIMENTAL EQUIPMENT

General design

This chapter describes the equipment used to measure the permeabilities of pure gases through a porous plug while simultaneously measuring the concentration profile within the porous solid. The equipment may be considered in two parts: the flow metering, temperature, and pressure control system and the x-ray absorption analytical system.

The complete flow system is shown in Figure 1. Generally, this consisted of a gas loading system, a combination flow metering and constant inlet pressure control system, the porous plug, an exit pressure control system with provision for intermittent flow measurement, and a vacuum system. The flow system was all pyrex glass and all stopcocks of the high vacuum types. Apiezon N grease (manufactured by the James G. Biddle Company) was used on all stopcocks. The flow system was vacuum tight down to less than 10^{-5} mm. Hg.

The following sections give the details of the various components of the equipment.

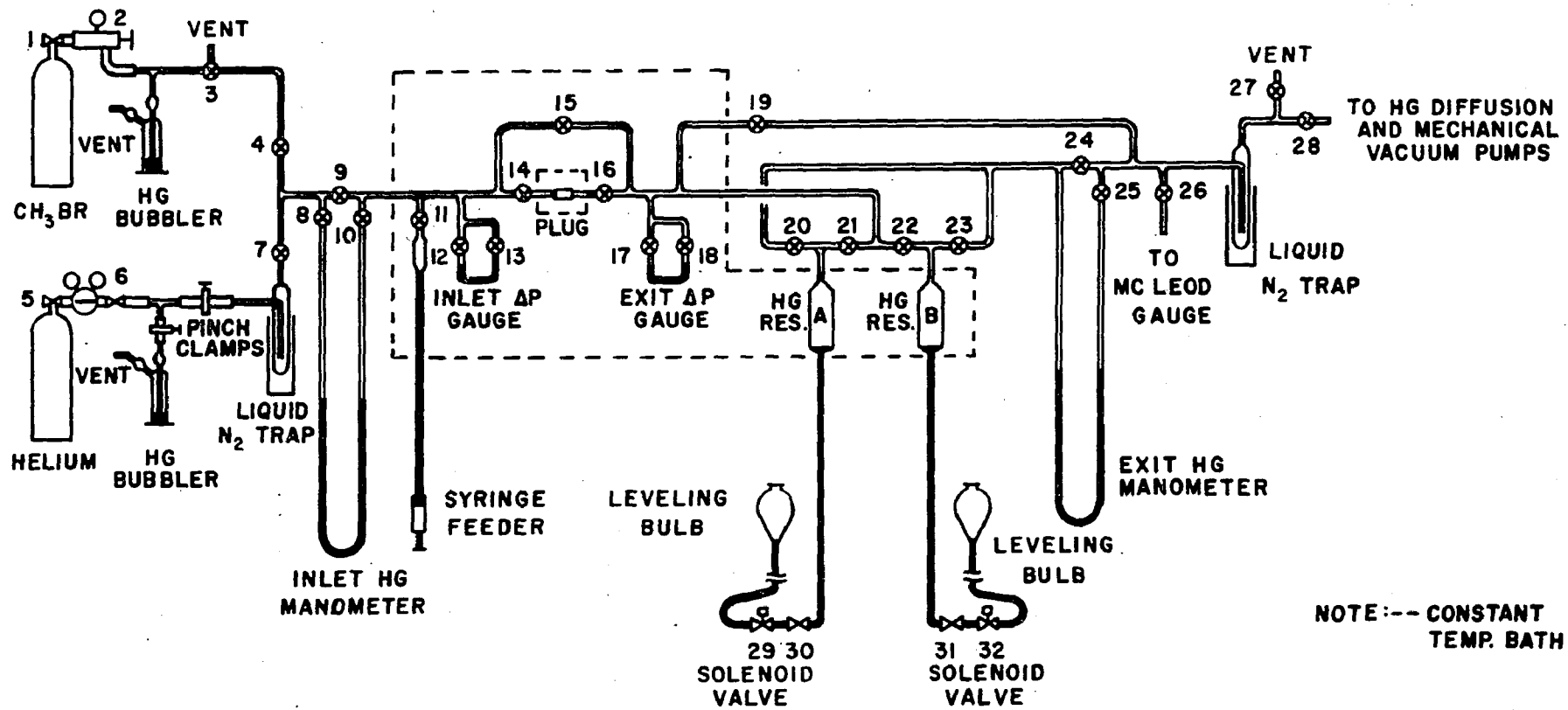


Fig.1. Gas flow system.

Gas loading system

This system as shown in Figure 1, consisted of a Hg-filled glass bubbler for the CH_3Br with a liquid nitrogen filled, glass cold trap added to remove water when helium was loaded. This system was necessary to allow purging of the feed lines to prevent contamination of the system with air. The flow system was generally purged two or three times by loading and evacuating with the porous plug valved out of the system. The Appendix on Operating Procedures gives the details.

Flow metering and inlet pressure control system

This system is shown in Figures 1 and 2. In essence, the operation consisted of feeding mercury into a 25 cc. reservoir on the inlet or upstream side of the plug to replace the gas which had flowed into the porous plug. Thus a constant upstream pressure was maintained. The upstream pressure change was monitored using a mercury filled U-tube with a tungsten contact in one arm. The contact on the U-tube was connected to a Thermocap relay (made by Niagara Electron Laboratories, Andover, New York) which sensed changes in the capacitance when the mercury made or broke contact with the tungsten wire. This in turn activated an automatic syringe feeder (made by Modern Metalcraft, Midland, Michigan) which fed mercury from a 25 cc. syringe

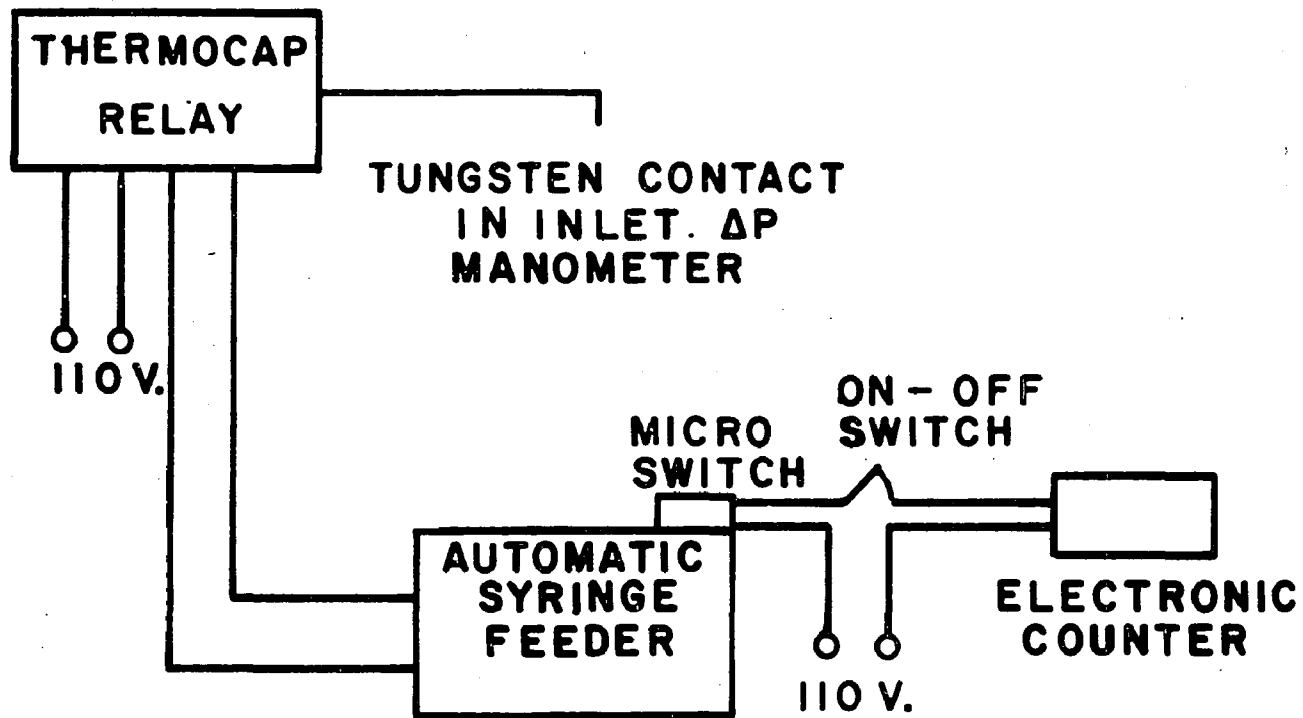


Fig.2. Flow metering and upstream pressure control system.

into the 25 cc. reservoir to restore the pressure. This system maintained the upstream pressure within approximately 0.1 to 0.2 mm.Hg.

The metering was done by installing a 112 tooth gear on the drive shaft of the syringe feeder. A microswitch was located so that each tooth closed and opened an electronic counter circuit thus giving 112 counts for each revolution. Calibration of this system showed a count for each 0.000817 cc. of Hg displaced. The counter was a model CE 600AS602 made by General Controls, Des Plaines, Illinois. This high count per unit volume ratio was necessary since the flow rates were low as a result of using a small diameter porous plug.

Porous plug system

It was necessary to attach inlet and outlet tubes as well as to seal the sides of the porous plug with a vacuum tight seal. After testing many sealing materials, Epocast 31-A resin with 9216-1 hardner (made by Furane Plastics, Inc., Los Angeles, California) was found to be satisfactory. By allowing it to partially polymerize before application, no apparent pore penetration was observed, the solubility of CH_3Br in it was not detectable in a two week test, it did not absorb x-rays too strongly, it cured at room temperature, and appeared to give a vacuum tight seal with glass as shown by an air permeability test. The details of

the plug embedding are reported in the Appendix on Equipment Details.

The inlet tube of the plug was made with two millimeter capillary tubing and the larger tube attached to the plug was partially filled with a glass rod so that the volume between the inlet stopcock and the plug could be held to a minimum. The object of this was to reduce the initial system pressure adjustment when the inlet stopcock was opened.

Exit pressure control, and flow measurement system

Figures 1 and 3 show this system. The exit or downstream pressure control system was exactly like the inlet pressure control system except that mercury was drained out of 500 cc. reservoirs through a barometric leg. A Thermocap relay opened or closed a stainless steel solenoid valve as dictated by the differential pressure mercury manometer to maintain a constant downstream pressure within about 0.2 mm. Hg.

As Figure 1 shows, there were two 500 cc. reservoirs and two solenoid valves arranged so that they could be used alternatively. While one was controlling the downstream pressure, the other could be emptied by mercury displacement into a known volume connected to an absolute pressure manometer so that the volume collected could be measured. Evacuation of the reservoir inlet lines completed the

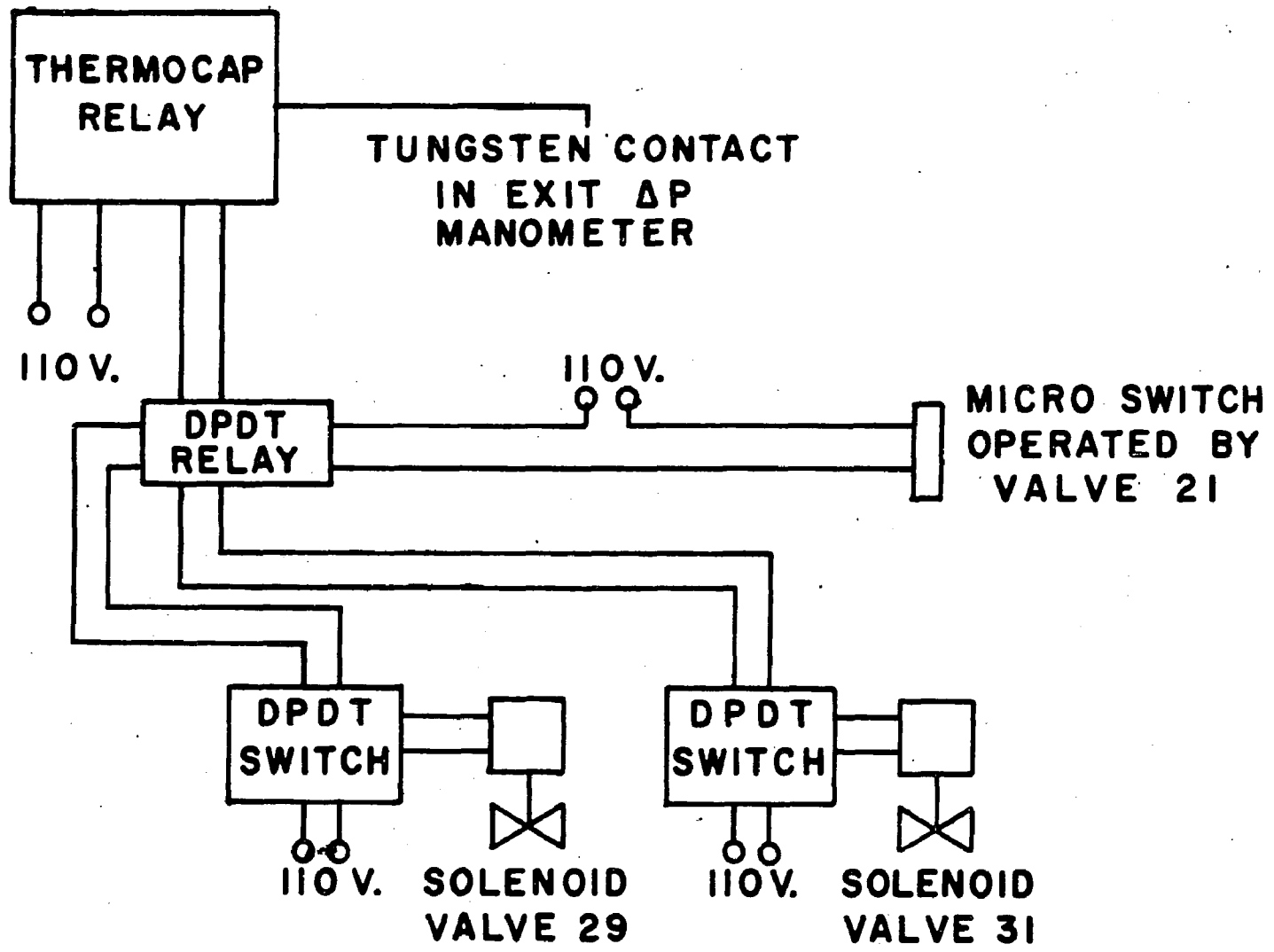


Fig.3. Exit pressure control circuit.

measuring cycle and the reservoir was again ready for pressure control use. In this manner, a material balance on the flow system would be possible.

Vacuum system

The vacuum system consisted of a McLeod gauge, a liquid nitrogen cooled cold trap, a mercury diffusion pump, and two mechanical vacuum pumps. The McLeod gauge was a model GM-100A manufactured by the Consolidated Vacuum Corporation and would measure down to 10^{-5} mm. Hg. The mercury diffusion pump was a number 8705 single stage pump manufactured by Ace Glass Incorporated. The two mechanical vacuum pumps were number 1405H Duo-Seal Vacuum pumps with a free air displacement at 33.4 liters/min. made by the Welch Scientific Company. One of the pumps was used as a fore pump for the Hg diffusion pump and the other was used to operate the McLeod gauge.

The system was capable of obtaining vacuums lower than 10^{-5} mm. Hg, probably as low as 10^{-6} mm. Hg.

Constant temperature baths

As shown by the dashed line in Figure 1, most of the flow system was enclosed in an airbath which maintained the system at $40^{\circ}\text{C} \pm 0.3^{\circ}\text{C}$. This air bath was lined with 1/16" lead to stop any scattered x-radiation. The air in the bath was circulated by an externally vented air motor with an

8 inch fan blade. This circulated air over two 600 watt No. E77 cone-shaped heating elements made by the Rodale Co., Emaus, Pennsylvania. Powerstat variable transformers were used to adjust the voltage for these elements and the temperature was controlled by a Model 63RA Termistemp temperature on-off controller made by the Yellow Springs Instrument Company, Yellow Springs, Ohio.

The lead box around the porous plug, to contain the x-rays, served as a separate air bath for the plug. The box was insulated and air was circulated from a heater through the box and back to the heater by a No. 2 3/4 L-R Blower (approximately 58 c.f.m.) made by the Ripley Company, Inc., Middletown, Connecticut. The heater consisted of two cone-shaped heaters like those previously described with eight 6 inch by two inch aluminum baffle plates to damp out temperature fluctuations. The elements were regulated by Powerstat variable transformers and controlled with an on-off controller like the one previously described. Temperature regulation within the lead box was about $\pm 0.1^{\circ}\text{C}$ when operated at 40°C .

The temperature in both air baths was measured using iron-constantan thermocouples with cold junctions located in ice baths. The temperatures were recorded on a Speedomax H Compact AZAR millivolt recorder manufactured by the Leeds and Northrup Company.

X-ray analytical system

Figure 4 shows the Analytical System. The X-ray system included a source of x-rays, two scintillation detectors, a scanning device, a dual count ratemeter, and a recorder.

The x-ray source was a number 6147 full wave rectified x-ray diffraction unit manufactured by the Picker X-Ray Corporation, Waite Mfg. Div. Inc., Cleveland, Ohio. A Machlett OEG-60 x-ray tube with a tungsten target and beryllium window was used. This was made by the Machlett Laboratories, Inc., Springdale, Connecticut. The source was capable of continuous operation with a maximum load current of 40 ma with 60 KV excitation voltage or 50 ma with 50 KV voltage. The tube had a focal spot of approximately 6 mm. square in projection and was of the end window type. Hence it was installed directly above (distance of about 18 inches) the porous plug. Normal operation was at 29 KV and 37 ma.

The x-rays were collimated through a three inch diameter ($1/4$ " wall thickness) lead pipe to the porous plug air bath which was also constructed of $1/4$ " thick lead. The tube was positioned so that the center of the focal spot would be as close as possible to being vertically above the center of the porous plug. Two holes were cut in the bottom of the porous plug air bath to allow both the part of the x-ray beam which had passed through the porous plug and a part of the uninterrupted beam to pass through to the scintillation detectors below. The holes were covered by

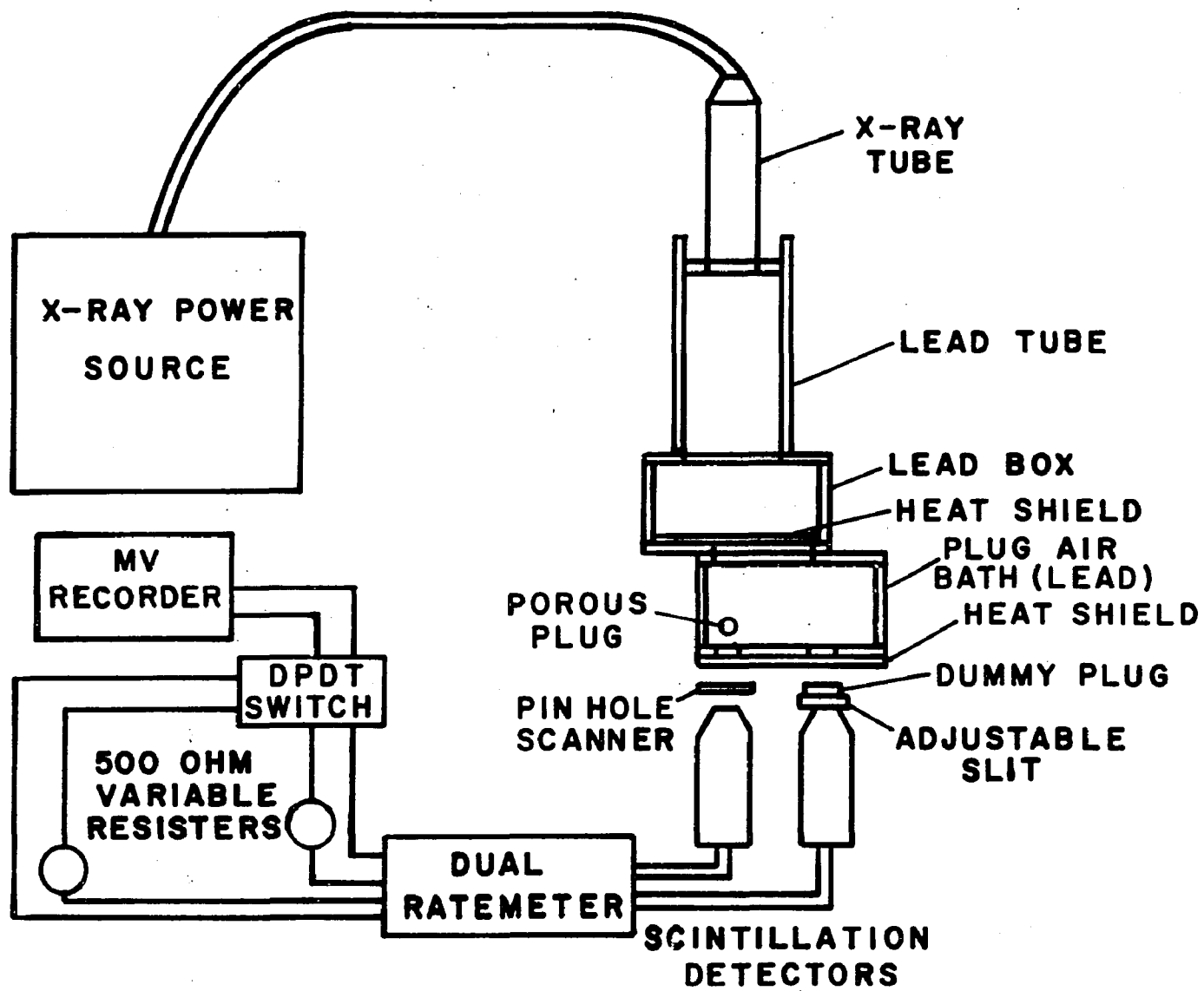


Fig.4. X-ray analytical system.

1/8" thick porous teflon (55% void teflon made by Fluoro-Plastics, Inc.) to act as a heat barrier.

Two model 2802G multiprobe scintillation detectors manufactured by the Picker x-ray Corporation, Waite Mfg. Div., Inc., Cleveland, Ohio, were used. These detectors employ a 1/2" diameter by 1/2" thick NaI (thallium activated) crystal with a Dumont 6291 photomultiplier tube and transistorized preamplifier.

In order to measure an axial concentration profile, it was necessary to scan axially along the plug with the scintillation detector. The simplest means for doing this was to use a stationary detector with a scintillation crystal larger than the porous plug and to scan the porous plug with a 1/8 inch thick lead shield which had a pin hole to allow only a small point of x-rays to pass through to the detector. The pin hole was measured using a 10 x microscope with a micrometer eyepiece. The average diameter was only 0.00816 millimeters. Using this small pin hole, it was possible to look at less than 1% of the plug length at any time. The details on the method of producing the pin hole are given in the Appendix on Equipment Details.

Figure 5 is a photograph of the entire scanning device. The whole assembly was made of aluminum with vertical and horizontal adjustment screws for aligning the entire assembly under the porous Vycor plug. The lead shield with the pin hole was driven by a gear train powered by a Hurst 80 in.-oz.

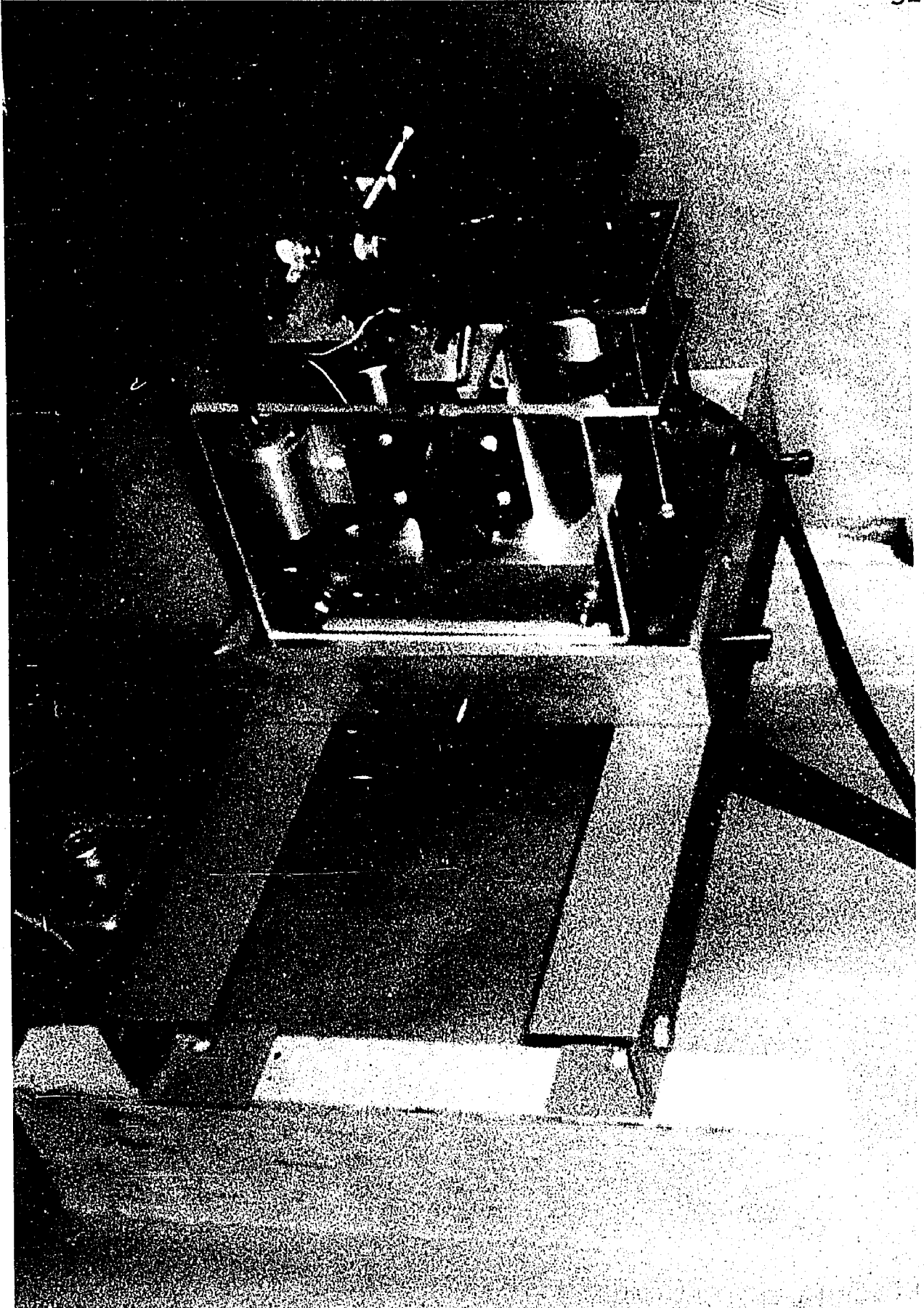


Fig. 5. X-ray scanning device.

synchronous motor at a linear travel of approximately 1 mm. per second. The gear train employed a double rack and pinion assembly from a Mitchell 500 fishing reel which supplied the back and forth motion required without reversing the drive motor. An overtravel of about 3 mm. on each end assured a constant scan rate while on the plug.

A reference plug similar to the actual porous plug was installed on the second scintillation detector. To further reduce the x-ray intensity, an adjustable pin hole was provided by an adjustable lead wedge sliding over a fixed 1/16 inch pin hole so that the proper detector output could be obtained. This reference beam provided a partial compensation for some of the variation in the x-ray source since the difference between the sample and reference beam intensities was used to measure the concentrations.

The output from the detector preamplifiers was fed into a model 600-046 transistorized dual ratemeter which also was manufactured by the Picker X-ray Company. This linear ratemeter converted the voltage signal to a meter indication in counts per minute and also provided a linear output of either detector or their difference for recording on a millivolt recorder. The ratemeter was generally operated on the 100,000 counts per minute scale using a 0.3 second time constant. This gave almost full scale count rates for the reference and sample beams when the porous plug was evacuated.

The millivolt recorder was a Speedomax H Continuously Adjustable AZAR recorder (manufactured by the Leeds & Northrup Company) with a nominal response time of one second. The 100 mv. scale was used.

The position of the pin hole was recorded by using a parallel plate capacitor which had one plate attached so that it moved with the scanning mechanism and the other plate was fixed. The change in capacitance was detected using a model 901-1 Decker Delta Unit (manufactured by the Decker Aviation Corporation). This unit converted the capacitance change into a voltage signal which was recorded on a model V.O.M.-5 recorder manufactured by Bausch & Lomb, Inc. The D.C. and filament power was supplied by a Model 760 voltage regulated power supply made by the Precise Development Corporation, Oceanside, New York. Constant voltage A.C. power was supplied to the regulated power supply by a No. 20-13-125 constant voltage transformer made by the Sola Electric Company, Elk Grove Village, Illinois.

The measurements of the concentration profiles with the previously described equipment were made in a step-scan fashion. The pinhole was placed near one end of the porous plug and the x-ray intensity measured for 11 seconds. Then the scan drive moved the pin hole for one second (hence about one millimeter) and the intensity at the new position was recorded for 11 seconds. The step-scan was continued in this manner over the length of the plug. This stepping was

performed automatically by using a Flexopulse timer-controller (made by the Eagle Signal Corp.) to activate the scan drive as required. Using this scheme, 9 to 11 points were measured on each scan which took approximately 2.5 minutes. The 11 second recording time was chosen so that the statistical error of the count rate meter due to the random x-ray source output would be about 2%.

The KV, ma, ratemeter time constant and scale, pin hole size, and recording time all effect the maximum range of absorptivity, the statistical error, and the response time. Consequently a compromise among these operating variables was necessary to obtain reasonable accuracy and response. A discussion of the effects of the x-ray system parameters and a computer program used in estimating absorptivities is given in the Appendix on the x-ray System Variables and Equations.

The details of the electrical circuits are given in the Appendix on Equipment Details.

A lead film holder which permitted the positioning of 1 1/4" x 1 5/8" Kodak dental x-ray film beneath the porous plug was used for taking some pictures of the concentration profile.

Porous Vycor plug characterization

The diameter of the porous Vycor plug was determined by averaging sets of two measurements at 90° to each other

at three positions along the axis of the plug. The length of the plug was measured using calipers and an inside type micrometer at 5 points and averaging.

It was felt that errors involved in these measurements would be negligible compared to the dimensions involved.

The plug was weighed, after degassing at 105°C under full vacuum over a period of 8 hours, on a Wm. Ainsworth & Sons Inc. Type LCB balance.

The N₂ surface area was determined by Dr. J. W. Lacksonen at the Battelle Memorial Institute, Columbus, Ohio, on a Dynamic Gas Adsorption Unit using the B.E.T. technique. The details of the method have been given previously by Dr. Lacksonen (11).

Operation of experimental equipment

The operation of the experimental equipment is detailed in the Appendix on Operating Procedures. The operation for the flow equipment was essentially the same for both helium and methyl bromide. The operation of the x-ray equipment was the same for all runs with methyl bromide in which concentration profiles were measured.

The manufacture's detailed operating manuals should be consulted before attempting to operate any of the major pieces of equipment.

CHAPTER V

RESULTS

Original data

The original data for calibrations, flow rates, and concentration profiles are tabulated in the Appendix on Original Data Tabulation. Approximately every other data point of the flow data for the six helium runs in Table 15 and the methyl bromide runs 1 through 7 in Table 17 is presented for the sake of brevity.

Porous Vycor plug physical data

Only one porous Vycor plug was used in this study.

The physical parameters of this plug were

$$L_p = 0.945 \pm 0.015 \text{ cm.}$$

$$D_p = 0.721 \pm 0.015 \text{ cm.}$$

$$A_p = 0.408 \text{ cm.}^2$$

$$W_p = 0.5557 \text{ gm.}$$

$$\rho_{\text{app}} = 1.441 \text{ gm./cc.}$$

$$\rho_s = 2.06 \text{ gm./cc.}$$

$$\epsilon = 0.301 \text{ cc. pore/cc. plug}$$

$$S_s = 192 \text{ m.}^2/\text{gm. for N}_2 \text{ at } 78^\circ\text{K}$$

S_s was measured by Dr. J. W. Lacksonen as previously mentioned. ρ_s was assumed to be the mid-range value of the

solid densities given by Engel (55), Russell (13) and Rutz (52). Their reported densities were 2.03, 2.05, and 2.10 gm./cc. respectively. Hence the assumed ρ_s has a maximum error of $\pm 3.4\%$. This leads to a maximum error in the calculated porosity, ϵ , of $\pm 4.0\%$.

Thermocouple calibration

The porous plug air bath and the air bath thermocouples (iron-constantan) were calibrated against calibrated thermometers to an accuracy of $\pm 0.1^\circ\text{C}$ over the range 0 to 48°C . The couples were taped to the thermometer, placed in a glass tube, and immersed in a dewar full of water at different temperatures. The data are given in Table 10 of the Appendix on Original Data Tabulation. The data were fitted by the least mean squares technique to the following equations.

$$\text{Plug Bath Thermocouple: } t' = 19.587 \text{ (mv.)} - .078 \text{ (6)}$$

$$\text{Air Bath Thermocouple: } t' = 19.587 \text{ (mv.)} - .071 \text{ (7)}$$

where t' = temperature in $^\circ\text{C}$

mv. = millivolt of thermocouple

Equations 6 and 7 may be shortened to:

$$t' = 19.58 \text{ (mv.)} \quad (8)$$

for an accuracy of $\pm 0.1^\circ\text{C}$.

A test of the bath temperature controllers indicated a sensitivity of $\pm 0.2^\circ\text{C}$.

Manometer scale calibration

The inlet and exit manometer scales (meter sticks) were calibrated using a cathetometer with an accuracy of 0.015 mm. The data are given in Table 11 of the Appendix on Original Data Tabulation. A least mean square fit of the data indicated that the scales were accurate to about 0.5%.

Syringe feeder calibration

A syringe feeder was used to measure the flow rates through the porous plug. The syringe mercury displacement was calibrated as a function of counts indicated on an electronic counter throughout the whole length of the syringe by weighing the mercury displaced. The data are given in Table 12 of the Appendix on Original Data Tabulation. The average mercury displacement was 8.171×10^{-4} cc./count with a standard deviation over the syringe length of 0.021×10^{-4} cc./count or 0.25%.

System volume measurement

The volumes of various parts of the system were measured to facilitate the flow measurements and the determination of the adsorption isotherm. The volume measurement data are given in Table 13 of the Appendix on Original Data Tabulation, and the calculation of the volumes is shown in the Appendix on Calculated Quantities. The volumes were measured with an accuracy of better than 0.5% and are given in Table 2.

TABLE 2
SYSTEM VOLUMES

Volume No.	Volume cc.
1 ^a	86.5
2 ^b	52.8
3 ^c	16.7
4 ^d	10.0

^aVolume 1 is the inlet system between valves 9, 14, and 15 with valves 12 and 13 closed and the manometer and syringe feeder reservoir mercury levels at the red marks. Valve numbers refer to Figure 1.

^bVolume 2 is the exit system between valves 15, 16, 19, 21 and 22 with valves 17 and 18 closed.

^cVolume 3 is the dead space before and after the plug between valves 14 and 16.

^dVolume 4 is the volume of the measuring system between valves 21, 23 and 24 with the mercury level in reservoir A at the red mark.

Differential pressure controller

The inlet and outlet pressures were controlled by mercury filled differential pressure manometers which had a tungsten contact in one arm. The mercury meniscus movement to make and break contact, hence to actuate the Thermocap relay controller, was barely observable and was estimated to be about 0.1 mm.

X-ray system calibration

Before each x-ray scan, the position along the plug axis of the x-ray detector was calibrated as a function of the voltage signal from the position indicator. These

position calibrations are given in Table 22 of the Appendix on Original Data Tabulation.

The x-ray system was calibrated by first obtaining a measurement of the x-ray intensity axially down the evacuated porous plug. These scan data are given in Table 23, in the Appendix on Original Data Tabulation and are shown graphically in Figure 6. The data from this scan were used as a base to which all further data were referred. For this scan $(I_R)_B$ was 97.5×10^3 counts/minute.

The porous plug was then equilibrated with CH_3Br for approximately 24 hours at different pressures. Axial x-ray scans gave the x-ray absorptions corresponding to the various pressures. The data for these scans are also given in Table 23. The x-ray attenuation function for reducing the x-ray data to a common base is derived in Appendix C. This x-ray attenuation function is defined as

$$F = (I_R - \Delta I) / (0.9I_R + 0.1(I_R)_B - (\Delta I)_B) \quad (9)$$

where F = x-ray attenuation factor
 I_R = x-ray intensity indication by the dummy plug
 or reference scintillation detector
 ΔI = difference in the x-ray intensity indicated
 by the reference and porous plug scintillation
 detectors

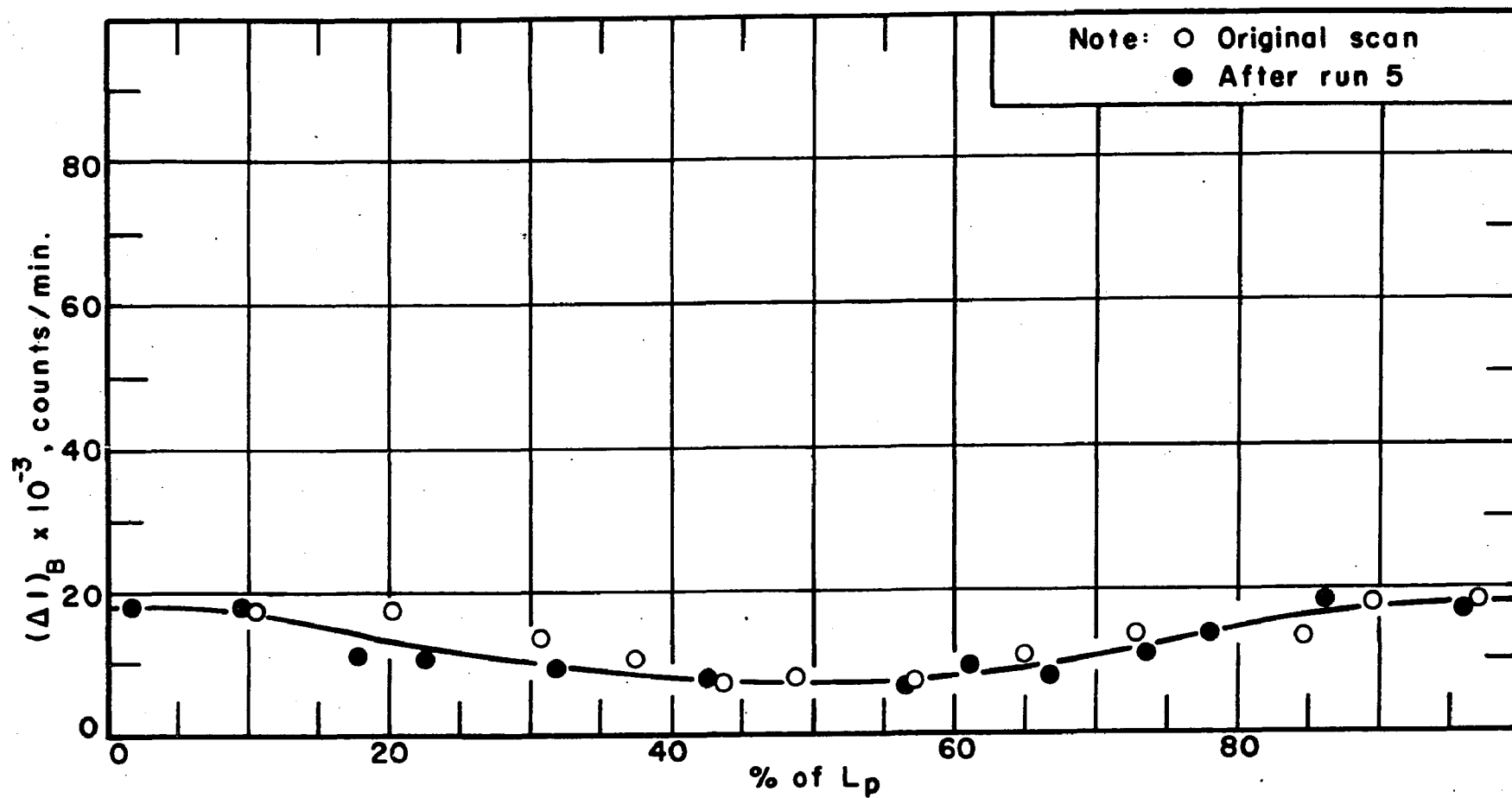


Fig. 6. Base line x-ray scan.

$(I_R)_B$ = x-ray intensity indicated by the reference scintillation detector during the base scan and hence is 97.5×10^3 counts/min.

$(\Delta I)_B$ = difference in the x-ray intensity indicated by the reference and porous plug scintillation detectors during the base scan at the same position on the plug where ΔI is measured.

Hence F is the x-ray attenuation corresponding to the equilibrium pressure with the effects of axial position and x-ray source intensity removed and should be unity for the evacuated plug. Figure 7 shows F as a function of length for various equilibrium pressures and Figure 8 shows F as a function of equilibrium pressure.

The equilibrium pressure, P_e , and the quantity adsorbed in the plug, C_s , is related through the adsorption isotherm. Since F as a function of P_e has been obtained experimentally, the dependence of F on C_s can be obtained through the adsorption isotherm. As shown in Appendix C, the semi-empirical relationship between C_s and F is given by

$$C_s = -K \ln F \quad (10)$$

$$\text{and } K = \frac{22,400}{\rho_{\text{app}} D_p M} (1/\mu/\rho) \quad (11)$$

where ρ_{app} = density of the plug

D_p = thickness of the plug

M = molecular weight of adsorbed material

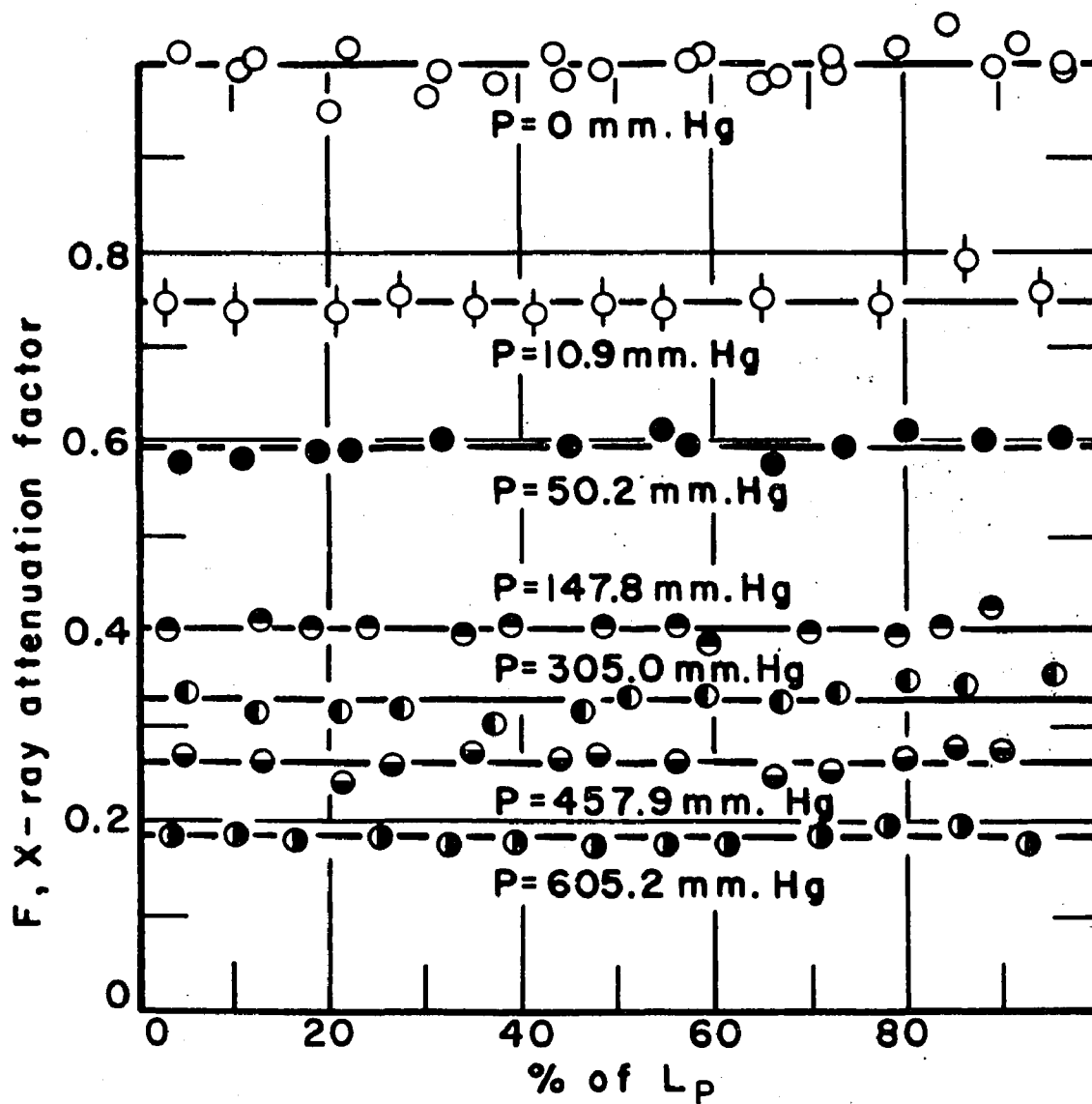


Fig. 7. Attenuation factor versus axial distance.

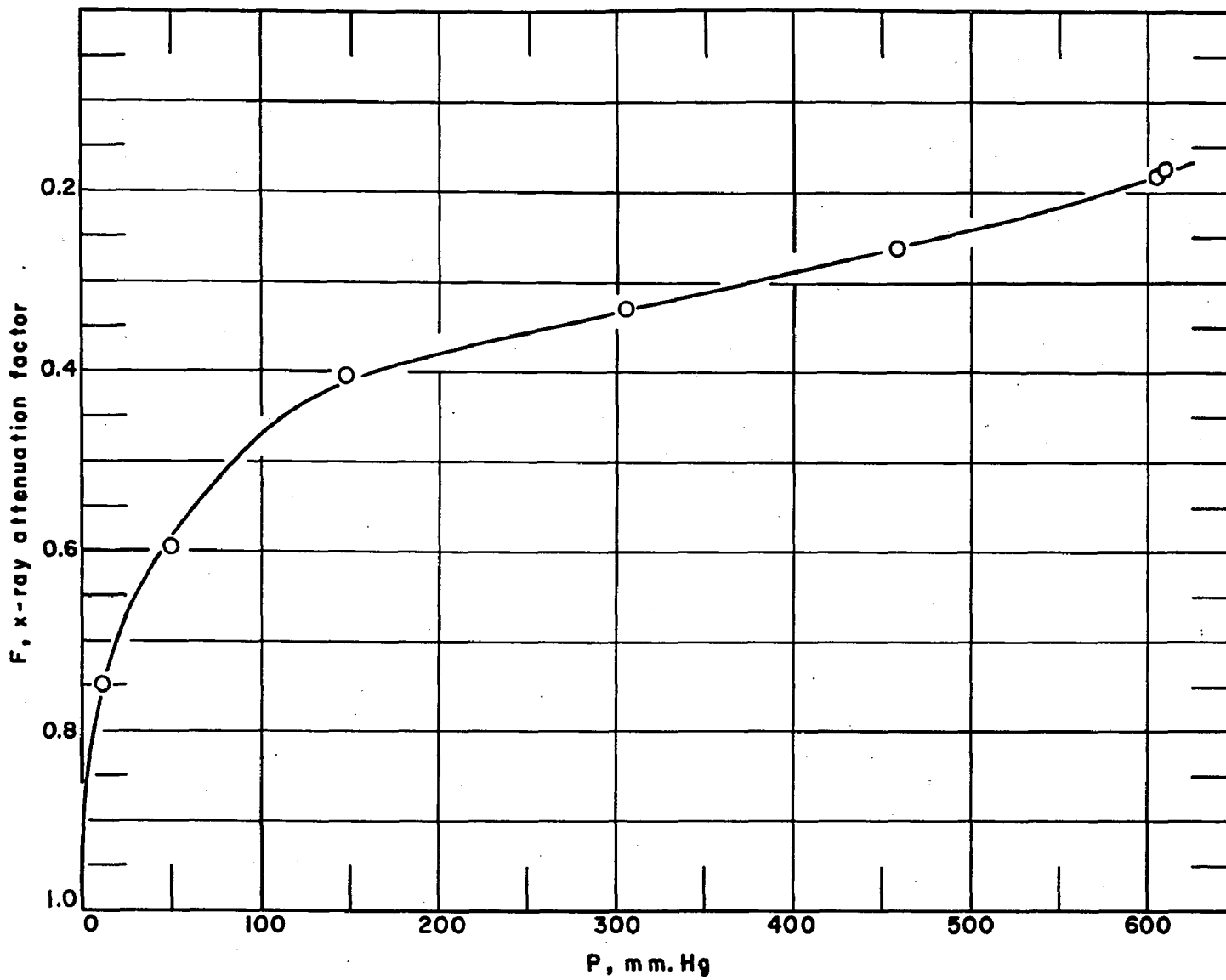


Fig. 8. Attenuation factor versus equilibrium pressure.

μ / ρ = x-ray mass absorption coefficient of
adsorbed material at the effective wave-
length

Three points on the adsorption isotherm were obtained by measuring the quantity of methyl bromide removed from the plug after equilibration at a given pressure. The experimental data are given in Table 19 and the isotherm points summarized in Table 20 of the Appendix on Original Data Tabulation. The quantity of material removed from the plug included both gas phase and adsorbed phase methyl bromide. However, as shown in the Appendix on Calculated Quantities, the amount of material in the gas phase was always negligible compared to the surface phase. Hence the quantity removed was essentially the quantity of material adsorbed.

The F values corresponding to the isotherm points were obtained from Figure 8 and C_s versus $\ln F$ for the three points is shown in Figure 9. Since these points did seem to establish the straight line predicted on the semi-log plot, three points were considered sufficient.

Adsorption isotherm

By plotting C_s and P_e from Figures 8 and 9 for the same values of F, the adsorption isotherm shown in Figure 10 was constructed. The data for this plot are given in Table 21 in the Appendix on Original Data Tabulation.

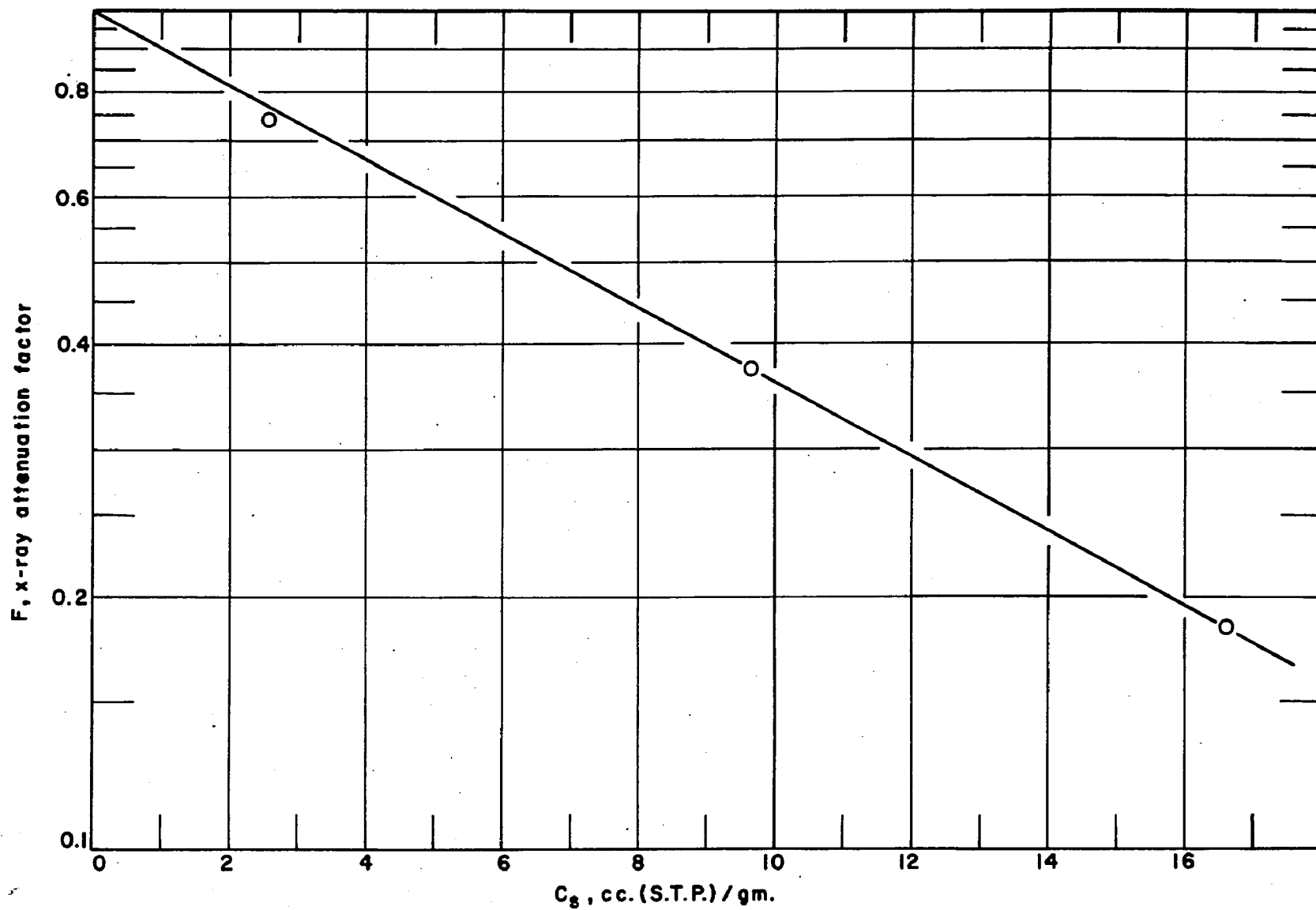


Fig.9. Attenuation factor versus volume adsorbed.

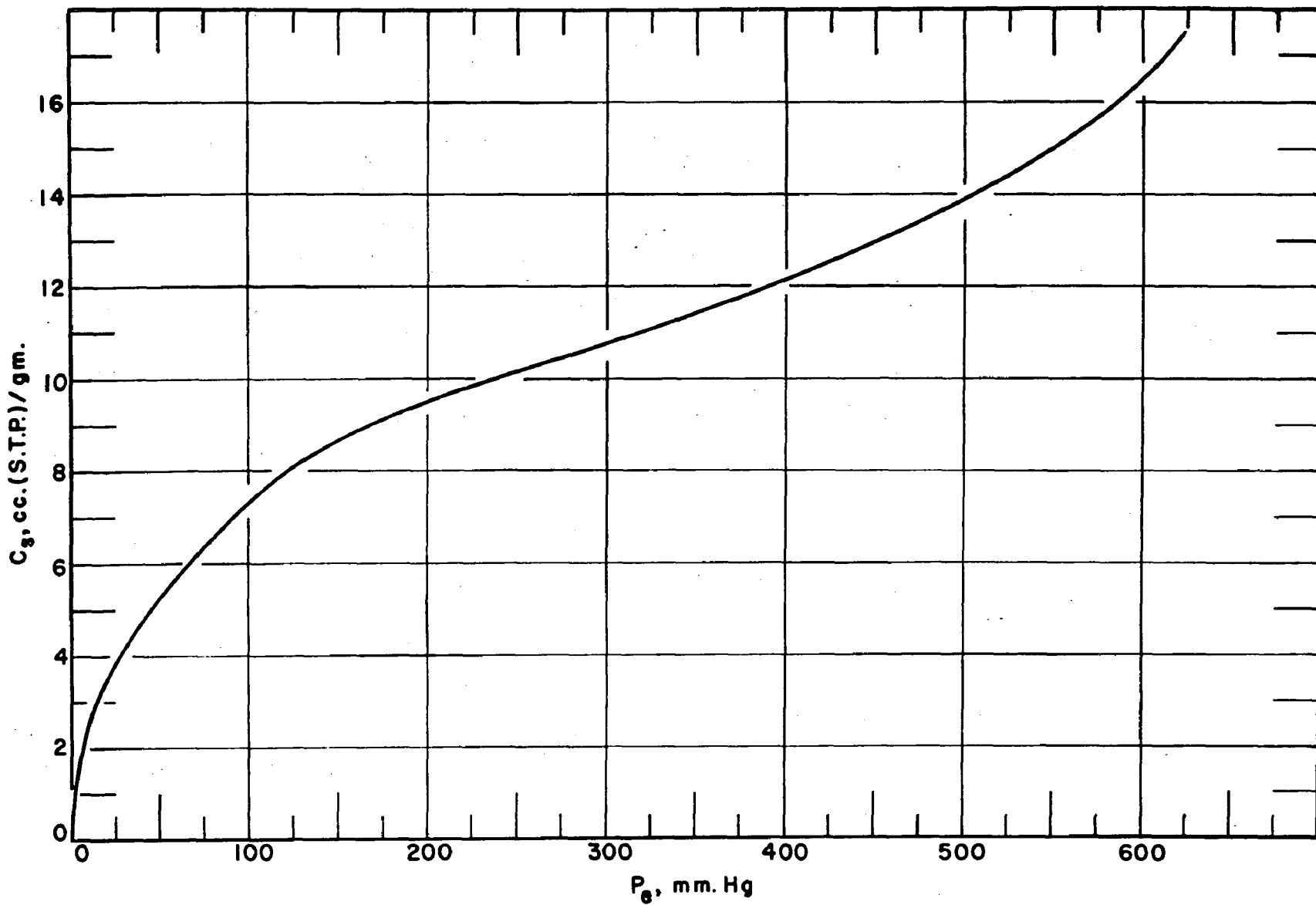


Fig.10. Adsorption isotherm for CH_3Br on porous Vycor at 40°C .

Helium permeability

The helium permeability was obtained by measuring the steady state flow rate of helium through the Vycor plug under various pressure differences and at different pressure levels at 40°C.

The helium flow data are given in Table 15 of the Appendix on Original Data Tabulation. Approximately every other data point has been included in this table for the sake of brevity.

The helium permeabilities were calculated as shown in the Appendix on Calculated Quantities and are summarized in Table 14 of the Appendix on Original Data Tabulation. These six permeabilities have been plotted against the average pressure level in Figure 11. Also shown in Figure 11 are the helium permeabilities measured by Engel *et al.* (38), Russell *et al.* (37), Barrer and Barrie (9), and Rutz (52) for various samples of porous Vycor. The porous Vycor physical parameters used by these investigators is given in Table 3. As shown in Figure 12, the average permeability is 0.00883 with maximum scatter of +2%.

Steady state methyl bromide permeability

The methyl bromide permeability was obtained by measuring the steady state flow rate of methyl bromide through the Vycor plug under various pressure differences and at different pressure levels at 40°C. Runs 1-8 and 13 were made

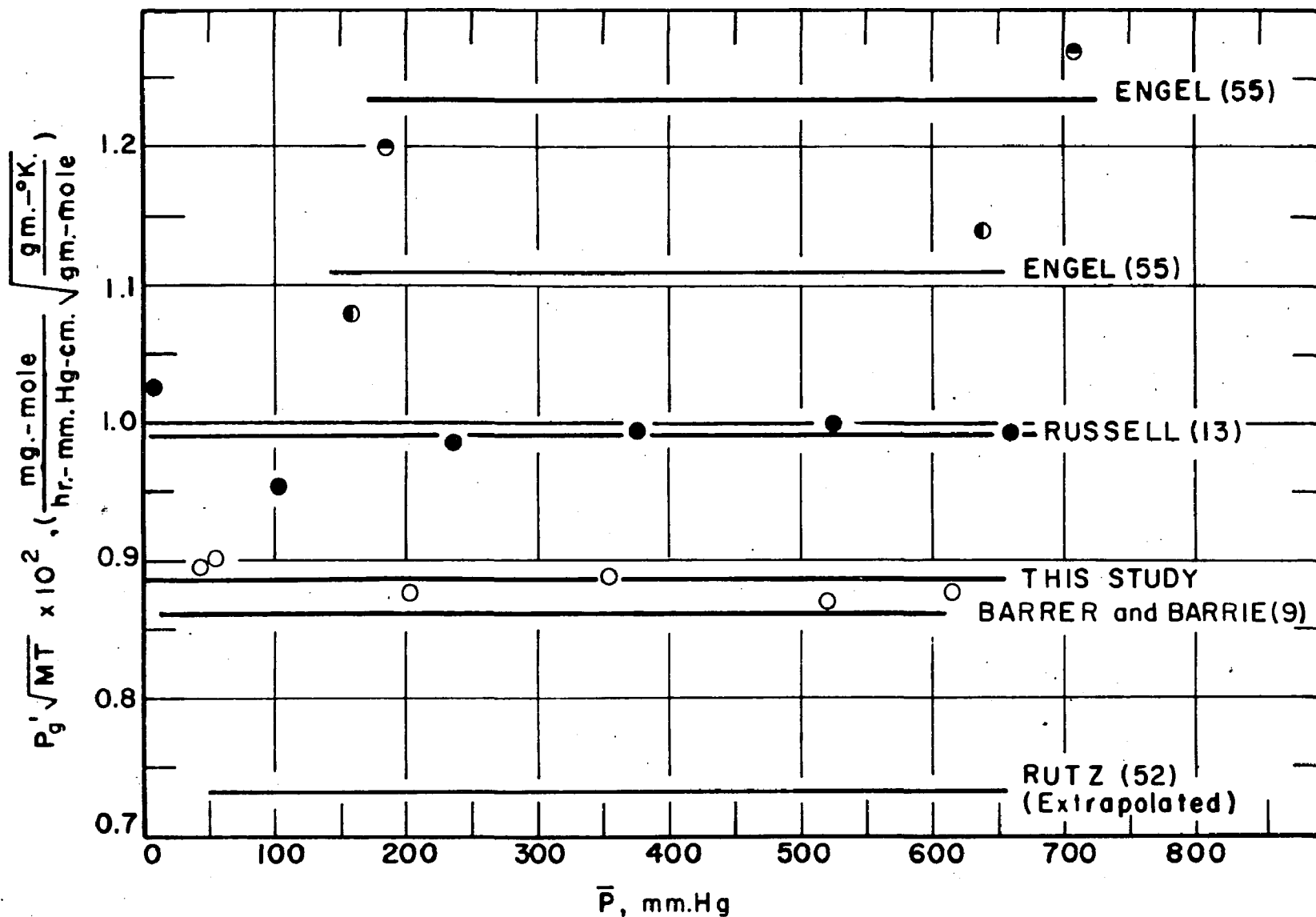


Fig. II. Helium permeability for porous Vycor.

TABLE 3

PHYSICAL PARAMETERS OF VYCOR PLUGS USED FOR HELIUM
PERMEABILITIES BY OTHER INVESTIGATORS

Reference	Engel <u>et al.</u> (38)	Russell <u>et al.</u> (37)	Barrer & Barrie (9)	Rutz (52)
L_p , cm.	1.41	0.372	2.64	0.5
A_p , cm. ²	1.32	1.412	0.924	19.635
S_s^a , m. ² /gm.	81.9	143	131	224
ϵ	0.28	0.31	0.298	0.284

^aSpecific surface areas were for nitrogen determine
by the B.E.T. method.

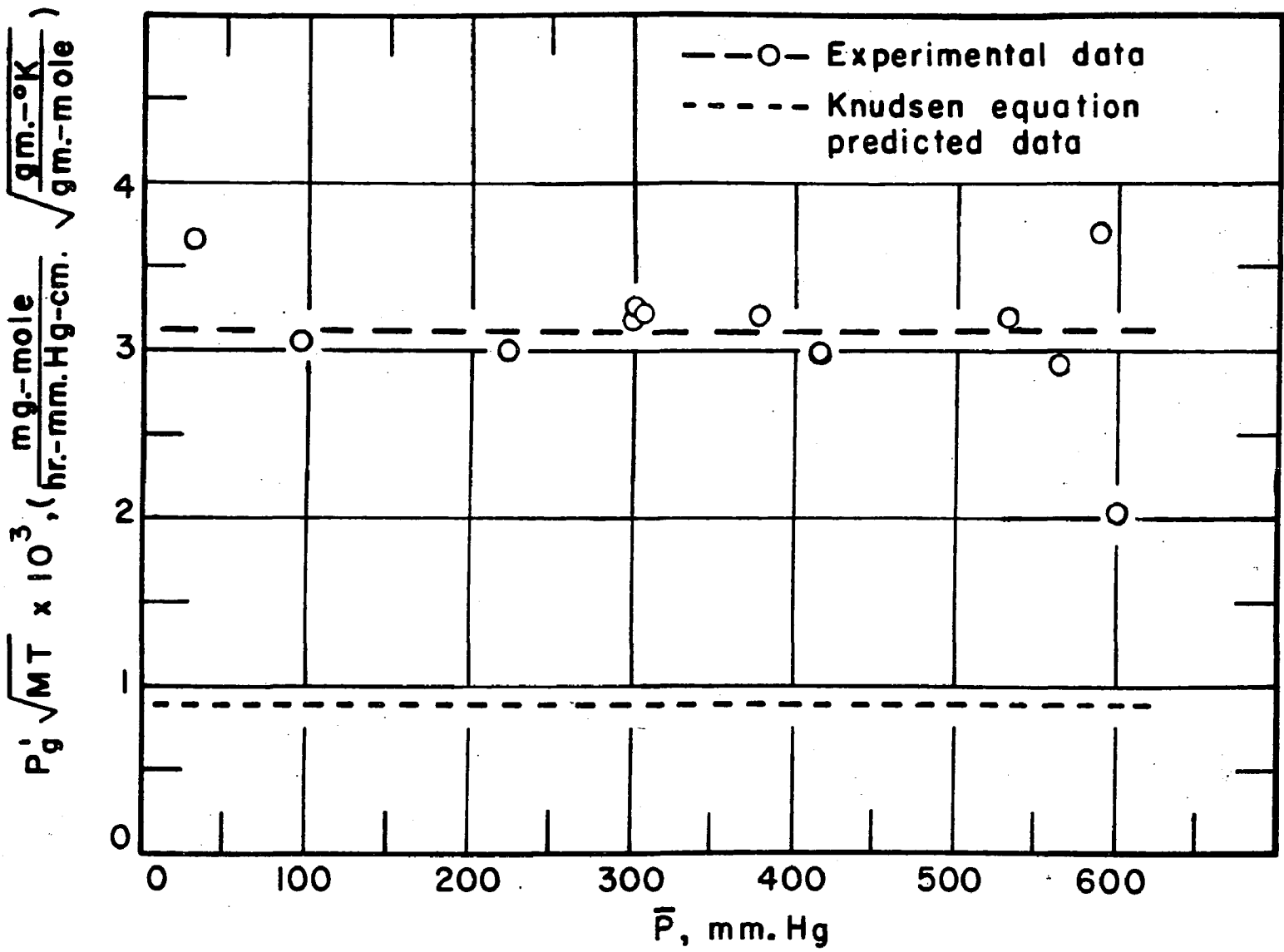


Fig.12. Steady state CH_3Br permeability at 40°C .

by equilibrating the plug at the exit (low) pressure before subjecting the inlet side of the plug to the inlet (high) pressure. Runs 9-11 were made by sequentially lowering the exit pressure after steady state operation of the preceding run starting with the steady state operation of run 8.

The steady state permeability for each run was calculated as shown in the Appendix on Calculated Quantities from the flow data given in Table 17 of the Appendix on Original Data Tabulation. These permeabilities are summarized in Table 17 of the same Appendix and are plotted in Figure 12 against the average pressure. The dashed (long) line is the average permeability for the ~~twelve~~ runs. Also plotted in Figure 12 is the permeability predicted by the helium flow measurements if we assume the Knudsen mechanism.

During the steady state portion of run 2, a material balance was made. All of the methyl bromide passing through the plug was collected for period of 5 hours. The calculations for this balance are shown in the Appendix on Calculated Quantities. 0.826 cc. (S.T.P.) were fed in during this 5 hour period and 0.804 cc. (S.T.P.) was collected downstream. The difference was 0.022 cc. (S.T.P.) or about 2.66%.

The reproducibility of the flow measurements seem excellent as indicated by runs 6, 7, and 13 which were made under essentially the same operating conditions and have the same permeabilities.

Concentration profiles of CH₃Br runs

The calibration data for the position of the x-ray detector along the axis of the plug for all the concentration profile measurements on the CH₃Br runs are given in Table 24 of the Appendix on Original Data Tabulation. As a sample, the position calibration curve for run 1 is shown in Figure 13. The standard deviation of the data about the curve is $\pm 2.3\%$ of L_p or ± 0.022 cm. These data are typical of the rest of the x-ray detector position calibration data.

The concentration profiles within the porous plug during the CH₃Br flow runs were measured by x-ray absorption measurements. The x-ray data were converted into concentration data using the relationship of equation 7 and Figure 9 as shown in the Appendix on Calculated Quantities.

Steady state concentration profiles were measured for runs 1 through 7 and run 11. The data for these profiles are tabulated in Table 25 of the Appendix on Original Data Tabulation and plotted in Figures 14 through 20. The data for runs 6 and 7 are plotted in the same figure since these were essentially duplicate runs. Also plotted on these figures is the concentration at the start of each run, time zero.

The concentration data scattered somewhat during the latter part of Runs 2 through 5. When scattering occurred, the line through the data has been extrapolated to the concentration in equilibrium with the exit pressure as shown by

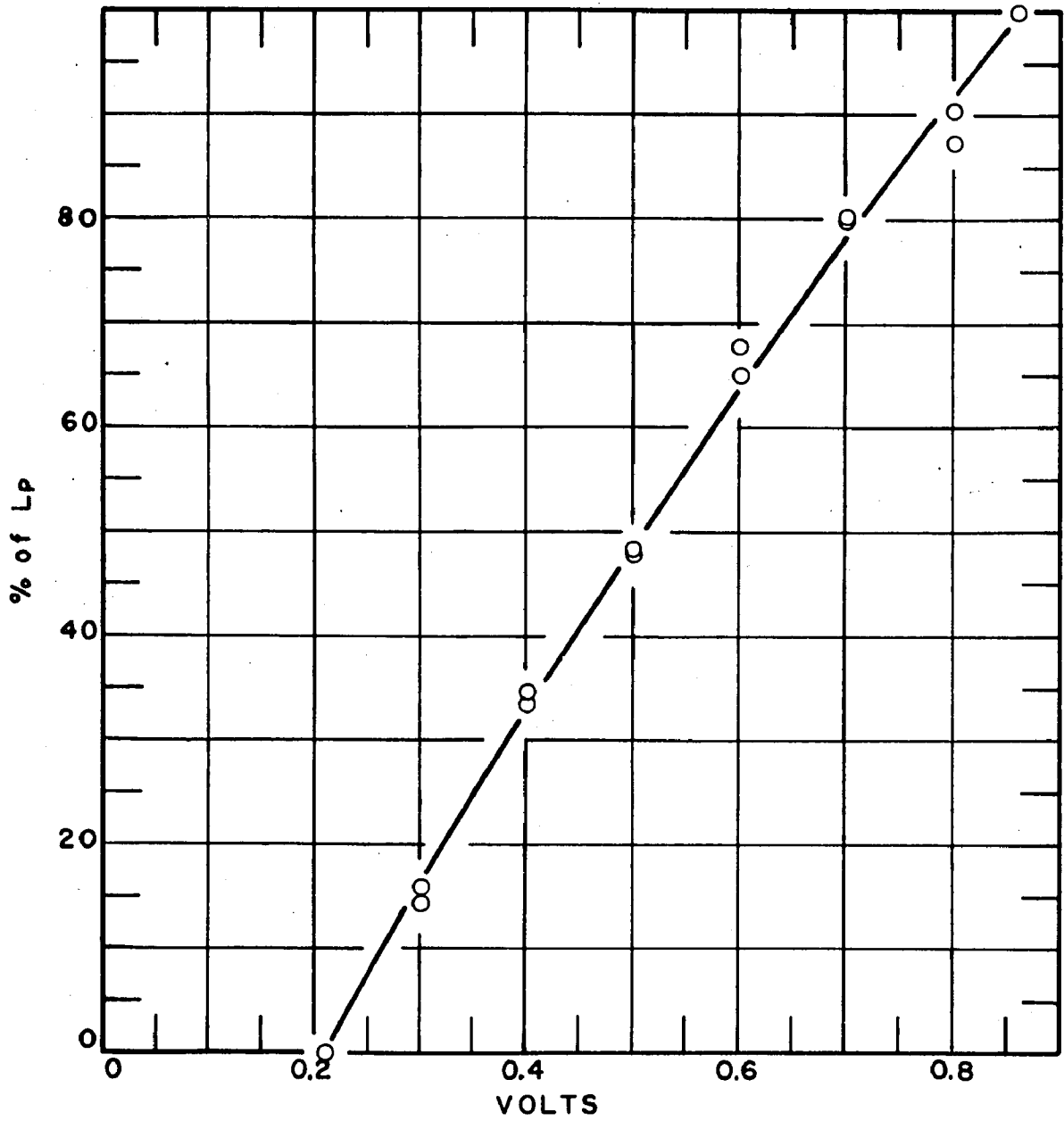


Fig.13. X-ray detector position calibration for run 1.

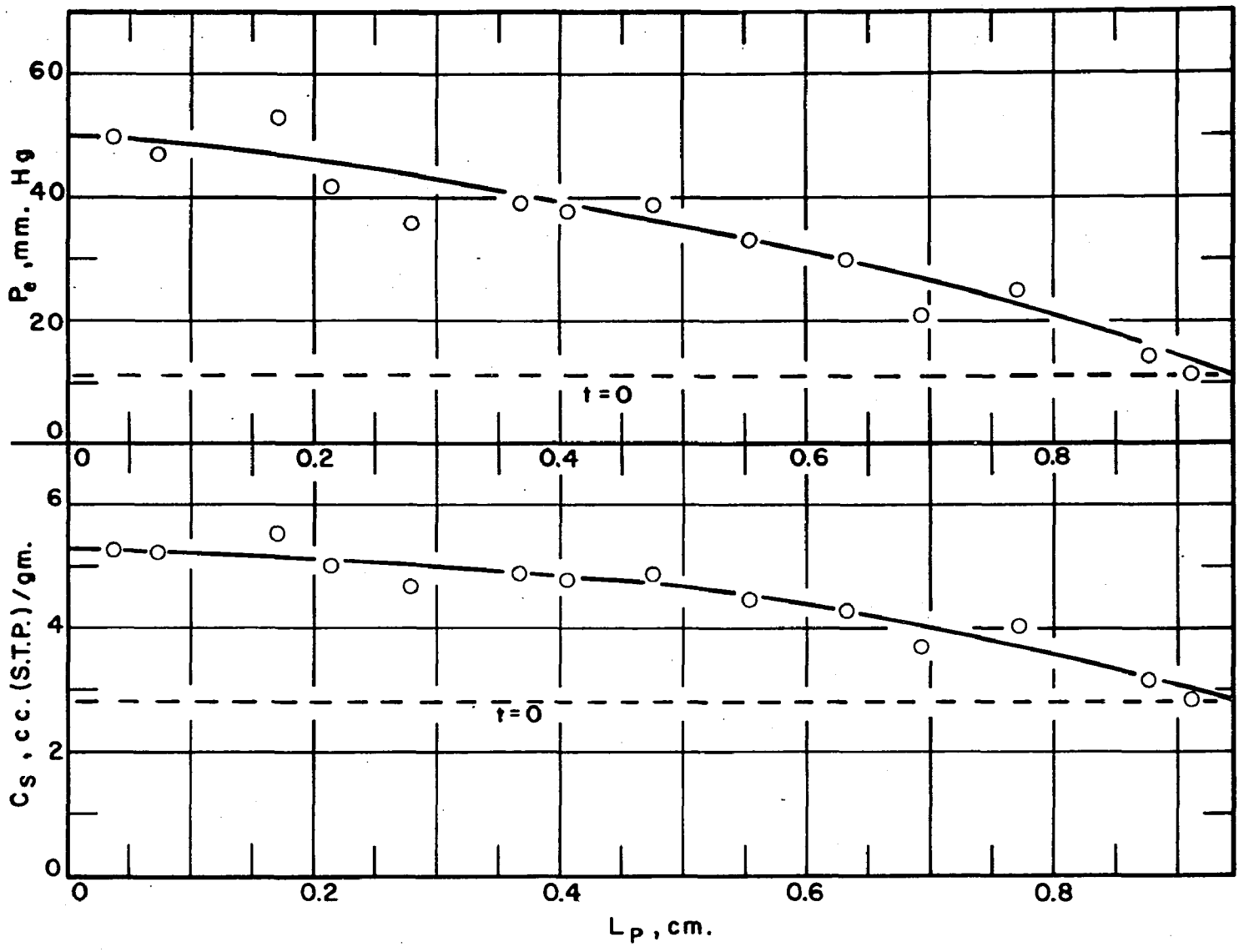


Fig. 14. Run 1 steady state concentration profile.

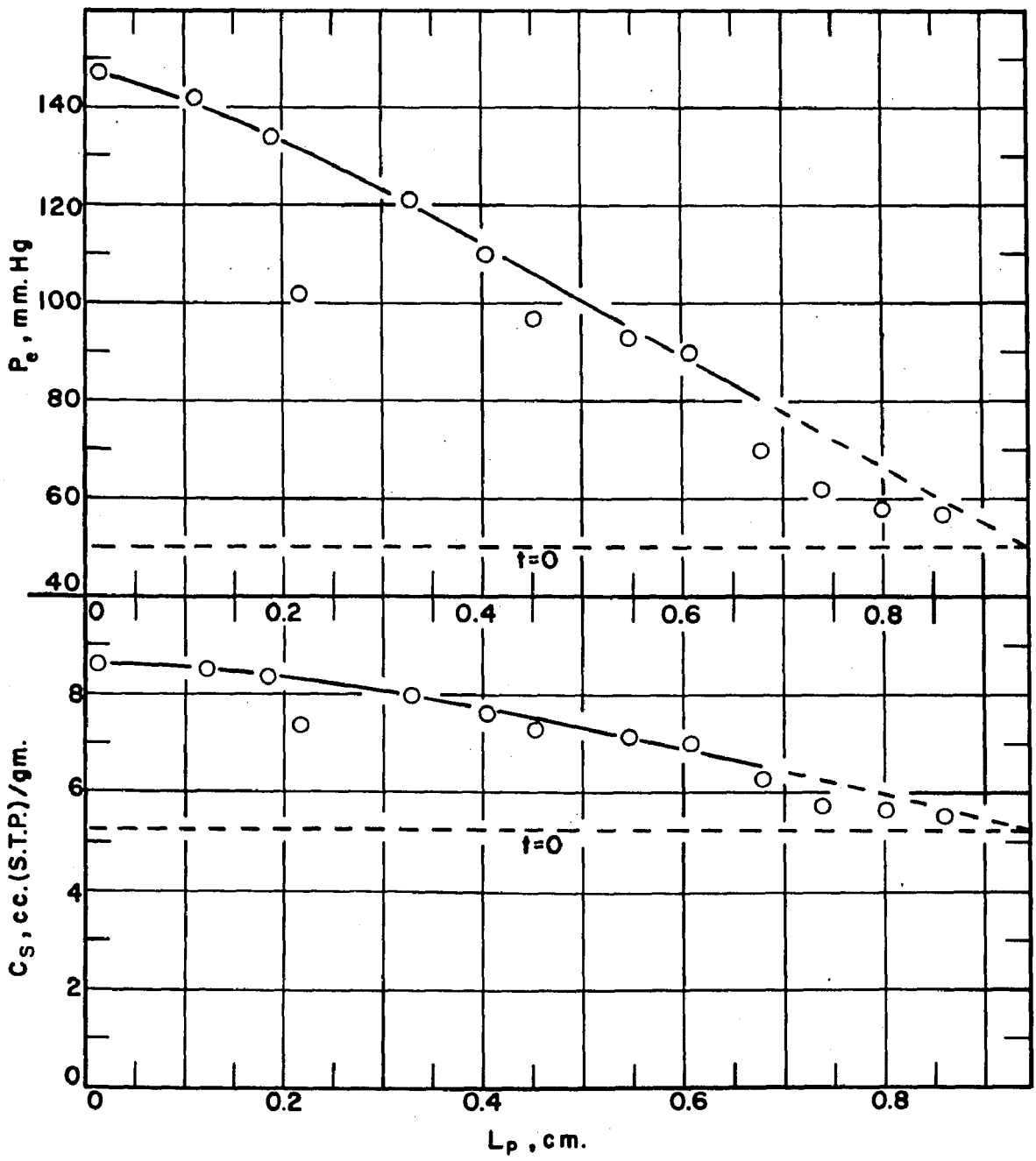


Fig.15. Run 2 steady state concentration profile.

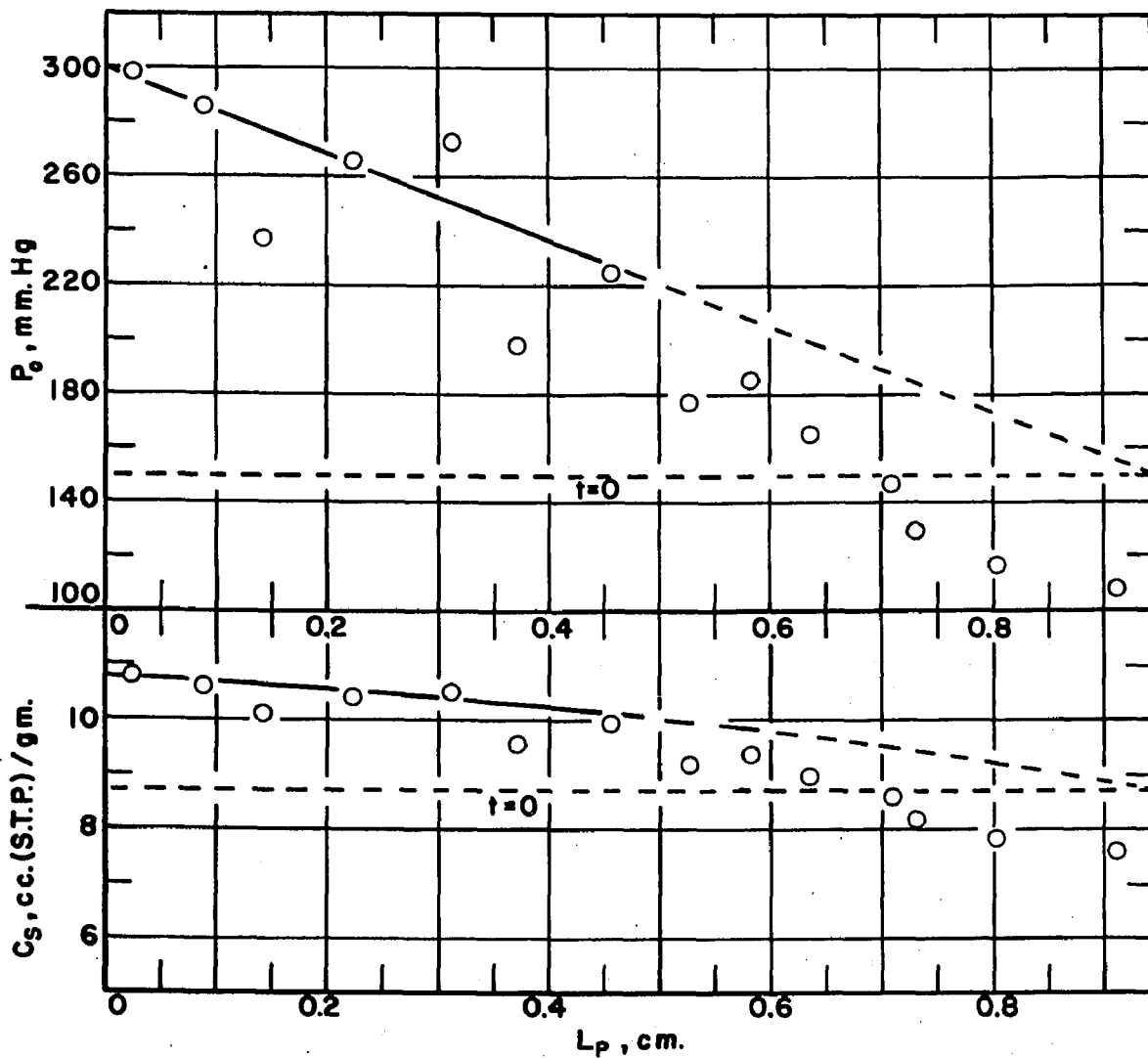


Fig.16. Run 3 steady state concentration profile.

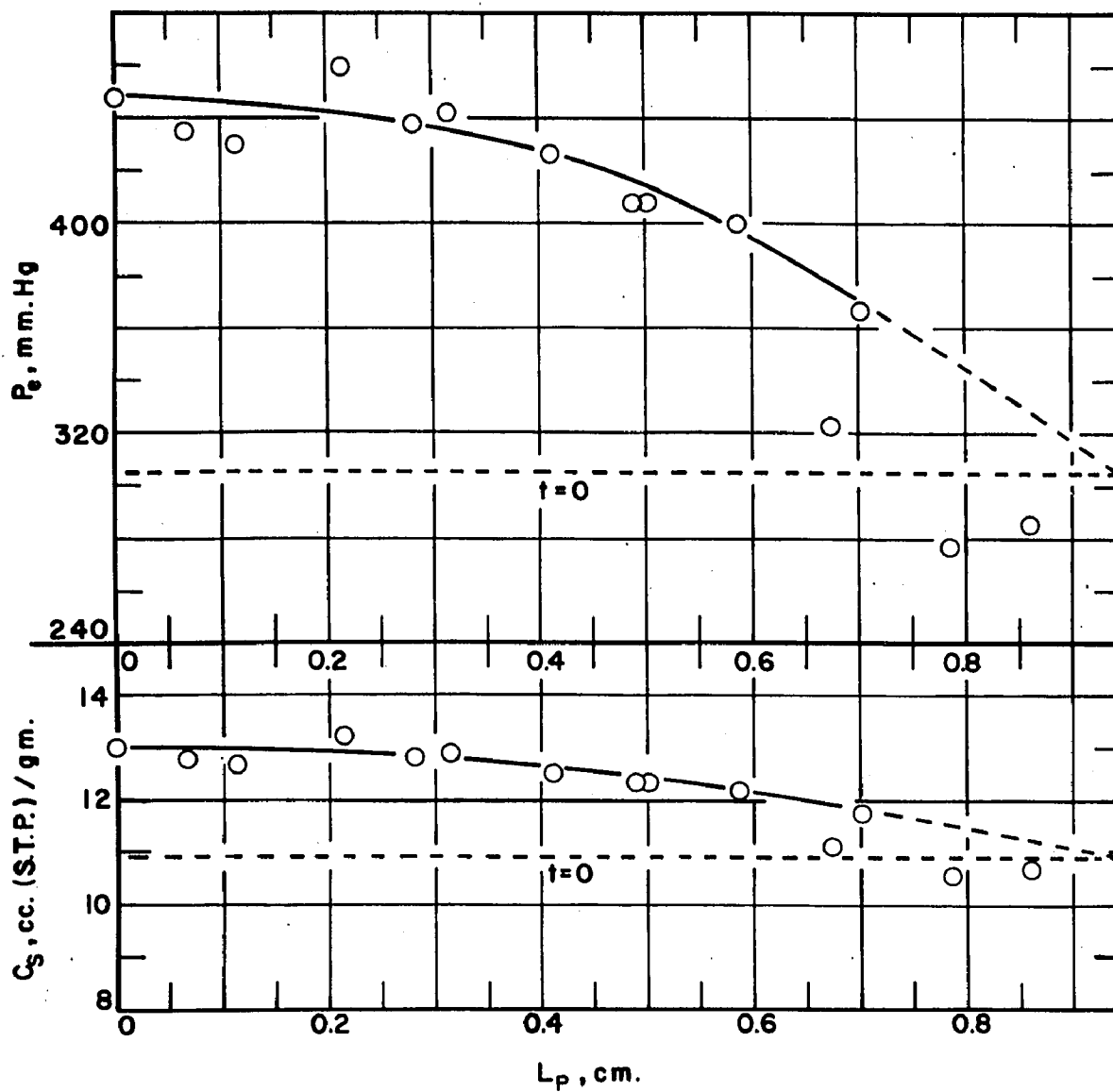


Fig. 17. Run 4 steady state concentration profile.

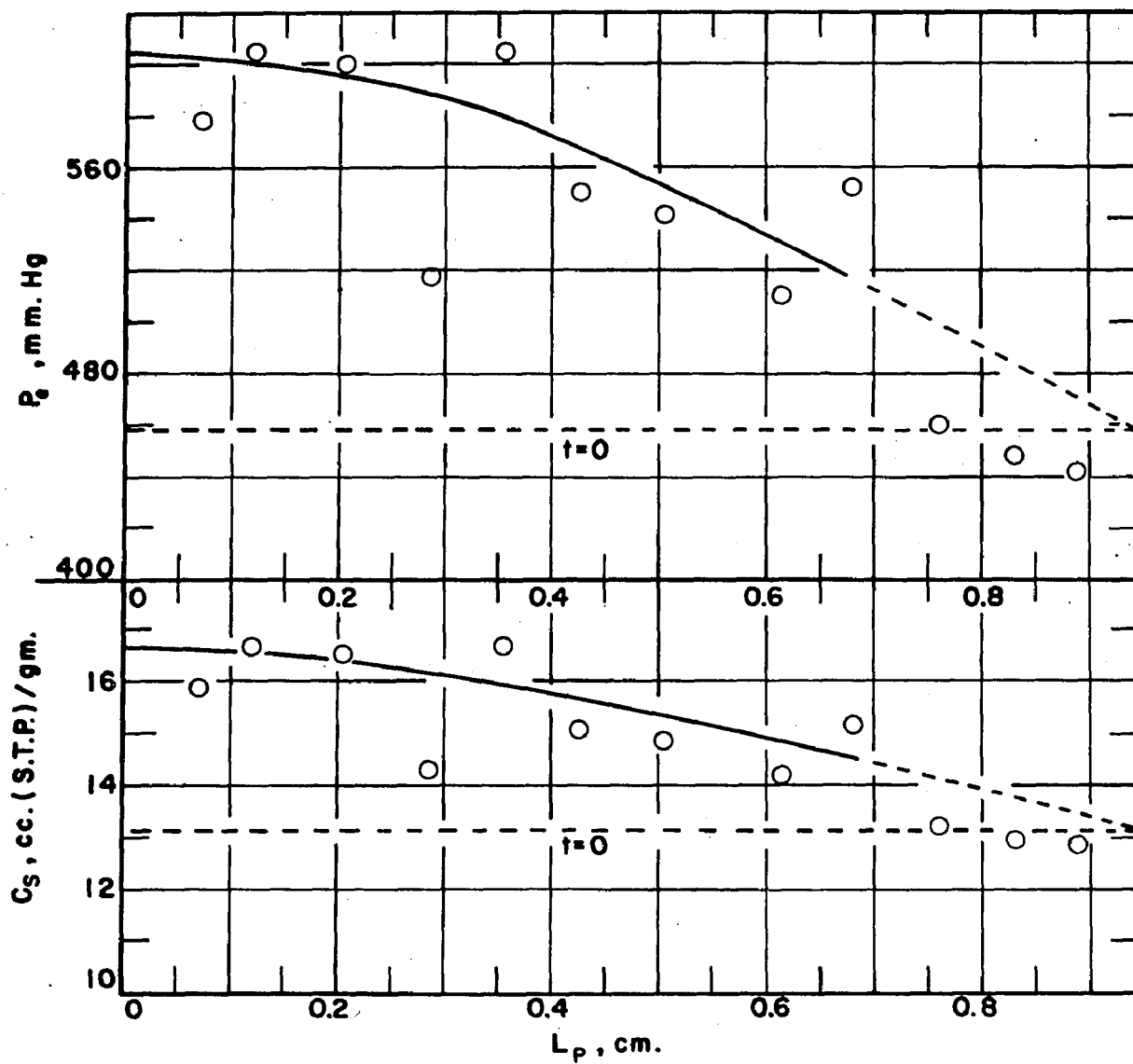


Fig. 18. Run 5 steady state concentration profile.

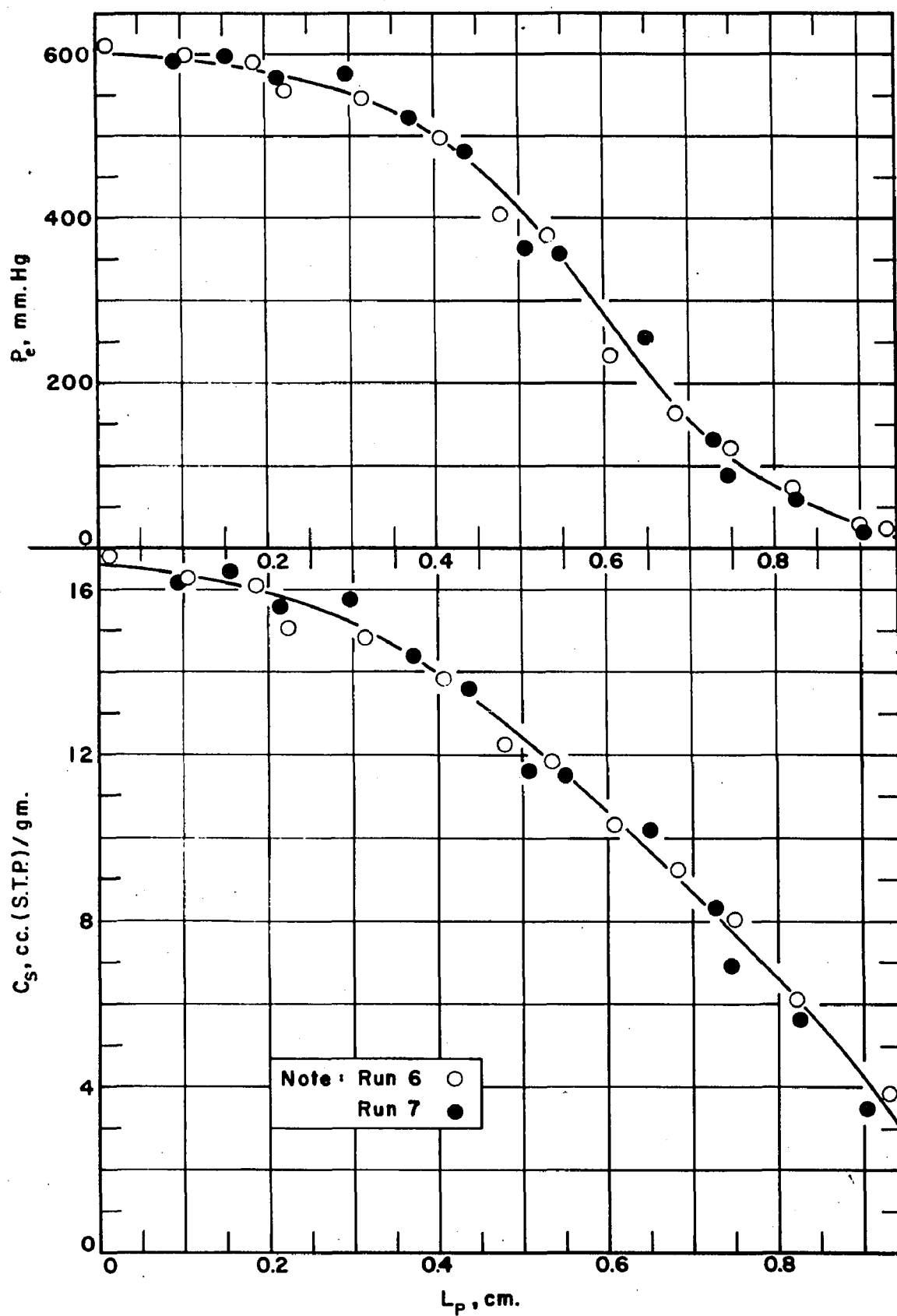


Fig. 19. Runs 6 and 7 steady state concentration profile.

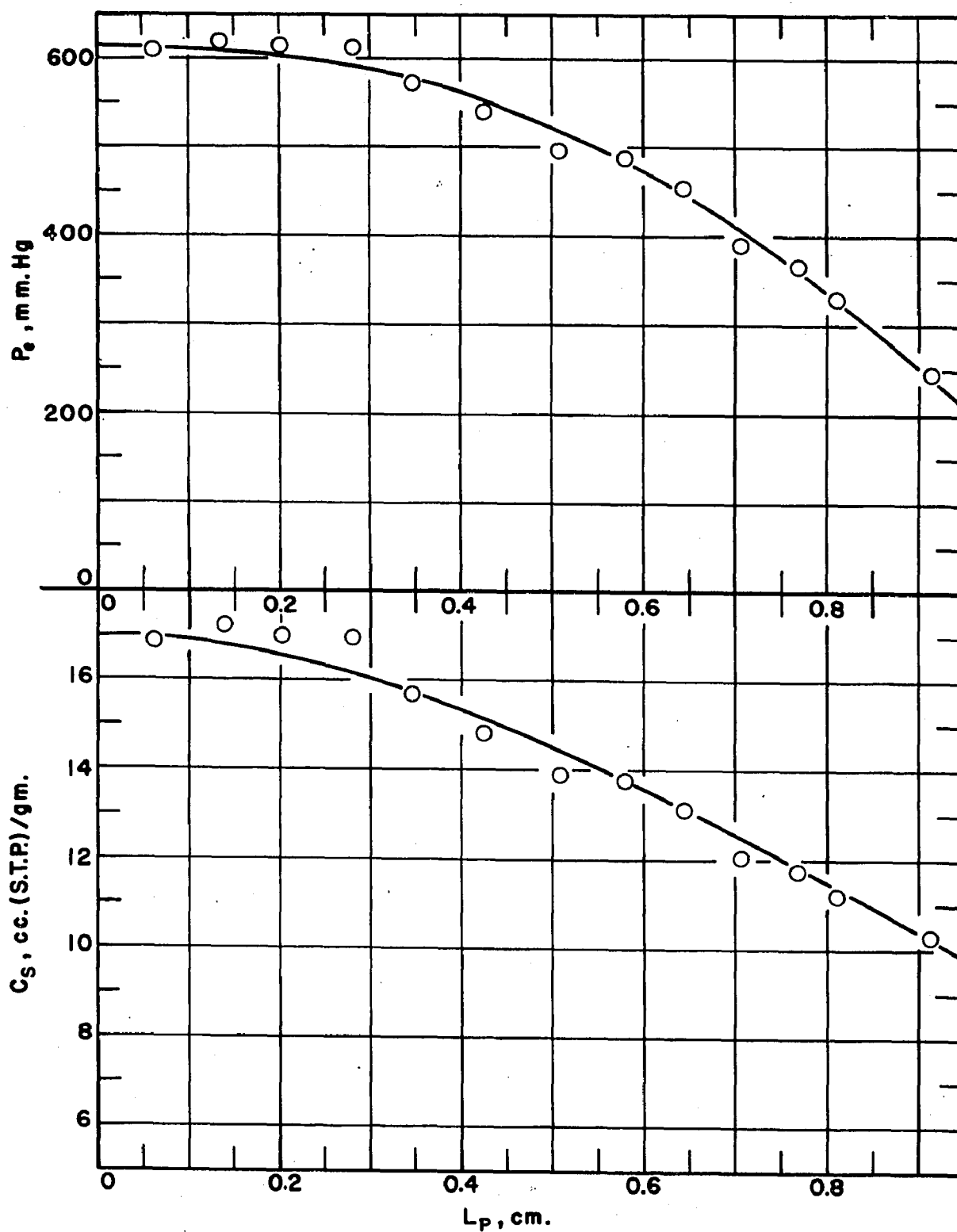


Fig. 20. Run II steady state concentration profile.

the dashed portion. The concentration profiles from these runs were only of value in the over-all qualitative picture.

This scatter in the profile data occurred especially at higher concentrations and at small concentration differences. This is not too surprising since the x-ray attenuation is logarithmic in nature and hence only small changes in x-ray absorption occur at higher concentrations. For example, runs 2 and 5 have essentially the same over-all concentration differences (3.35 and 3.5 cc.(S.T.P.)/gm. respectively), but very different average concentration levels (6.92 and 14.95 cc.(S.T.P.)/gm. respectively). Consequently their x-ray intensity measurement differences, Δ (ΔI), are 13.0×10^3 and 3.0×10^3 counts/min. respectively.

A contributing factor to the scatter in the data is the variation in the reference detector x-ray intensity measurement, I_R . I_R was only measured at the beginning and end of the x-ray scan. Since I_R is used in reducing the x-ray data to a common base, any fluctuations in I_R during the scan would tend to scatter the data even though the changes are partially compensated for by similar fluctuations in the plug detector intensity measurement. The value of I_R has been observed to fluctuate as much as $2-6 \times 10^3$ counts/min.

In addition to any error in I_R , there is the statistical error due to the random nature of x-rays as discussed in the Appendix on x-ray system variables and equations. The statistical error varies from about 2.0 to 0.8% when the

concentration measured varies from about 16.7 to 0 cc. (S.T.P.)/gm.

The other errors in the measuring system are minor compared to the statistical error, the error due to variation of I_R , and the error in the detector position measurement since relative, rather than absolute, count rates were used.

As is shown in Figure 19, the reproducibility of the concentration profile measurements seems excellent when large changes in concentration are observed.

For runs 6 and 7, unsteady state concentration profiles were also measured. The data for these profiles are given in Table 26 of the Appendix on Original Data Tabulation and shown graphically in Figures 21 and 22. The times indicated on the figures are the average times after time zero when the profiles were measured.

When run 6 was made, concentration profiles were not made after about one hour until steady state operation was reached. Thus the run 6 profiles do not show the building up of an apparent end effect. Consequently, run 7 was made under essentially the same operating conditions as run 6 to show the reproducibility of the flow and concentration profile measurements and to obtain concentration profiles for this period between one hour and steady state operation.

Each profile measurement took about two and one-half minutes. As a check on the dynamic error introduced by this scan time, alternate profiles were made starting at the

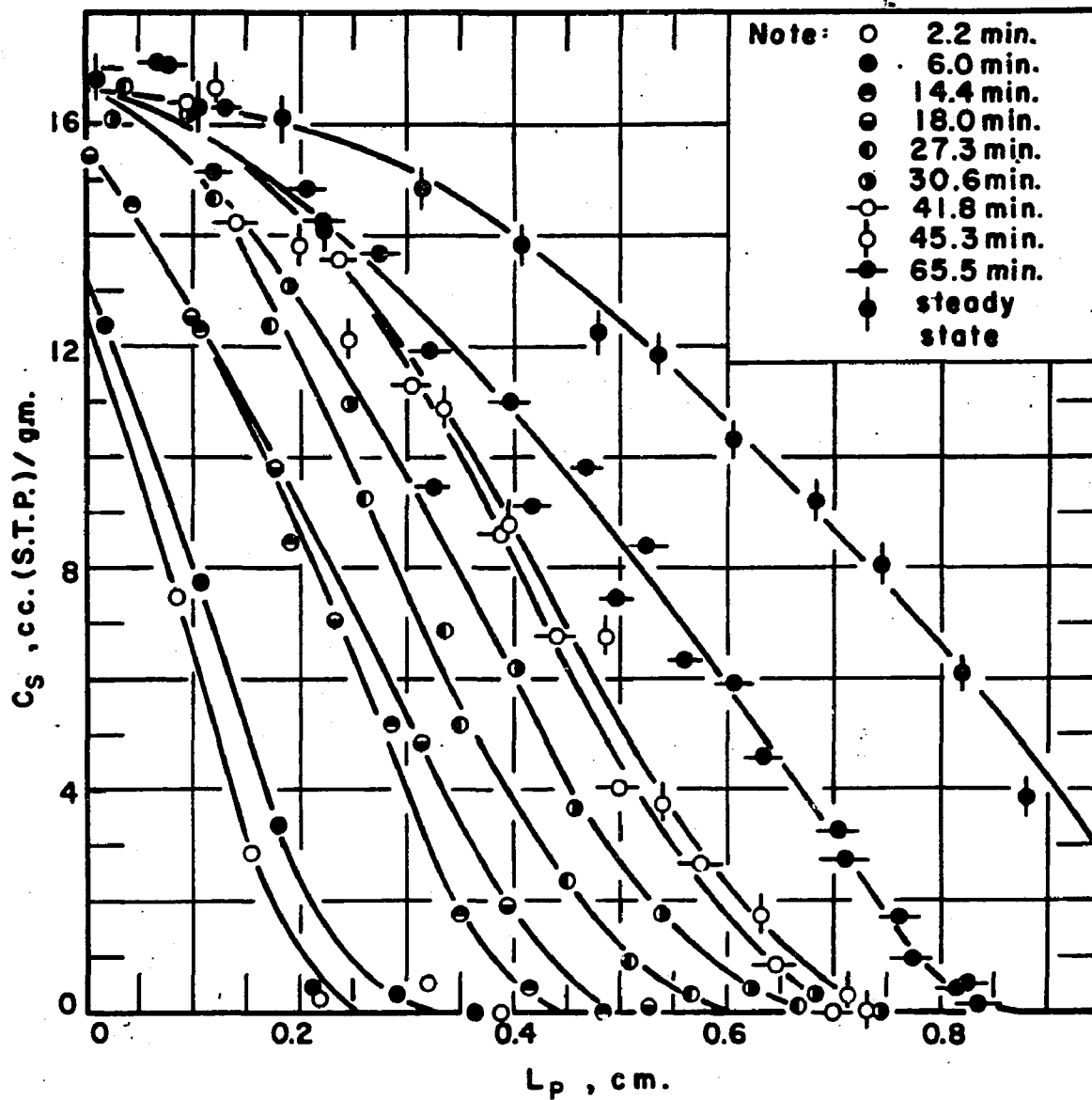


Fig. 21. Run 6 unsteady state concentration profiles.

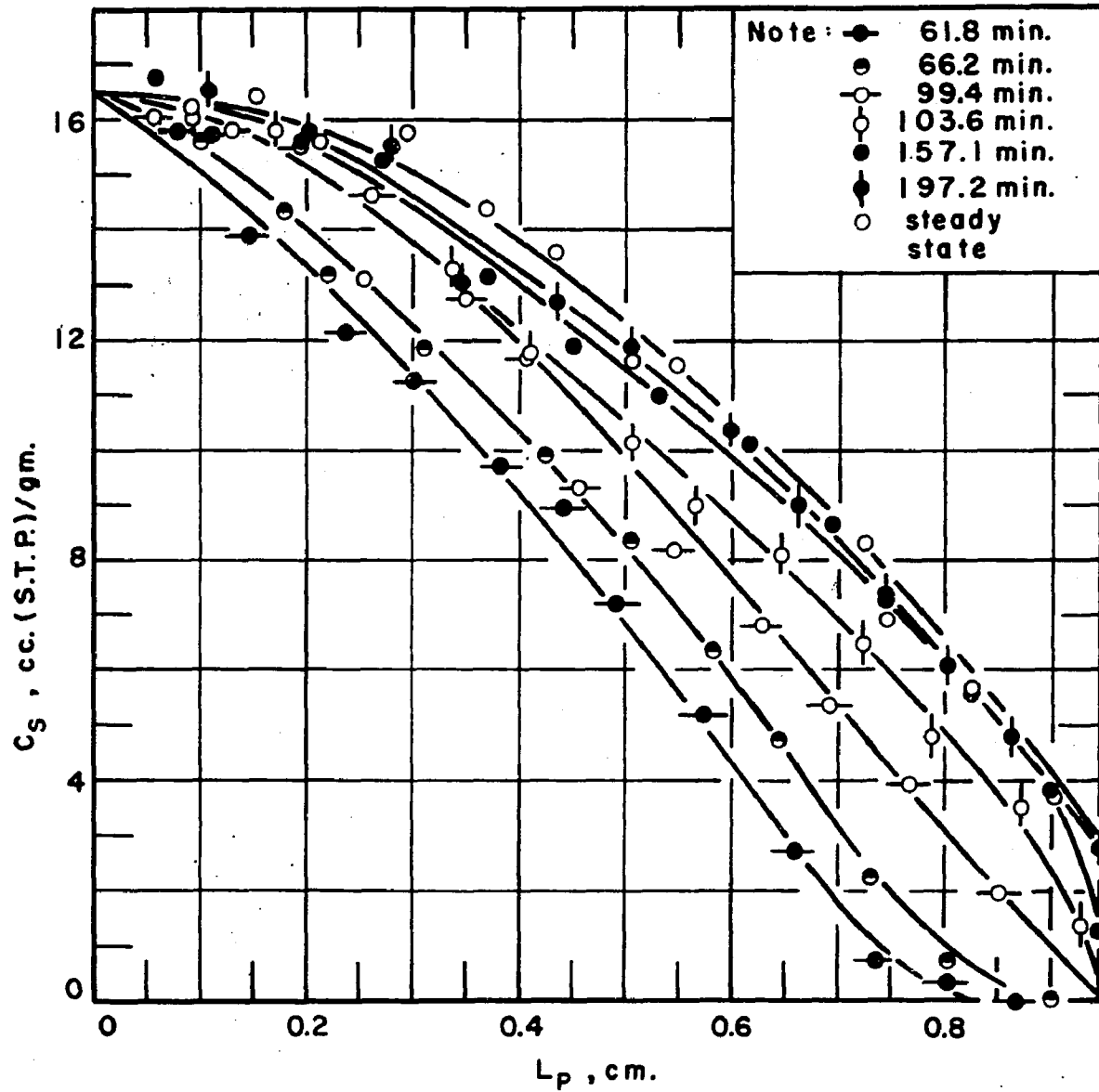


Fig.22. Run 7 unsteady state concentration profile.

opposite end of the plug. As the profiles indicate, the flow rate appears to be too slow to introduce much dynamic error.

Run 13 was essentially a repeat of runs 6 and 7 except that only flow data were obtained and the x-rays were on only for 5 second intervals to take radiographs of the developing profile. The x-rays were on for a total of only 102 seconds during the entire run. The fact that the permeability calculated for run 13 was the same as for runs 6 and 7 indicates that the x-rays, used substantially during runs 6 and 7, had a negligible effect on the profile and flow measurement. To further substantiate the negligible x-ray effect, the x-rays were turned off and on for periods of one hour during the steady state part of run 7 with no observable effect on the flow rate. In addition, the x-rays were left on throughout run 11 and the material passing through the plug was collected. A sample of this material was compared to a sample of methyl bromide from the methyl bromide supply cylinder by gas-liquid chromatography. The chromatography unit used was a home-made unit in the Engineering Experiment Station at the Ohio State University. The column was a 6 mm. O.D. pyrex tube, 4 ft. long, packed with 48-60 mesh Chromosorb W support with di-octyl phthalate substrate and operated at room temperature. The chromatographs indicated no detectable differences between the pure methyl bromide and that which had passed through the plug under x-radiation.

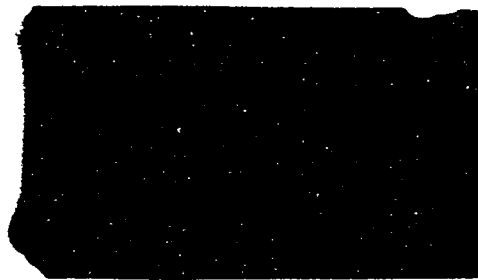
Thus any effect of the x-rays on the methyl bromide was negligible.

Some of the radiographs obtained during run 13 are shown in Figure 23. These pictures are actually the negatives of the x-ray exposures made at 41 KV. and 43 ma. with a 5 second exposure time using Kodac Dental X-ray film. Consequently the light area on the porous plug is the methyl bromide gas entering the plug. The very light area at the left hand edge of each picture is the solid glass used to fill the glass inlet tube. The shade of this area gives an indication of the comparability of the exposure and processing technique among the pictures. The somewhat parabolic profile of the methyl bromide filling the plug is due to the geometric effect of the cylindrical cross-section of the plug. Had a plug with a rectangular cross-section been used, the parabolic effect would not be present. The times given under each picture are the times after the beginning of the run.

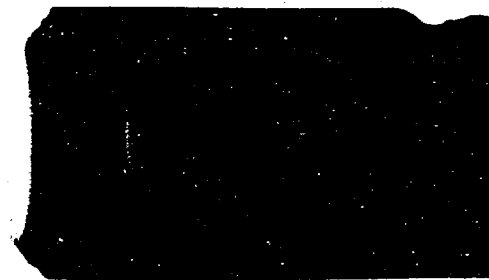
Only one desorption run was made. This was run 12. No flow data was taken, however concentration profiles were measured. These data are given in Table 26 of the Appendix on Original Data Tabulation and are shown in Figure 24. This run was made by equilibrating the plug with methyl bromide at 613.1 mm. Hg. Evacuation of the plug from both ends was started at time zero. As can be seen, the end effect observed in runs 6 and 7 is again evident. The symmetry of the profiles about the center of the plug indicates that the



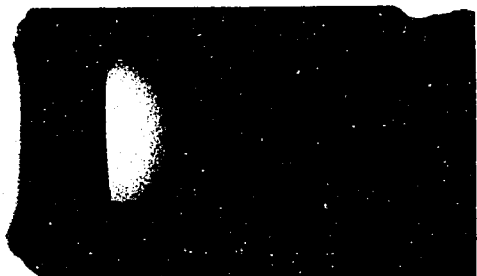
T = 0 sec.



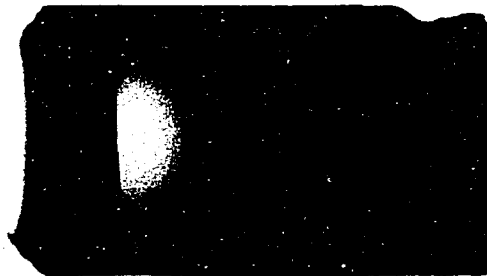
T = 10 sec.



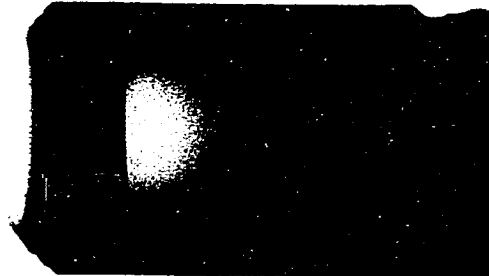
T = 2 min.



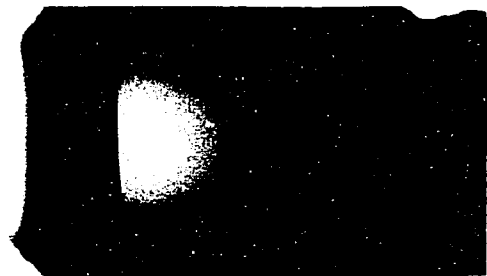
T = 10 min.



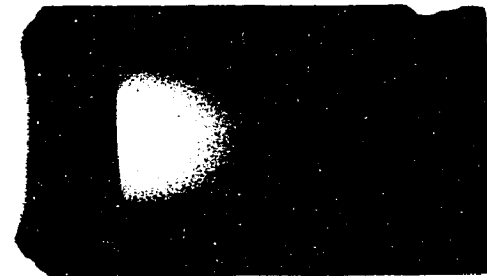
T = 20 min.



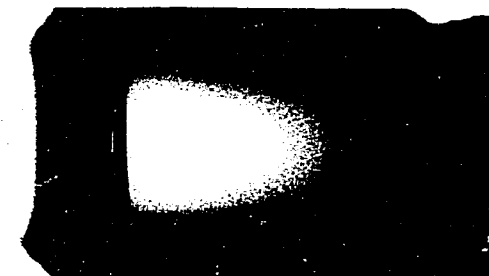
T = 30 min.



T = 40 min.



T = 1 hr.



T = 5 hrs.

Fig. 23. Radiographs of run 13 concentration profile development.

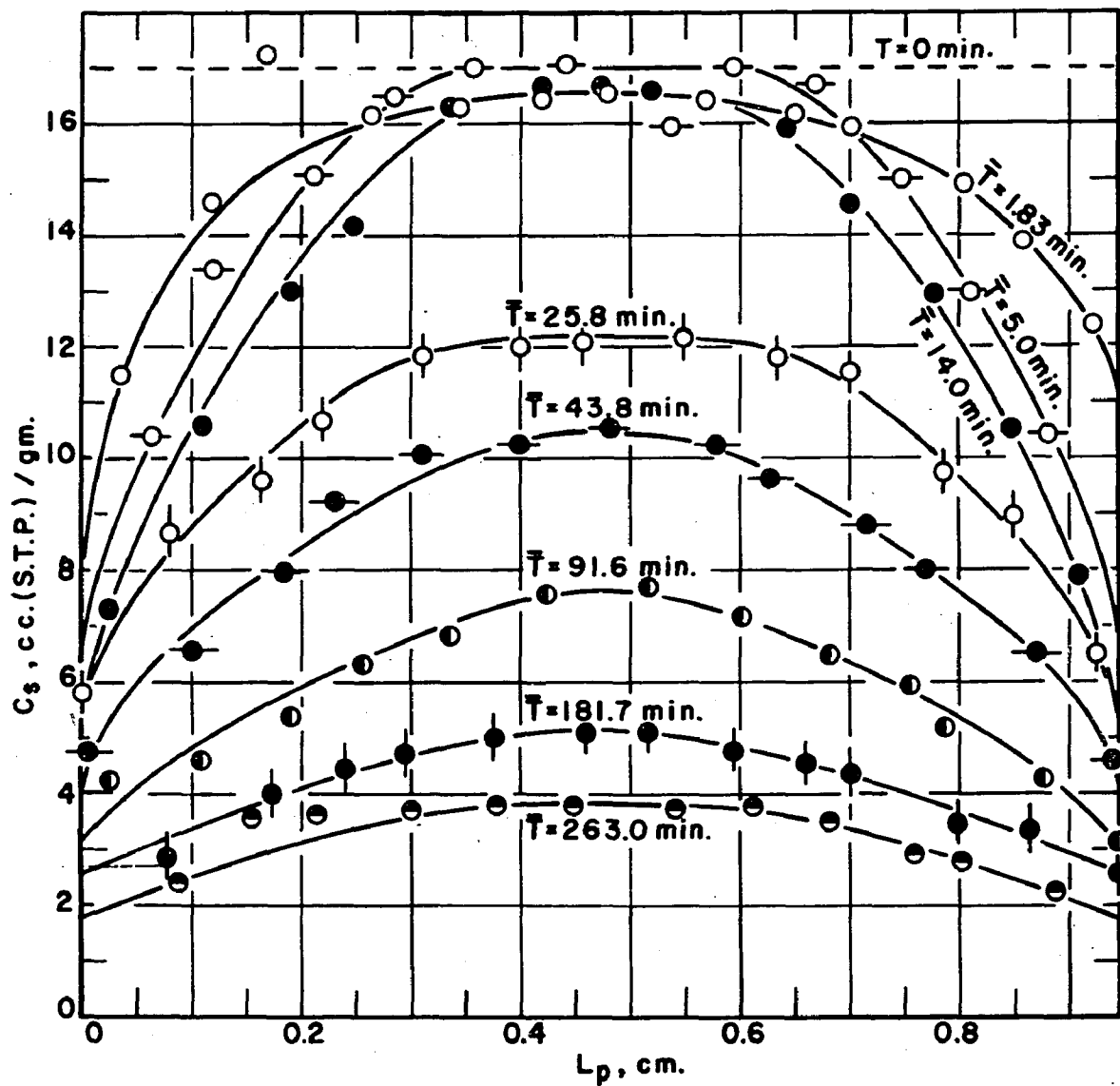


Fig. 24. Run 12 desorption concentration profiles.

end effect is not peculiar to the normally exit end. The times indicated on Figure 24 are the average times after time zero when the profiles were measured.

As can be noted on Figure 24, the first scan at an average time of 1.83 minutes is not symmetrical. This was due to the rapid flow rate combined with the relatively slow step scan. The scan started at 0.55 minutes at the exit end ($L_p = 0.945$ cm.) and ended at 3.10 minutes at the inlet end ($L_p = 0$ cm.). The crossing over of the scan at $t = 1.83$ minutes and $t = 5.0$ minutes was apparently due to the previously mentioned error encountered at high concentrations.

During runs 6, 7, and 13 the exit pressure was maintained by evacuation with the vacuum pumps. The exit pressure was measured using a McLeod gauge. These pressures are given in Table 18 of the Appendix on Original Data Tabulation.

CHAPTER VI

DISCUSSION OF RESULTS

Adsorption isotherm

To aid in the study of the transport of adsorbable gases through porous materials, it is desirable to measure and interpret the adsorption isotherm for the system under study. This has been done for the system methyl bromide-porous Vycor glass, used in this investigation. The measurements were made on the actual plug as it was actually used in the flow studies of this research. The method of determination of the isotherm, which employed the x-ray system for interpolating between the measured isotherm points, has been given previously. The isotherm obtained is given in Figure 10.

This adsorption isotherm data were fitted to the linear form of the B.E.T. equation (51):

$$\frac{(P/P^0)}{C_s(1-(P/P_0))} = \frac{(C-1)(P/P^0)}{CC_m} + \frac{1}{CC_m} \quad (12)$$

where P^0 = vapor pressure of pure material, mm.Hg

C = empirical constant, dimensionless

C_m = monolayer volume, cc.(S.T.P.)/gm.

The plot of equation 12 is shown in Figure 25. The equation for the straight line portion (approximately up to 350 mm.Hg) is

$$C_s = \frac{455 (P/P^0)}{(1-(P/P^0))(1-38.4(P/P^0))} \quad (13)$$

This gives the constant $C = 39.4$ and the monolayer capacity for methyl bromide of 11.55 cc. (S.T.P.)/gm. at 40°C.

The molecular area of methyl bromide, 23.1 \AA^2 , was calculated using the close packing formula given by Emmett and Brunauer (53) and the liquid density at 40°C. This calculation is given in the Appendix on Calculated Quantities. The specific surface area of the Vycor plug can then be estimated from this molecular area and the monolayer capacity:

$$S_s = C_m A_m N / V_0 \quad (14)$$

where A_m = molecular area of CH_3Br

N = Avogadro's number

V_0 = volume of gm.-mole at S.T.P.

The surface area calculated from equation 14 was $71.7 \text{ m.}^2/\text{gm.}$

The surface area per gm. can also be estimated from the helium permeability. The method and calculations are given in the Appendix on Calculated Quantities. The area based on the helium permeability was $121 \text{ m.}^2/\text{gm.}$

All of these areas are compared to the nitrogen-B.E.T. area in Table 4. Also included in Table 4 are the data of Yates and co-workers (10) for CH_3Br and N_2 , the monolayer

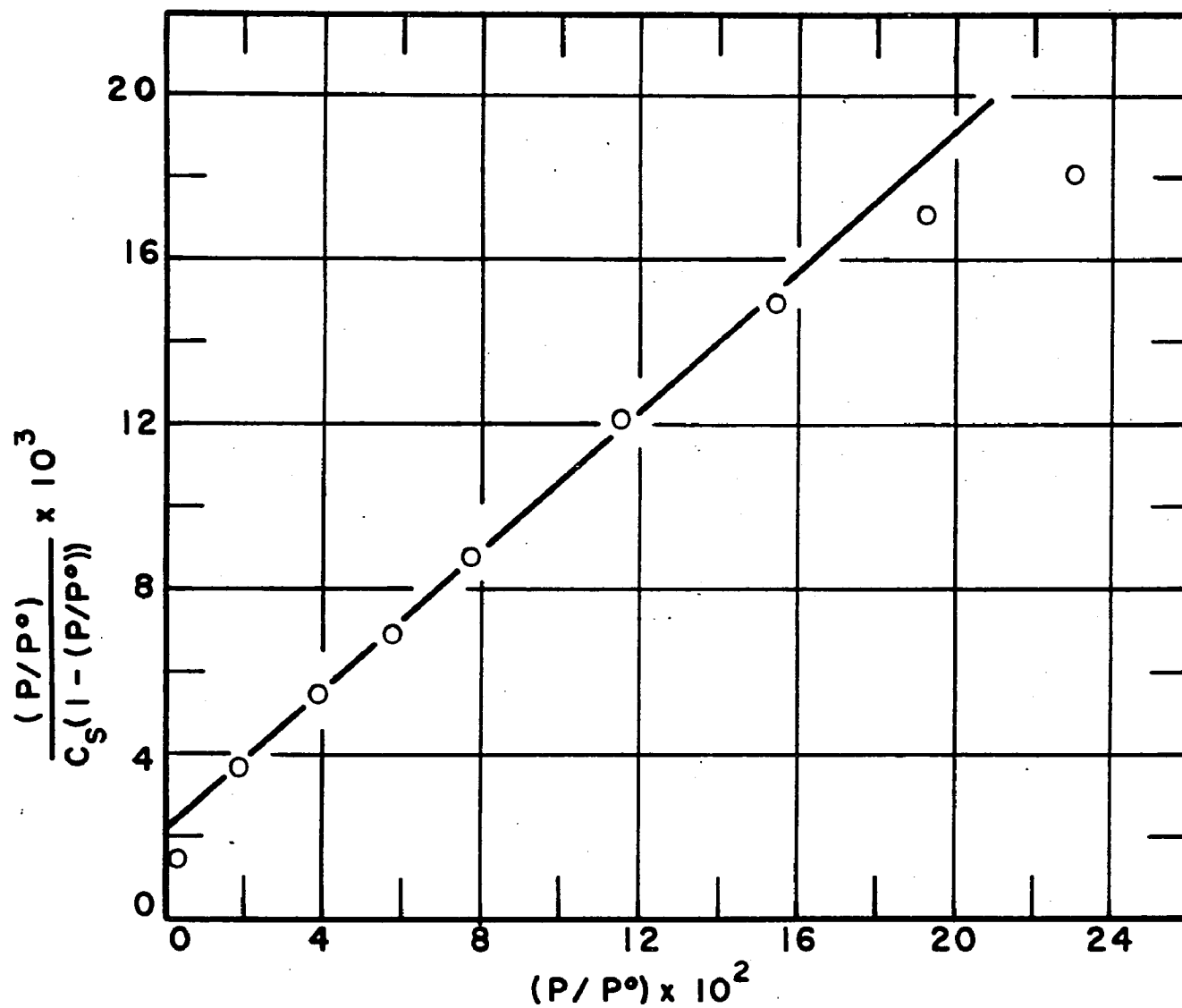


Fig. 25. B.E.T. plot for CH_3Br on porous Vycor at 40°C .

capacities, and parallel pore model average radii. The calculation of the average pore radius is also given in the Appendix on Calculated Quantities.

TABLE 4
SPECIFIC SURFACE AREAS

Source	T °K	S_s m. ² /gm.	\bar{r} Å	C_m cc.(S.T.P.)/gm.
N ₂ - B.E.T.	79	192	21.8	---
CH ₃ Br - B.E.T.	313	72	--	11.55
He Permeability	313	122	34.2	---
Yates and Co-workers (10);				
N ₂ - B.E.T.	79	180	--	43.5
CH ₃ Br - B.E.T.	273	145	--	24.5 ^a

^a Based on $A_m = 22.1 \text{Å}^2$ at 0°C.

The difference between the B.E.T. surface area and the surface area calculated from the helium permeability can probably be attributed to the assumption of a tortuosity factor of 2.56, given by Barrer and Barrie (9), for the calculation of \bar{r} and hence S_s . If the tortuosity factor for the porous Vycor glass used in this study were 2.04, the B.E.T. and the permeability surface areas would be the same. Calculation of this tortuosity is given in the Appendix on Calculated Quantities. Similar calculations of the tortuosity factors from the data of Russell (37), Engel (38), and Rutz (52) give values of 2.3, 2.42-2.55, and 1.91

respectively. Hence the value of k seems to become smaller as the B.E.T. surface area increases and the average pore radius decreases.

Another possible explanation for the discrepancy in the surface areas by the two methods is that there are dead end pores which do not contribute to the He steady state permeability. However, as will be discussed later in this chapter, the unsteady state CH_3Br concentration profile data predicts reasonably well the steady state CH_3Br flow rate. This seems to negate the idea of blind pores.

Resolution of the difference in surface areas by the two methods must await closer study of the pore size distribution and more accurate measurement of the N_2 - B.E.T. surface area.

The difference between the CH_3Br -B.E.T. and the N_2 - B.E.T. surface areas is quite striking. This difference would seem to indicate that not all of the surface area available to nitrogen is available for CH_3Br . Again further study of porous Vycor is necessary to explain these differences.

There is also a wide discrepancy between the monolayer CH_3Br coverage reported by Yates and co-workers (10) and that found in this study. A measurement of the CH_3Br -Vycor adsorption isotherm in a conventional adsorption apparatus is needed to resolve this difference.

Helium permeability

The measurement of the flow rate of helium through the porous Vycor plug was used to establish the adequacy of the flow measuring equipment and the applicability of the Knudsen type flow equation for describing the flow of relatively non-adsorbable gases through the porous Vycor used in this investigation. This is shown clearly in Figure 11 by the nondependence of the helium permeabilities on the pressure level over the pressure range used in this study. The helium permeabilities are comparable to those found by other investigators (9,37,38,53) for porous Vycor. The helium permeability measurements were spaced throughout the experimental study as a check on any possible effect of methyl bromide on the porous Vycor. Hence runs H-1 through H-4 were made before any methyl bromide was used, run H-5 was made after methyl bromide runs 1 through 5, and run H-6 was made after methyl bromide run 12.

The Knudsen relationship has been generally found to apply when the molecular mean free path is approximately ten times the average pore diameter. This condition validates the Knudsen equation basic assumption that the flow is governed by the wall collisions with a negligible number of intermolecular collisions.

The mean free paths for helium and methyl bromide for the maximum pressure used in this study (615 mm.Hg) are 3,580 and 541 ⁰Å respectively (see the Appendix on Calculated

Quantities for calculation of these figures). The ratio of the minimum mean free path to the average pore diameter (by N₂-B.E.T. method $\bar{d} = 43.6\text{\AA}$) was 82.0 and 12.4 for helium and methyl bromide respectively. Hence the applicability of the Knudsen flow mechanism was anticipated.

The Knudsen equation for flow in porous media can be written as:

$$N'_K = \frac{8}{3} \frac{n\pi \bar{r}^3}{\sqrt{2} \pi R T M} \left(\frac{2-f}{f} \right) \frac{dP}{k^2 a L} \quad (15)$$

where N'_K = flow in g-mole/sec.

n = number of pores in the parallel pore model

\bar{r} = average pore radius, cm.

R = gas constant, joules/g.mole-°K.

T = temperature, °K.

M = molecular weight

f = fraction of molecules diffusely reflected

k = tortuosity factor

P = pressure, dynes./cm.

L = distance along plug axis, cm.

The other assumptions for deriving the Knudsen equation are cosine law wall reflections (i.e., the molecules leave the wall in a direction independent of their incident direction but with an equal probability for all directions), a slowly varying density or pressure gradient axially along the pore

such that a two term Taylor series approximation is applicable, and no radial density or pressure gradient. The added assumptions for obtaining equation 15 from the original Knudsen equation (54) for use on porous material are the assumptions of a parallel pore model and the use of a tortuosity factor to include all effects not included in the derivation such as the tortuous path.

Equation 15 is useful for predicting the Knudsen flow of another gas from the experimentally measured flow of one gas through the same porous plug. Thus the flow of methyl bromide by the Knudsen mechanism can be predicted using equation 15 in the form

$$\frac{(N_K)_{\text{CH}_3\text{Br}}}{(N_K)_{\text{He}}} = \sqrt{\frac{M_{\text{He}}}{M_{\text{CH}_3\text{Br}}}} \quad (16)$$

for the same plug at the same temperature. Or, as shown by equation 15 and used by Russell (13), the modified permeability, $P'_g \sqrt{MT}$ should be constant for all gases in the same plug. P'_g is the permeability or flow rate per unit area per unit pressure drop multiplied by the plug length.

Methyl bromide permeabilities

As shown in Figure 12, the experimental permeabilities for methyl bromide were 2-4 times as high as predicted from the experimental helium data. An excess flow (over the predicted Knudsen flow) for adsorbable gases has been

observed by many previous investigators as indicated in the Related Literature Chapter. Thus an anticipated excess flow was experimentally observed. This measured excess flow is much greater than could possibly be attributed to experimental error. This excess flow has generally been attributed to some surface transport process.

In order to show the nature of the transport observed in this study, let us first consider the porous plug as a "blackbox," then treat the flow data as proposed in previous investigations, and finally consider the transport in the light of the concentration profiles actually measured experimentally.

Black box treatment

In a black box type treatment, only the external pressure difference and flow rate are known. By analogy with other transport processes, let us consider the flow to be proportional to the pressure difference. A plot of flow versus pressure difference should yield a straight line. Such a plot of the data for methyl bromide flow through Vycor is shown in Figure 26. The investigators of previous studies on Vycor glass pointed out similar correlations. The ranges of their data and the over-all diffusion coefficients are given in Table 5. These diffusion coefficients are reasonably consistent for each gas considering that different Vycor plugs and pressure ranges were used. It is

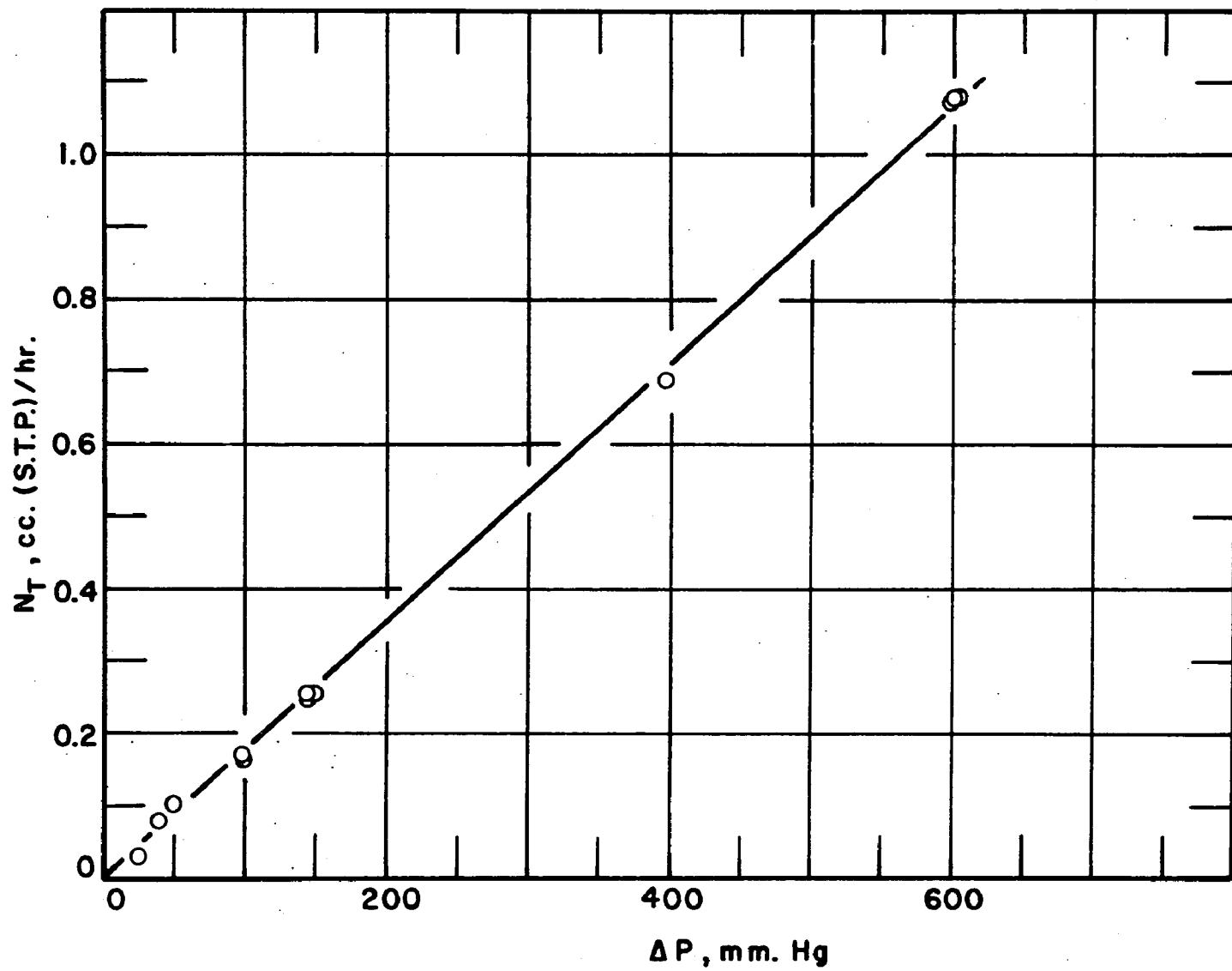


Fig. 26. Total flow versus pressure difference.

TABLE 5
DATA FOR BLACK BOX TYPE CORRELATIONS

Investigator	Gas	T, °C	\bar{P} range mm.Hg	ΔP range mm.Hg	$D_T \times 10^4$ cm. ² /sec.
Russell (13)	C ₂ H ₄	0	16 -740.3	6.6 -723.0	7.80
		25	11.1-744.0	6.1 - 83.3	7.81
		40	12.6-739.9	8.6 - 87.0	7.24
	C ₃ H ₆	0	9.9-747.2	3.1 -171.1	10.05
		25	12.9-726.1	4.95- 68.7	8.37
		40	14.0-733.4	9.15- 77.6	8.35
	i-C ₄ H ₁₀	25	12.8-758.6	7.55- 76.3	7.86
		40	9.6-741.7	6.7 - 89.6	6.92
	Engel (55)	C ₂ H ₄	25	212.0-737.7	56.0 -167.4
40			235.0-631.0	112.0 -200.0	7.96
C ₃ H ₆		25	132.2-590.8	55.5 -217.5	7.89
		40	246.7-620.5	76.5 -176.5	7.34
Rutz (52)	CH ₄	25	1,393-6,660	320.6 -539.8	6.61
	C ₂ H ₄	25	1,181-6,640	232.7 -532.7	6.20
	C ₃ H ₆	25	1,167-5,000	227.3 -418.9	6.34
	C ₃ H ₈	40	1,098-7,860	315.4 -465.4	5.80
This study	CH ₃ Br	40	30.6-601.1	25.4 -602.6	10.00

interesting to note that for any one gas the diffusion coefficients decrease with increasing temperature. This is the reverse of the effect of temperature on either Knudsen or molecular diffusion coefficients and suggests that some process other than gas phase transport is occurring.

One exception to the pressure drop correlations for Vycor glass was the data on i-C₄H₁₀ at 0°C given by Russell (13). However, these measurements were under conditions where capillary condensation was occurring. Hence the lack of correlation is not surprising.

The black box type treatment correlates the data within about $\pm 15\%$. These correlations are useful for interpolation for the particular solid over the range of experimental measurements for porous Vycor. However, similar correlations have not been found for other porous materials by other investigators. Therefore, this sort of treatment, though interesting, has not been considered significant from a theoretical standpoint and interpretation of its meaning must await a better understanding of the transport processes occurring.

Literature correlations

Now let us consider the approach taken by many previous investigators. In order to study the surface transport process by measuring total flow rates through porous materials, some assumption by which the total flow could be separated into gas and surface phase components had to be made. The usual method was to assume no net flux interchange between the gas and surface phases. The gas phase flux was then calculated by assuming a linear pressure gradient and using the Knudsen mechanism with some correction for the blockage of the pore by the adsorbed phase. This gas phase flux was then subtracted from the measured total flux and the excess was attributed to some surface transport process. Hence, with this approach, the surface concentration profile was fixed by assuming adsorption equilibrium at each point.

This separation of fluxes was generally justified by showing that the predicted gas phase flux was small compared with the total flux and hence any net flux interchange would have had a negligible effect.

For the system used in this investigation, the predicted gas phase flux amounted to a maximum of about 50% and was generally about 25%. Hence the utility of the previously presented division of fluxes is certainly questionable.

However, let us apply these methods to the flow data measured in this study. First the gas phase flow by the Knudsen mechanism must be estimated.

Since there is pore blockage by the CH_3Br in the adsorbed phase, the permeability obtained from the helium flow data must be modified to $B P_g' \sqrt{MT}$. Let us use the blockage factor, B , proposed by Russell (13):

$$B = \left[1 - \left(\frac{\rho_{\text{app}} M C_S}{22,400 \rho_L \epsilon} \right) \right]^{3/2} \quad (4)$$

where ρ_L = density of the adsorbed phase

ϵ = porosity of Vycor plug

This blockage factor was derived by Russell (13) based on the fact that Knudsen flow is proportional to r^3 . To evaluate B , the density of the adsorbed phase was assumed to be that of the CH_3Br liquid and the arithmetic average concentrations C_S , was used. The value, 1.618 gm./cc., for ρ_L was obtained

by extrapolating the density data for CH_3Br , given by Dreisbach (56), to 40°C .

By subtracting the partially blocked gas flow from the total measured flow, the excess flow attributed to surface transport was obtained. A sample of these calculations is given in the Appendix on Calculated Quantities and summarized in Table 5.

Up to this point, most previous theories are similar. However, in the treatment of the excess or surface flow, three possibilities (as discussed in the Related Literature Chapter) have been proposed. The simplest is that of a surface diffusion coefficient as expressed by equation 1:

$$N_s = - D_s \frac{dC_s^I}{dL} \quad (1)$$

Since N_s is considered to be independent of L ,

$$D_s = N_s (\Delta L / \Delta C_s^I) \quad (17)$$

The calculated values of D_s are given in Table 6 and plotted as a function of \bar{C}_s in Figure 27. The non-linear shape of the curve rules out a constant D_s . However, since relatively large values of ΔP were used, the curve does not give the true dependence of D_s on \bar{C}_s . The maximum exhibited by this plot does occur in the region of a monolayer coverage based on the CH_3Br isotherm. A maximum in the $D_s(\bar{C}_s)$ curve in the monolayer region has been found in most previous studies reported in the literature (12). Generally the maximum is

TABLE 6

SUMMARY OF DIFFUSION COEFFICIENT CALCULATIONS BASED ON OVER-ALL FLOW DATA

Run No.	$N_T \times 10^2$ cc.(STP) hr.	$N_K \times 10^2$ cc.(STP) hr.	B	$N_{KB} \times 10^2$ cc.(STP) hr.	$N_g \times 10^2$ cc.(STP) hr.	ΔC_g cc.(STP) gm.	$D_g \times 10^5$ cm ² /sec.	\bar{C}_g cc.(STP) gm.
1	7.96	1.96	0.925	1.81	6.15	2.5	2.28	4.05
2	16.60	4.88	0.873	4.26	12.34	3.4	3.37	6.92
3	24.70	7.39	0.822	6.08	18.62	2.1	8.24	9.75
4	25.80	7.22	0.784	5.66	20.14	2.1	8.89	11.95
5	25.90	7.33	0.732	5.37	20.53	3.5	5.44	14.95
6	108.10	30.10	0.848	25.50	82.60	16.6	4.62	8.3
7	107.90	29.90	0.848	25.40	82.50	16.5	4.64	8.25
8	2.86	1.25	0.704	0.88	1.98	0.8	2.30	16.60
9	10.20	2.48	0.710	1.76	8.44	1.5	5.21	16.25
10	16.30	5.03	0.722	3.63	12.67	2.8	4.19	15.60
11	68.90	19.90	0.759	15.11	53.79	7.2	6.94	13.40
13	107.50	29.90	0.849	25.40	82.10	16.5	4.62	8.25

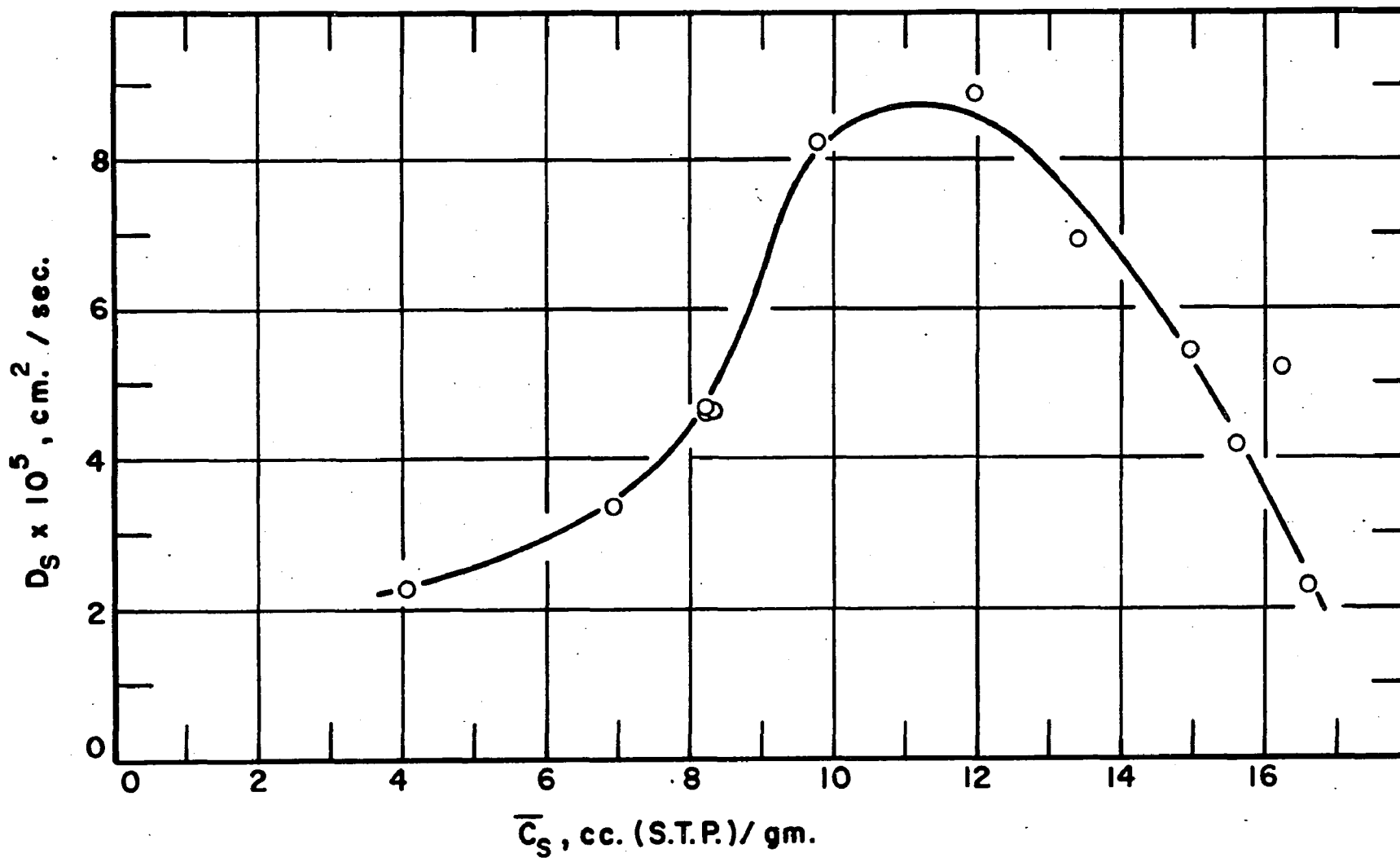


Fig. 27. D_S versus \bar{C}_S based on CH Br permeability runs.

not as pronounced; however, Haul and Peerbooms (24) did find a very large maximum in $D_S(\bar{C}_S)$ for the system N_2 - Spheron 6 (2700°) at 77.4 and 90.2°K. They also found that the activation energy increased with coverage. They explained the maximum in D_S as possibly being due to a corresponding increase in the activation entropy since calculations showed the ΔS of adsorption had a distinct minimum in the vicinity of a monolayer. However, they felt that the idea of activated diffusion was not applicable above a monolayer. The utility of a surface diffusion coefficient which varies so non-linearly with concentration is thus very questionable.

The second proposed way to describe surface transport is the Babbitt-Gilliland, Baddour, and Russell hydrodynamical approach. This employs a spreading pressure driving force and leads to equation 2, as presented in the Related Literature Chapter.

$$J_S = \frac{RT \rho_{app}}{22,400k^2 C_R S_S L_p} \int_{P_0}^{P_1} \left(C_S^2/P \right) dP \quad (2)$$

Hence a plot of J_S or N_S versus $\int (C_S^2/P)dP$ should yield a straight line passing through the origin. Values of C_S^2/P for methyl bromide were plotted and the integral was evaluated graphically. The values of the integrals thus obtained are given in Table 7 and plotted versus N_S in Figure 28. The correlation is quite good despite the low ratio of surface to gas phase flow components. The resistance coefficient, C_R ,

TABLE 7

DATA FOR TESTING THEORETICAL EQUATIONS BASED ON MEASURED FLOWS

Run No.	$N_S \times 10^{+2}$ $\frac{\text{cc. (STP)}}{\text{hr.}}$	$\int_{P_1}^{P_0} (C_S^2/P) dP$ $\left(\frac{\text{cc. (STP)}}{\text{gm.}} \right)^2$	$\frac{\Delta P}{\Delta L}$ $\frac{\text{mm. Hg}}{\text{cm.}}$	$N_S / (\Delta P / \Delta L)$ $\frac{\text{cc. (STP) - cm.}}{\text{mm. Hg}}$	$[1.637 C_S P \frac{dC_S}{dP} + C_S^2]$ $\left(\frac{\text{cc. (STP)}}{\text{gm.}} \right)^2$
1	6.15	25.0	41.6	0.1480	29.9
2	12.34	53.2	103.3	0.1193	82.9
3	18.62	65.7	156.3	0.1191	146.8
4	20.14	54.2	152.9	0.1315	245.6
5	20.53	60.1	155.0	0.1322	560.0
6	82.60	252.6	638.0	0.1295	157.8
7	82.50	251.7	634.0	0.1302	157.5
8	1.98	11.6	26.9	0.0736	901.0
9	8.44	20.1	52.7	0.1600	817.0
10	12.67	40.6	106.3	0.1190	663.0
11	53.79	156.6	422.0	0.1274	343.4
13	82.10	251.6	632.0	0.1299	157.1

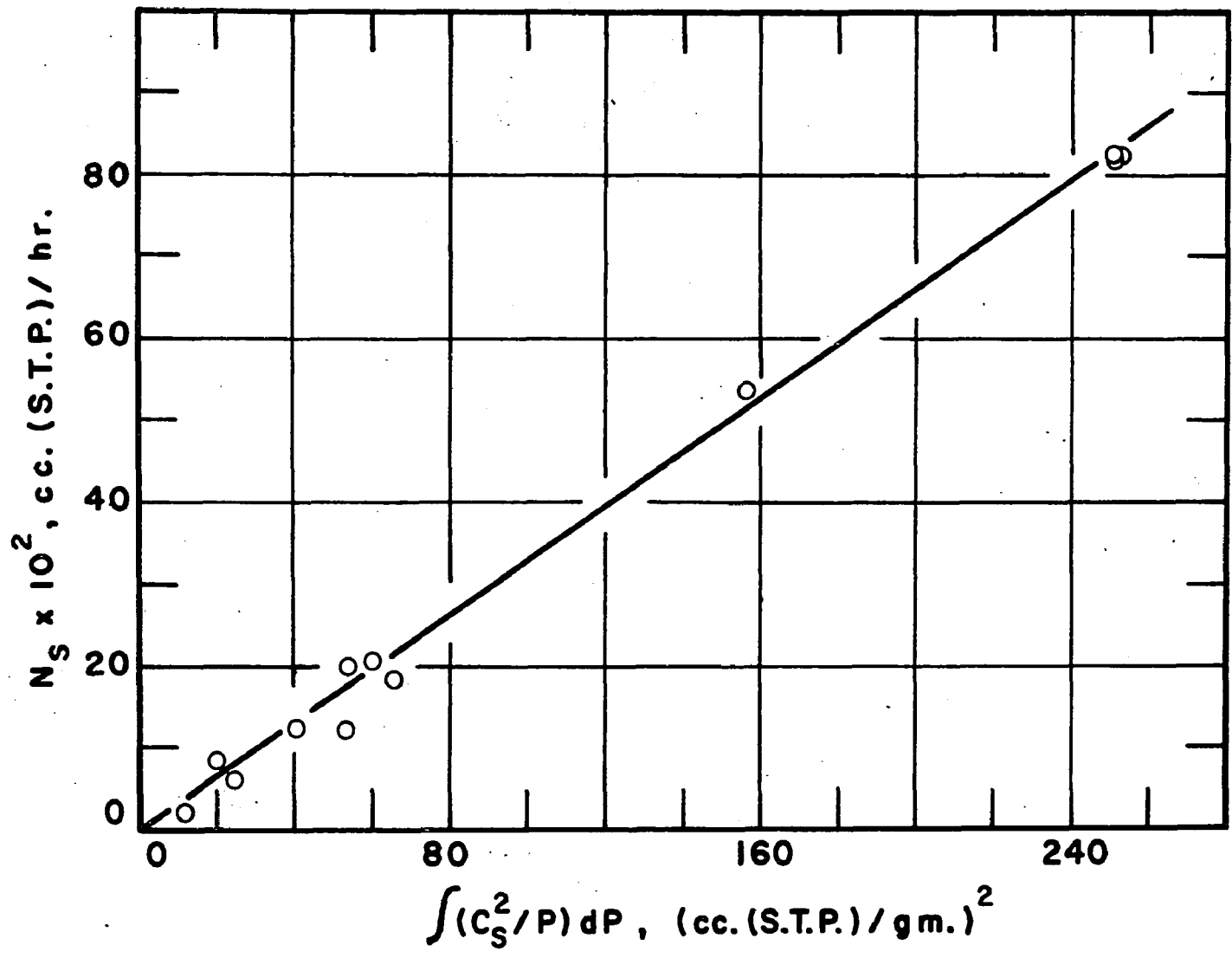


Fig. 28. N_S versus $\int (C_S^2/P) dP$.

was calculated from the slope of the curve, using $S_s = 192 \text{ m}^2/\text{gm.}$, and assuming $k = 2.56$. C_R was found to be $0.6 \times 10^5 \text{ gm./sec.-cm.}^2$ For hydrocarbons, Gilliland and co-workers (37,38) found C_R values in the range $0.65 - 1.43 \times 10^5 \text{ gm./sec.-cm.}^2$

It is interesting to note the good correlation for Vycor found by Gilliland and co-workers (37,38) and this author contrasted with the poor correlation cited by Barrer and co-workers (43) for carbon and by Metzner and Smith (32) for Alumina. This apparently good correlation seems only applicable to Vycor. More will be said about this correlation later in this discussion.

The third proposed method for describing surface transport is that by Metzner and Smith (32). Their derivation is based on a surface concentration driving force as discussed in the Related Literature Chapter. As they point out, their theory is only applicable to surface concentrations less than a unimolecular layer. Their final equation is:

$$N_s = -K_M [1.637C_sP(dC_s/dP) + C_s^2]dP/dL \quad (18)$$

where $K_M =$ empirical dimensional constant

Hence a plot of $N_s/(dP/dL)$ versus $[1.637C_sP(dC_s/dP) - C_s^2]$ should give a straight line passing through the origin.

This correlating function is given in Table 7 and plotted against $N_s/(dP/dL)$ in Figure 29. Only runs 1, 2, and 3 were below a monolayer coverage where equation 18 was proposed to

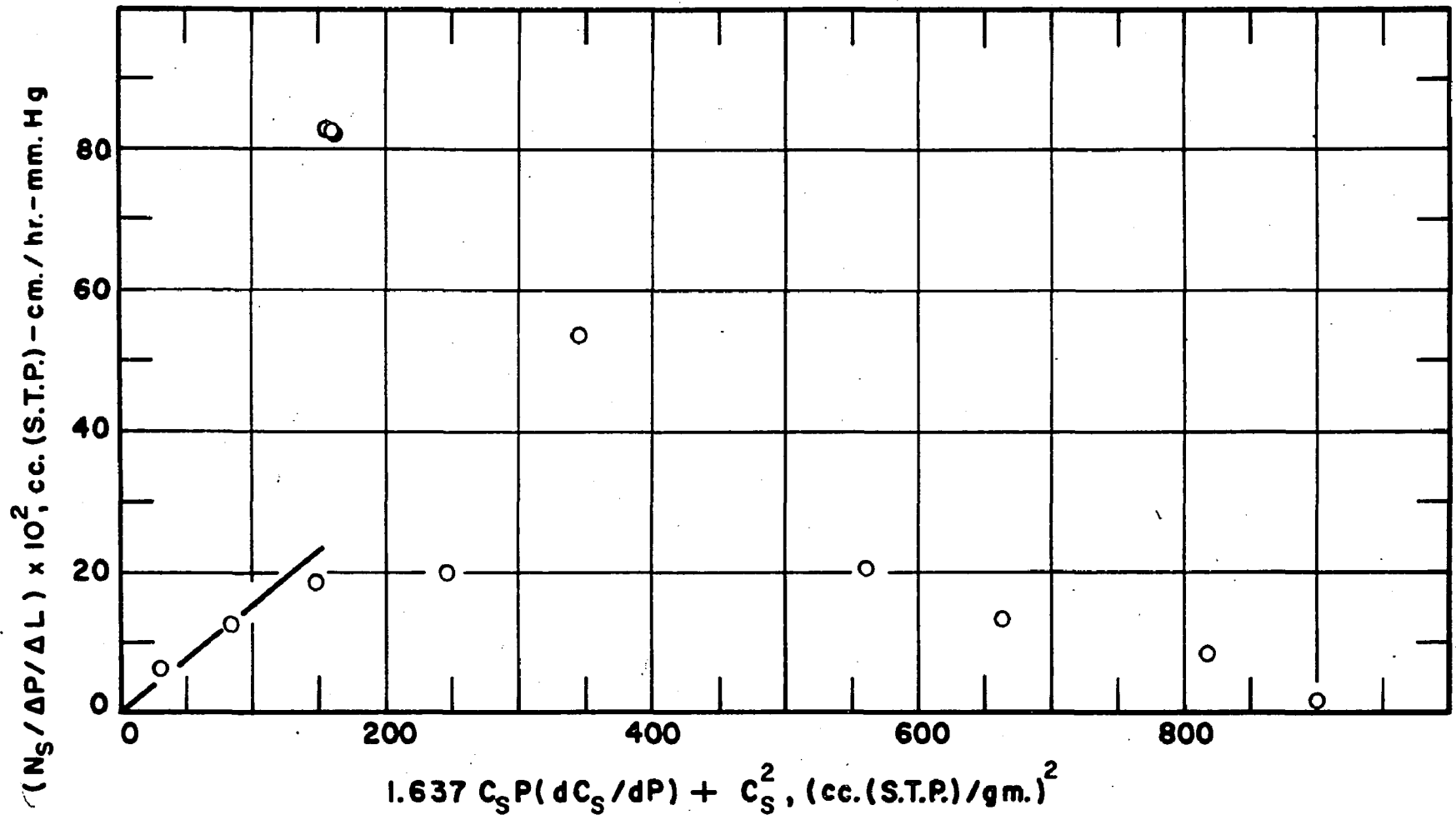


Fig. 29. Metzner and Smith type plot.

be applicable. These three points do give a correlating line with a slope in the right direction which tends toward zero; however, the correlation is not as good as it appears on the small scale in Figure 29. Further discussion of this correlation will be given later in this chapter.

Steady state concentration profiles

In this study, an attempt was made to get a better picture of the actual transport process for adsorbable gases in microporous media by measuring the concentration profiles within the porous material rather than to rely on deductions from external measurements. These internal concentration profiles were measured simultaneously with the flow measurements by x-ray absorption. The profiles during the steady state period of the methyl bromide flow runs are shown in Figures 14 through 20. The gas phase pressure profiles were calculated from the measured surface concentrations by assuming equilibrium at all points. To the author's knowledge, this is the first time such internal concentration profiles have ever been measured.

In Figures 30 and 31, the concentration profiles based on the previous assumptions of a straight line pressure gradient and equilibrium at each point are compared with the experimentally measured profiles for run 1 and for runs 6 and 7 respectively. As shown in these figures, the gas phase pressure profile, in addition to the surface phase

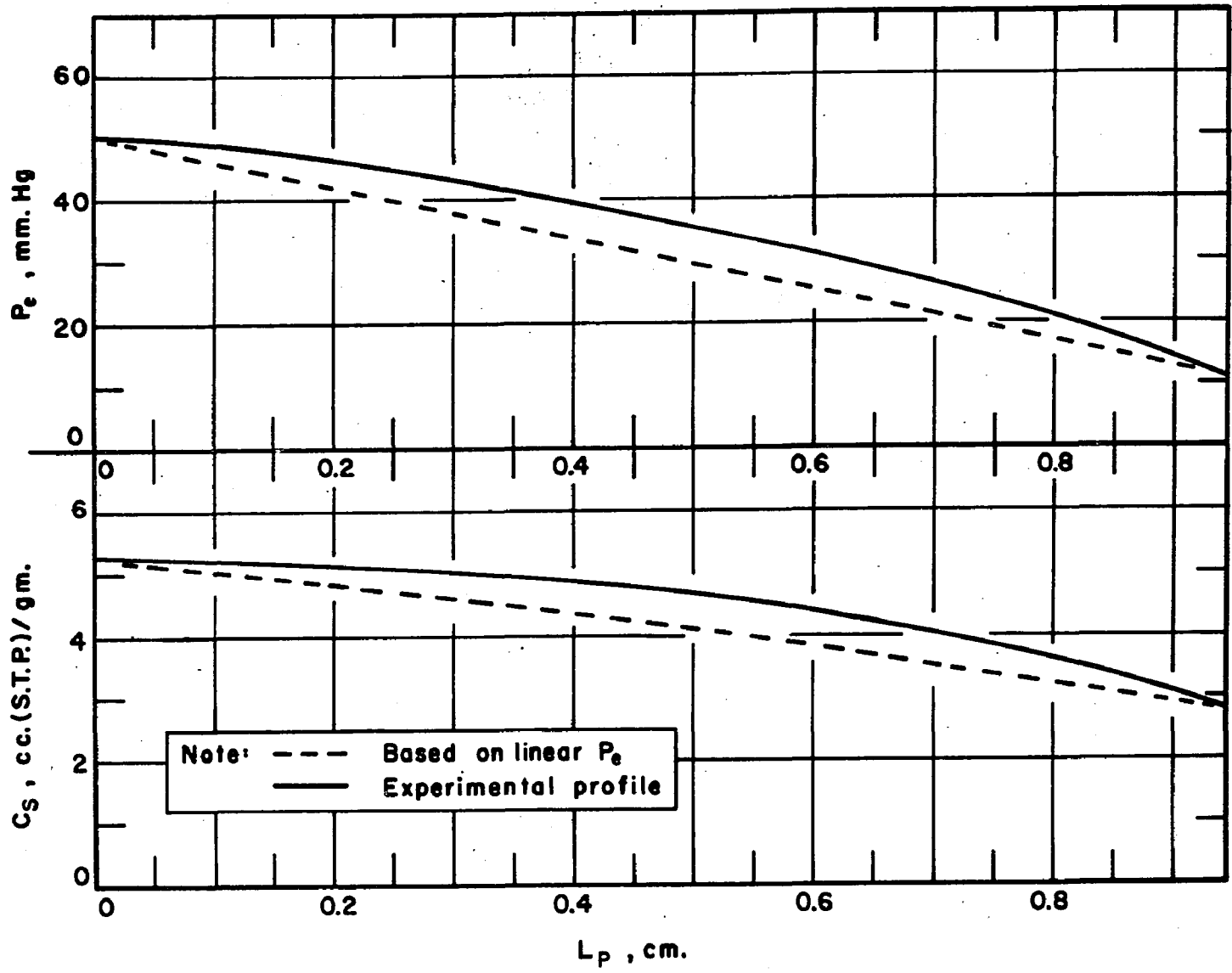


Fig. 30. Comparison of experimental with assumed concentration profiles for run 1.

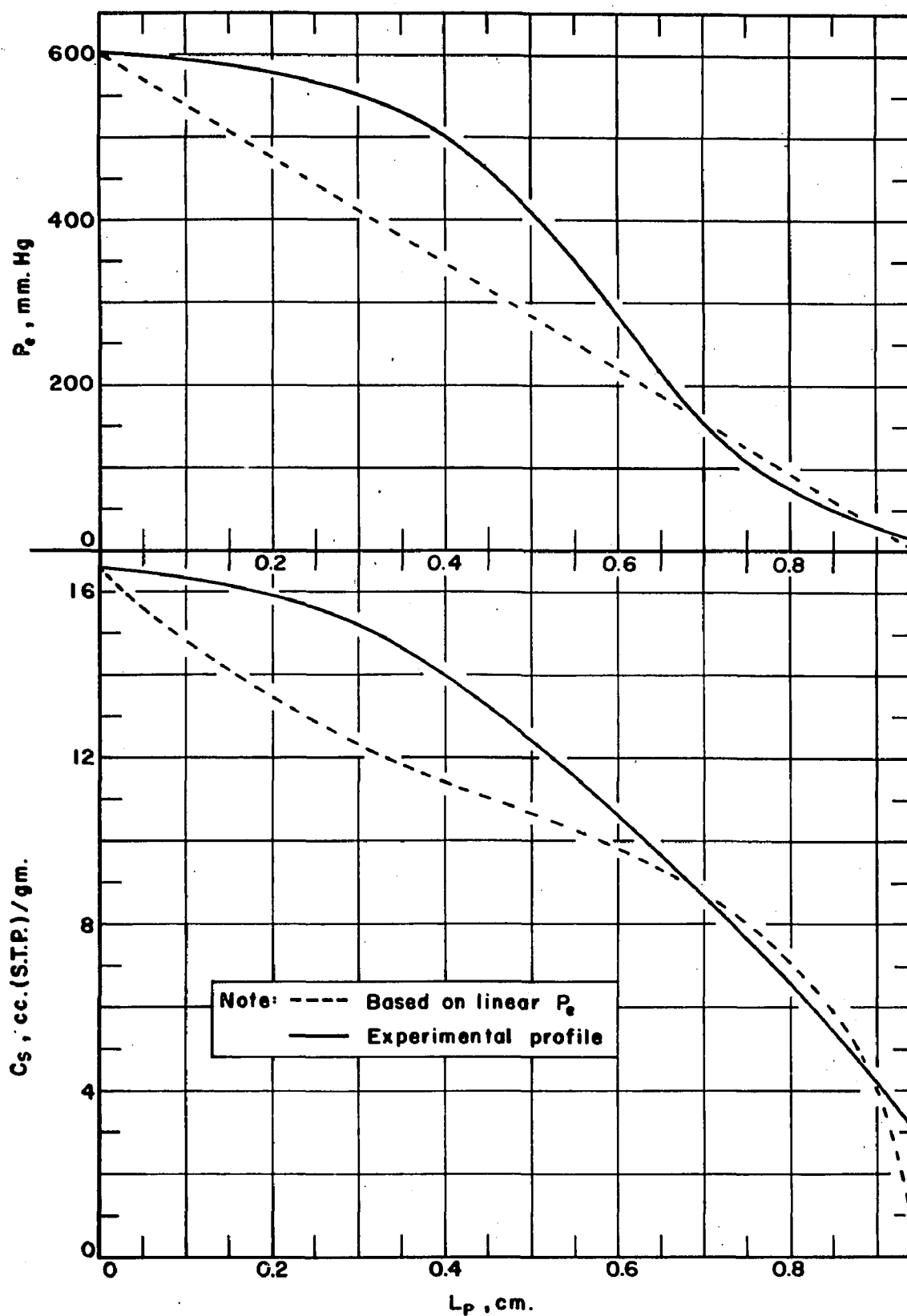


Fig. 31. Comparison of experimental with assumed concentration profiles for runs 6 and 7.

concentration profile, is non-linear. This fact seems to indicate some net surface phase-gas phase flux interchange, even with small pressure differences, unless the mathematical relationships describing these fluxes are similarly non-linear. If there is flux interchange, a material balance on the gas phase and surface phase would yield the following respective equations.

$$-\frac{\partial J_g}{\partial L} + \frac{2}{r} Q(L) = \frac{22,400}{RT} \frac{\partial P}{\partial t} \quad (19)$$

$$-\frac{\partial J_s}{\partial L} - \frac{2}{r} Q(L) = \frac{2}{22.4S_s r} \frac{\partial C_s}{\partial t} \quad (20)$$

where $Q(L)$ = flux interchange between the adsorbed and gas phase in cc.(S.T.P.)/sec.-cm² (surface area)

The flux interchange term cannot be evaluated with the experimental information available at this time.

The steady state concentration profiles can be employed to make a more critical test of the transport equations proposed in previous studies based on the differential rather than the integral form of these equations. The differential forms of equations 1, 3, and 18 combined with equations 2 and 4 with Knudsen type gas phase flow are

$$J_T = \frac{-22.4 B P_g' \sqrt{MT}}{3600 \sqrt{MT}} \frac{dP_e}{dL} - D_s P_{app} \frac{dC_s}{dL} \quad (21)$$

$$J_T = \frac{-22.4 B P_g' \sqrt{MT}}{3600 \sqrt{MT}} \frac{dP_e}{dL} - \frac{RT \rho_{app}}{22,400 k^2 C_R S_S} \frac{C_S^2}{P_e} \frac{dP_e}{dL} \quad (22)$$

$$J_T = \frac{-22.4 B P_g' \sqrt{MT}}{3600 \sqrt{MT}} \frac{dP_e}{dL} - K_M [1.637 C_S P_e (dC_S/dP_e) + C_S^2] dP_e/dL \quad (23)$$

since

$$J_T = \frac{-22.4 B P_g' \sqrt{MT}}{3600 \sqrt{MT}} dP_e/dL \quad (24)$$

Equations 21, 22, 23 can be rearranged to solve for the appropriate parameters D_S , $k^2 C_R S_S$, and K_M respectively.

$$D_S = \frac{J_T - J_g}{-\rho_{app} dC_S/dL} \quad (25)$$

$$k^2 C_R S_S = \left(\frac{-RT \rho_{app}}{22,400} \frac{C_S^2}{P_e} \frac{dP_e}{dL} \right) \left(\frac{1}{J_T - J_g} \right) \quad (26)$$

$$K_M = \frac{J_T - J_g}{-(1.637 C_S P_e (dC_S/dP_e) + C_S^2) dP_e/dL} \quad (27)$$

$k^2 C_R S_S$ should be constant over the entire range of C_S and K_M should be constant below C_m . From the steady state concentration profiles, the gas phase flux can be estimated as a function of axial position in the plug by using equation 24. The slopes dP_e/dL , dC_S/dL , and dC_S/dP_e were obtained from the concentration profiles using a mirror method. The calculated values are shown in Table 8 for runs 6 and 7. A sample calculation is given in the Appendix on Calculated Quantities.

TABLE 8

DATA FOR TESTING THEORETICAL EQUATIONS BASED ON EXPERIMENTAL PROFILES FOR RUNS 6 AND 7

L_p	C_s	P_e	$-\frac{dC_s}{dL}$	$-\frac{dP_e}{dL}$	$\frac{dC_s}{dP_e}$	B	$J_g \times 10^4$	$k^2 C_R S_s \times 10^{-11}$	$K_M \times 10^8$	$D_s \times 10^5$
0.1	16.3	594.5	3.0	111	0.0357	0.709	0.252	1.17	7.68	16.40
0.2	15.9	582.5	5.2	203	0.0323	0.716	0.465	2.14	5.98	9.33
0.3	15.2	557.0	10.3	378	0.0276	0.728	0.880	4.06	2.84	4.36
0.4	14.0	505.0	13.7	685	0.0205	0.748	1.638	7.77	1.93	2.89
0.5	12.4	416.0	16.9	1,140	0.0152	0.776	2.830	15.62	1.40	1.86
0.6	10.6	287.5	19.3	1,571	0.0127	0.807	4.030	30.90	1.20	1.19
0.7	8.7	152.0	20.0	1,107	0.0193	0.841	2.980	21.10	3.37	1.52
0.8	6.6	80.5	21.5	576	0.0354	0.878	1.620	9.10	13.38	1.85
0.9	4.2	31.0	25.7	404	0.0650	0.921	1.190	6.23	48.60	1.67

As shown in Table 8, $k^2 C_R S_S$ is certainly not a constant as the Gilliland and co-workers (37) theory requires. Hence the seemingly good correlation of their equation for the over-all flow data obtained in this study (Figure 28) does not stand up under a more critical test. Similarly the theoretically constant K_M in the Metzner and Smith theory is not constant even for values of C_S less than C_M .

This same calculation approach can be used to obtain the phenomenological coefficients appearing in the equation derived by Barrer (41) by irreversible thermodynamics. Such tests indicate non-constant coefficients and hence seem to refute the proposed equation.

The surface diffusion coefficient, evaluated using equation 25, is also included in Table 8. The surface diffusion coefficients for run 11 were calculated in the same manner. These calculations are summarized in Table 9. D_S is plotted as a function of C_S in Figure 32. The difference between D_S values of runs 6 and 7 from those of run 11 at the values of C_S above 14 cc. (S.T.P.)/gm. is attributed to the inaccuracy of the x-ray measurement at high concentrations coupled with the fact that D_S is changing so rapidly in this range. The curve was drawn through the runs 6 and 7 points since this duplication of profile measurements increased their accuracy. The curve was extrapolated to zero as shown by the dashed line.

TABLE 9

 D_s VALUES FROM THE CONCENTRATION PROFILE OF RUN 11

L_p	C_s	P_e	$-\frac{dC_s}{dL}$	$-\frac{dP_e}{dL}$	B	$J_g \times 10^4$	$D_s \times 10^5$
0.1	16.9	610	2.9	29	0.7000	0.065	11.25
0.2	16.6	603	4.9	124	0.705	0.280	6.20
0.3	16.0	588	5.8	187	0.713	0.426	5.09
0.4	15.4	562	8.2	384	0.725	0.890	3.22
0.5	14.4	520	9.3	455	0.741	1.079	2.69
0.6	13.6	473	10.3	540	0.756	1.309	2.28
0.7	12.5	411	10.3	666	0.774	1.651	2.05
0.8	11.5	335	10.3	766	0.792	1.942	1.85
0.9	10.4	253	12.0	889	0.810	2.300	1.38

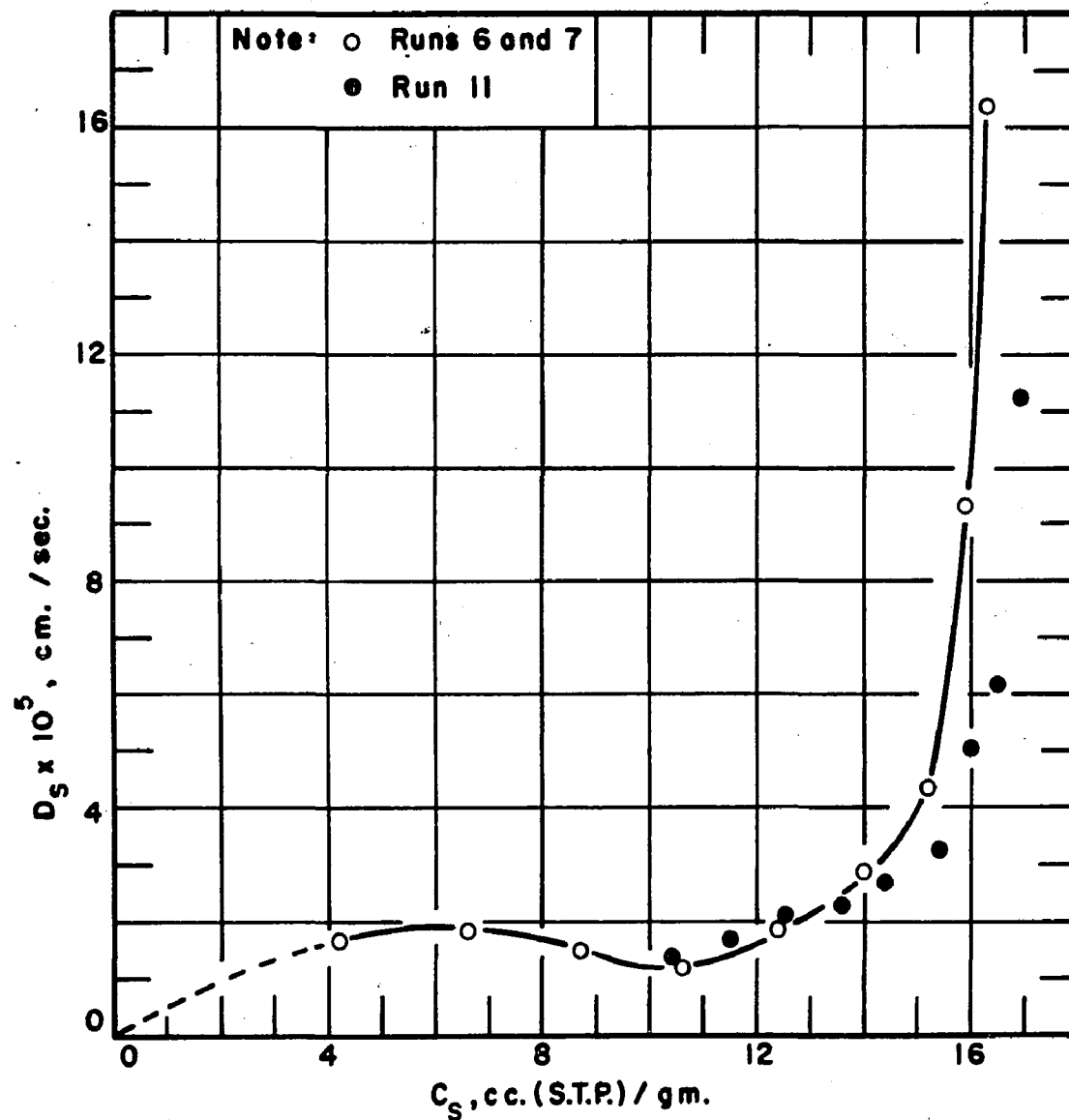


Fig. 32. D_S based on steady state profiles.

The rapid increase in D_S above monolayer coverage (11.5 cc. (S.T.P.)/gm.) may indicate that the mobility in the multilayer region is much higher than in the monolayer region.

If one compares Figures 27 and 32, there appears to be a considerable difference between a D_S evaluated from the external measurements and a D_S evaluated from internal plus flow measurements. A minor part of this difference is due to the use of relatively large ΔC_S values in the flow runs. Even if D_S from internal measurements were averaged over the corresponding ΔC_S intervals, there would still be a large difference. Actually, the two ways of calculating D_S are basically different. The D_S evaluated from external measurements requires a linear dP/dL , constant J_g , no flux interchange and hence a constant J_S , a linear surface concentration profile, some average blockage factor, and no end effect at the exit end. The D_S evaluated from internal and flow measurements requires only that the gas phase flux be described by the Knudsen mechanism, some sort of blockage, and adsorption equilibrium at all points. The fact that the two sets of D_S values are different merely reflects the differences in the assumptions required in their calculation. The most important differences are due to the fact that dC_S/dL continually increases and dP_e/dL passes through a maximum for the experimental profile D_S calculations. The steady state pressure gradient, dP_e/dL , would have been

constant if there were no flux interchange as assumed in the calculation of the D_S from the external steady state measurements. Hence this non-constant gradient indicates considerable flux interchange. The shape of the curve of Figure 32 more closely resembles the $D_S(C_S)$ curves found in most investigations (12).

The primary assumptions which still must be made to evaluate D_S , even with experimentally measured concentration profiles, are some sort of a blockage factor of the gas phase flux by the adsorbed layer, adsorption equilibrium, and some assumption regarding the mechanism of the gas phase flux. The assumption of Knudsen type flow in the gas phase seems somewhat questionable when pores of 20-30^oÅ radius are involved. The usual assumption requires a relatively dense adsorbed layer with a vapor space, at the equilibrium pressure, above it. This idea of such a sharp boundary may be acceptable when large pores are involved, but in pores of 20-30 Å radius, it seems rather unrealistic. If the boundary were not sharp, gas phase intermolecular collisions could occur and the Knudsen mechanism for the gas phase transport would not be valid. Hence when the Knudsen mechanism is used to evaluate the possible flow through a porous plug, the measured excess flow may or may not be entirely on the surface.

End effect

An important new phenomenon was shown experimentally in runs 6 and 7. Some sort of an end effect does exist at the exit side of the plug when the downstream pressure is maintained at essentially zero. This effect, which was duplicated, is shown clearly in Figures 21 and 22. The surface phase concentration measured near the end of the plug corresponds to an equilibrium pressure of about 15 mm.Hg while the measured outlet pressure was 8 microns. Hence there is a tremendous concentration gradient or a desorption barrier at the exit end. As the unsteady state profiles show, the methyl bromide seems to flow into the plug as a slanted front moving from inlet to exit until the leading edge reaches the end of the plug. Then the methyl bromide seems to pile up from exit to inlet as if some barrier or additional resistance had been added at the exit end. This apparent end effect was only observed for runs where the downstream pressure was essentially zero. This end effect was not found at higher downstream pressures although the sensitivity of the x-ray measuring system was not sufficient to show that it did not exist. Also, it should be pointed out that at the end of the plug there must be a balancing of the rates of adsorbed layer flow and desorption. Hence, in the higher downstream pressure runs, the adsorbed layer flow may not have been high enough to show the end effect.

In light of the end effect observed in this study, care

must be exercised in interpreting adsorbable gas flow studies in other porous materials where the exit pressure is very low.

There are at least three possible explanations for the end effect observed. One is that there is an external back pressure at the exit end due to flow through the exit tubing. This exit tube was 6 mm. and 10 mm. glass tubing. If the Knudsen long tube formula (33) is used to calculate the minimum flow which could occur with the exit equilibrium pressure of 15 mm.Hg and the pressure 0.008 mm.Hg measured approximately 250 cm. downstream, the minimum flow is 100 times the actual steady state flow rate. This calculation is given in the Appendix on Calculated Quantities. Hence an external back pressure seems highly unlikely.

Another possible explanation was offered in the discussion by Barrer and Dacey (50) in 1958 as given in the Related Literature Chapter. They speculated that an end effect might occur due to the adsorbed material having to obtain the necessary energy to desorb at the end of the plug. This appears to be a possibility since the heat of adsorption is generally higher at low surface concentrations. The relation between heat of adsorption with surface coverage has not been measured for methyl bromide on Vycor.

One other possible explanation is that surface diffusion coefficients generally decrease with surface concentration. Hence if the idea of a diffusion coefficient with a concentration gradient driving force is applicable, a very

small diffusion coefficient at low concentrations would require a large concentration gradient to maintain a constant total flow rate.

Sufficient information to determine the actual cause of this end effect has not been obtained. This end effect was not peculiar to only one end of this one plug as shown by the desorption concentration profiles in Figure 24.

Unsteady state concentration profiles

The unsteady state concentration profiles were measured in flow runs 6 and 7 since only these runs had concentration differences which would give large enough x-ray absorptions for reasonably accurate unsteady state measurements. The profiles obtained are shown in Figures 21 and 22. As previously discussed, these profiles certainly add to the end effect picture.

The unsteady state profiles can also be used to estimate a concentration dependent diffusion coefficient. Crank (57) gives a number of solutions, for concentration dependent diffusion coefficients, to the unsteady state equation

$$\frac{\partial C_S}{\partial t} = \frac{\partial}{\partial L} \left(D_T \frac{\partial C_S}{\partial L} \right) \quad (28)$$

with the boundary conditions for a semi-infinite medium

$$C_S = C_0, \quad L = 0, \quad t > 0$$

$$C_S = 0, \quad L > 0, \quad t = 0$$

The solutions to equation 28 are given by Crank (57) as reduced plots of C_S/C_0 versus $L/(4D_T^0 t)^{1/2}$, where D_T^0 is the diffusion coefficient at $C_S = 0$. Since it is difficult to separate gas phase and surface phase components of the total flux, one might try to gain some idea of the nature of the transport by empirically determining the total diffusion coefficient, D_T , as a function of C_S using the solutions to equation 28 given by Crank (57). In order to do this, some value of D_T^0 must be chosen. One way to obtain a D_T^0 value is to determine D_T as a function of C_S from the steady state concentration profiles and extrapolate to $C_S = 0$. $(D_T)_{SS}$ can be evaluated by the equation 25 if J_g is omitted. A summary of such $(D_T)_{SS}$ values for runs 6 and 7 are plotted in Figure 33.

Extrapolation of $(D_T)_{SS}$ to $C_S = 0$ leads to a D_T^0 value of 1.6×10^{-5} cm²/sec. Using this value of D_T^0 , the reduced plot of C_S/C_0 versus $L/(4D_T^0 t)^{1/2}$, shown in Figure 34, was calculated from the unsteady state profiles of runs 6 and 7. Comparison of this plot with the plots given in Crank (57) pp. 268-274, indicates the form of D_T to be

$$D_T = D_T^0 / (1 - \alpha C_S/C_0) \quad (29)$$

where α is a constant

The reduced curves from Crank (57) Figure 12.12 with $1/(1 - \alpha) = 5$ and 10 are also shown in Figure 34. This

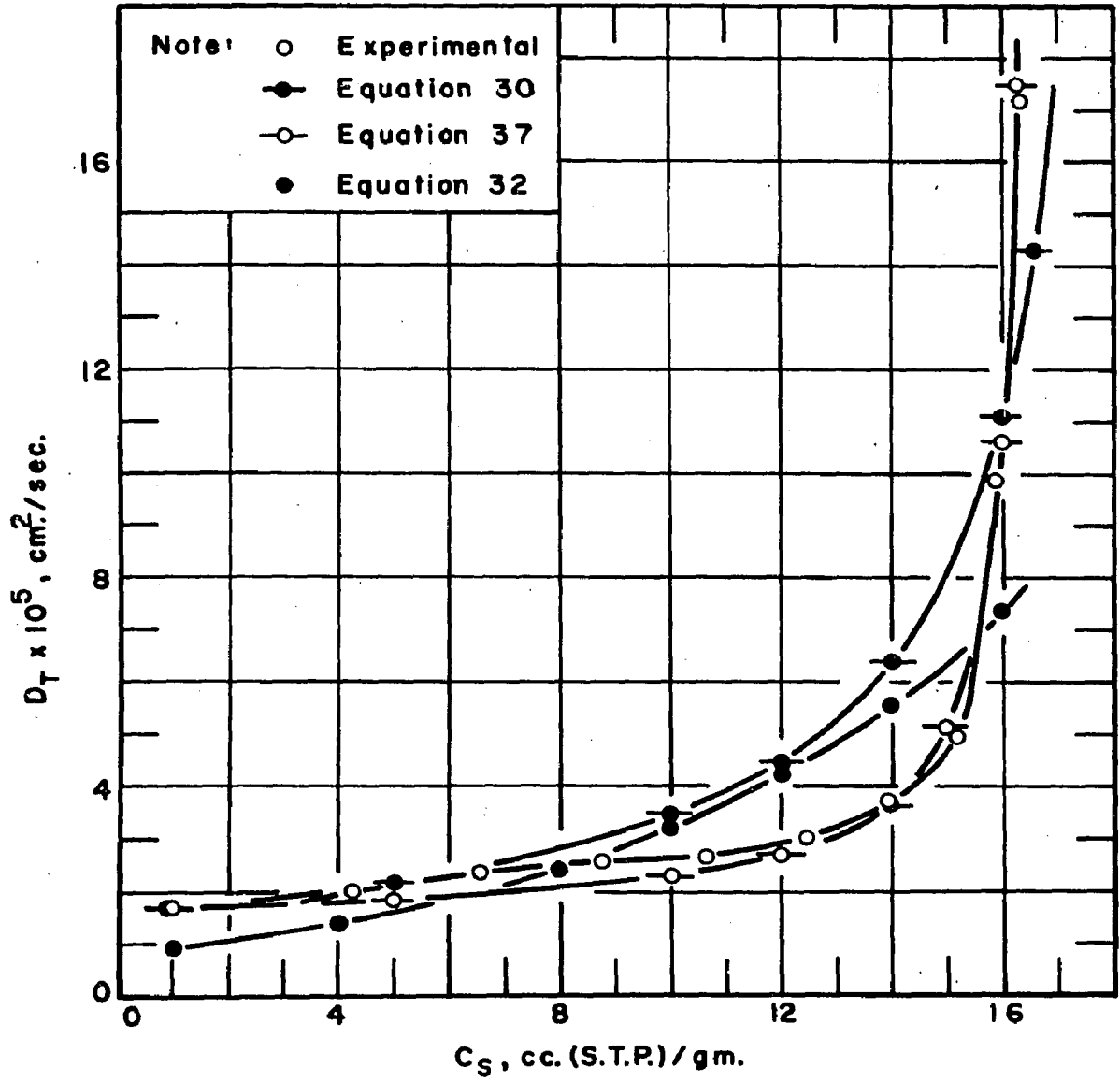


Fig. 33. D_T versus C_S .

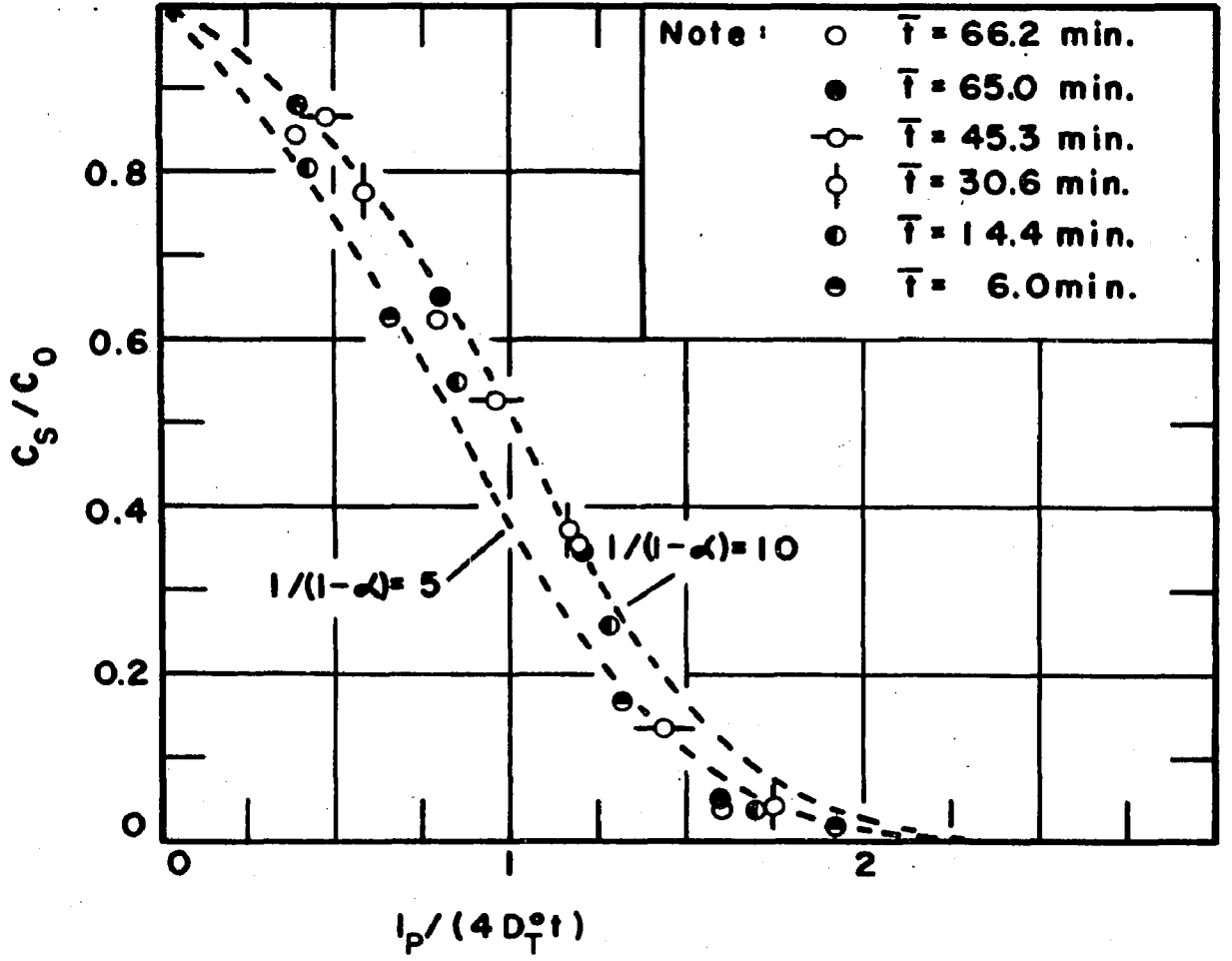


Fig. 34. Reduced unsteady state plot for D_T form A.

plot indicates that the value of $1/(1-\alpha)$ should be approximately 9. Thus the total diffusion coefficient would be

$$D_T = 1.6 \times 10^{-5} / (1 - 0.889 C_S/C_O) \quad (30)$$

Equation (30) is plotted in Figure 33 for comparison to $(D_T)_{SS}$. Let us designate the form of D_T of equation 30 as form A.

If the value of D_T^0 is arbitrarily taken as 0.8×10^{-5} cm²/sec., another reduced plot of C_S/C_O versus $1/(4D_T^0 t)^{1/2}$ can be prepared. This plot is shown in Figure 35. Again comparison with Crank's plots (57) indicate the form of D_T to be

$$D_T = D_T^0 e^{\alpha C_S/C_O} \quad (31)$$

where α is a constant

The reduced curve from Crank (57) Figure 12.9 with $e^{\alpha} = 10$ is also shown in Figure 35. Thus the total diffusion coefficient would be

$$D_T = 0.8 \times 10^{-5} e^{2.3 C_S/C_O} \quad (32)$$

Equation 32 is also plotted in Figure 33 for comparison.

Let us designate D_T of equation 30 as form B.

D_T for forms A and B can be used to estimate the steady state concentration profile by solving the steady state equation

$$\frac{d(D_T dC_S/dL)}{dL} = 0 \quad (33)$$

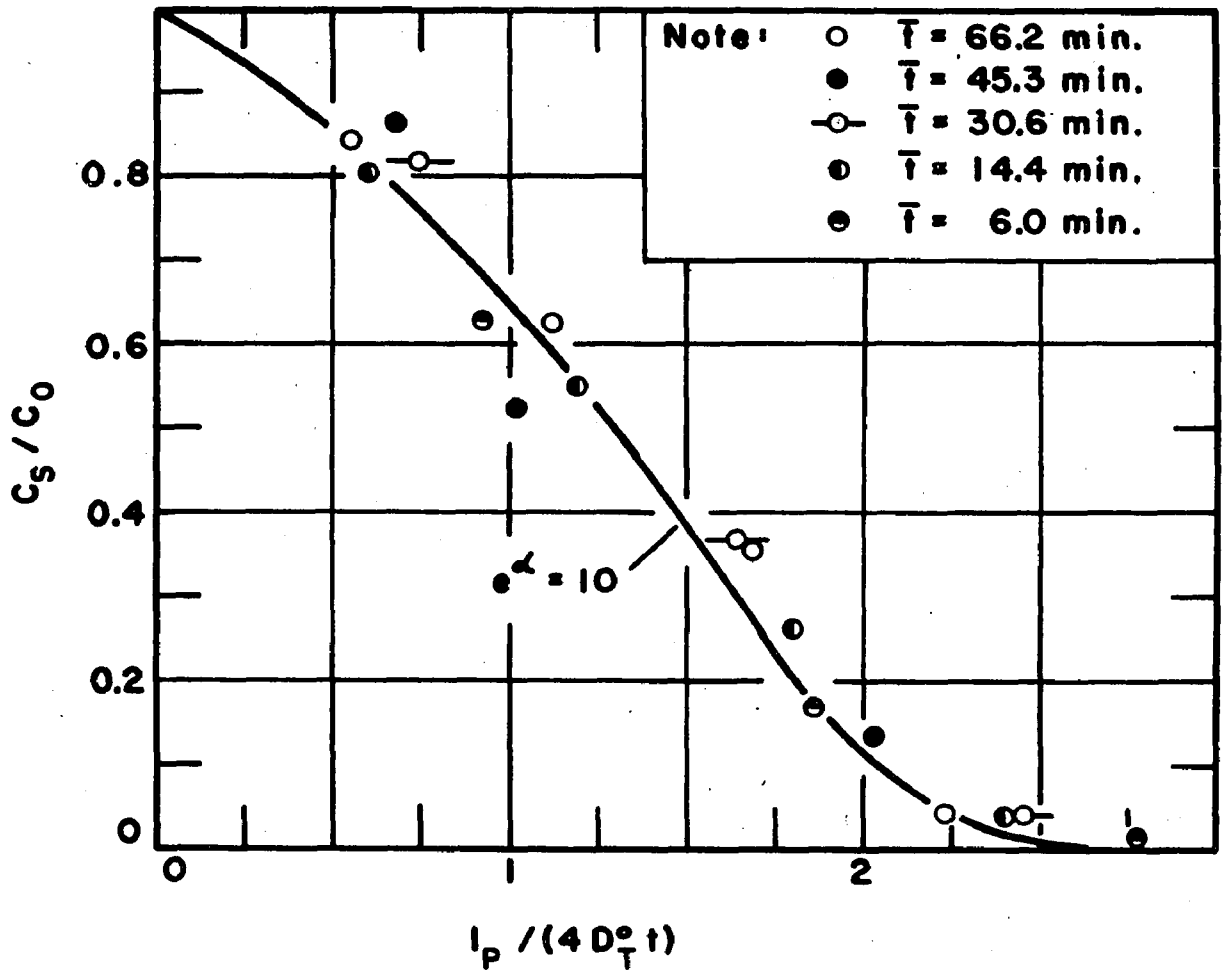


Fig. 35. Reduced unsteady state plot for D_T form A.

with the boundary conditions

$$C_S = C_0, \quad L = 0$$

$$C_S = C_L, \quad L = L_p$$

Equation 33 has been solved for both forms A and B as shown in the Appendix on Calculated Quantities. The equations for the steady state concentration profiles for D_T of forms A and B respectively are

$$C_S/C_0 = \frac{1-(1-\alpha) \left(\frac{1-\alpha}{1-\alpha C_L/C_0} \right)^{-L/L_p}}{\alpha} \quad (34)$$

$$C_S/C_0 = \frac{1}{\alpha} \ln \left\{ \frac{L}{L_p} (e^{\alpha C_L/C_0} - e^{\alpha}) + e^{\alpha} \right\} \quad (35)$$

Equations 34 and 35 were plotted in Figure 36 for the values of α previously given and $L_p = 0.945$ cm., $C_L = 3$ cc. (S.T.P.)/gm., and $C_0 = 16.6$ cc. (S.T.P.)/gm. The experimental steady state profile for runs 6 and 7 is also given in Figure 36 for comparison. Both forms of D_T give reasonable approximations to the steady state concentration profiles.

The two forms of D_T can be used to predict the steady state flow rate by solving the equation

$$N_T = \frac{3600 \rho_{app} A_p}{L_p} \int_{C_L}^{C_0} D_T dC_S \quad (36)$$

The solutions of equation 36 for the two forms of D_T are given in the Appendix on Calculated Quantities. D_T forms A and B given N_T values of 1.357 and 1.096 cc.(S.T.P.)/hr. respectively for runs 6 and 7. Hence form B estimates

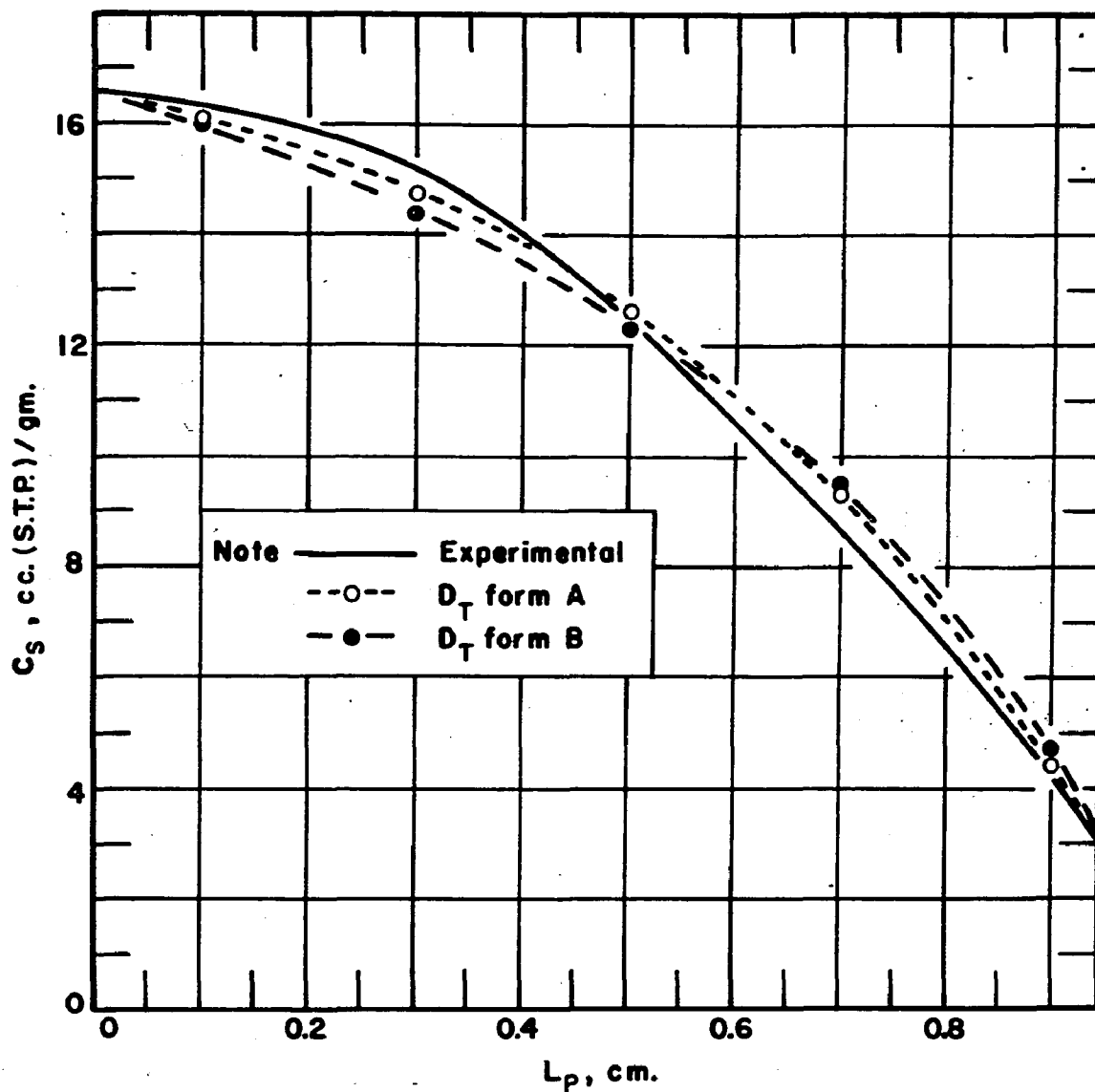


Fig. 36. Steady state profiles predicted from unsteady state profiles.

the steady state flow much closer to the measured value of 1.08 cc.(S.T.P.)/hr. for runs 6 and 7.

Inspection of $(D_T)_{ss}$ plot in Figure 33 suggested still another form of the D_T equation. This shape is similar to a translated hyperbola. The equation for a translated hyperbola (58) was fitted to $(D_T)_{ss}$ to give the equation (form C)

$$D_T = \left(\frac{1.3C_S - 28.18}{C_S - 16.7} \right) 10^{-5} \quad (37)$$

This equation is also plotted in Figure 33 for comparison with $(D_T)_{ss}$.

The general conclusion from this sort of mathematical treatment is that there are probably many such forms of D_T which will fit the data. The theoretical significance of any of these forms is not understood. It is of interest that the unsteady state data is consistent enough to give such reduced plots of C_S/C_0 and $L/(4D_T^0 t)^{1/2}$ and that these plots lead to diffusion coefficients which describe reasonably well the steady state data. This applicability of unsteady state data for predicting steady state data seems to indicate that the transient and steady state transport are very similar. Hence it appears that there is a negligible effect of blind or dead end pores which would be expected to effect only the transient measurements.

Time lag

The time lag of a flow system, as originally proposed by Daynes (59), was the time axis intercept of the extrapolation of the steady state portion of the exit pressure to zero pressure for a system having a constant downstream volume, an exit pressure much smaller than the inlet pressure, and having been subjected to a step-function inlet pressure at time zero. Clausing (29) and Knuyser (30) have interpreted t_L to be the average time required by a molecule to pass through a porous material under steady state two or three dimensional Knudsen conditions.

The time lag has been related to the total diffusion coefficient by solving the unsteady state flow equation 28 with suitable boundary conditions. For a constant total diffusion coefficient,

$$D_T = k^2 L_p^2 / 6t_L \quad (38)$$

where k is the tortuosity factor

Frisch (46) has solved equation 28 for any concentration dependent diffusion coefficient. His equation is

$$t_L = \frac{\int_0^{kL_p} LC_s dL}{\int_0^{c_0} D_T dC_s} \quad (39)$$

These integrals were evaluated graphically by plotting LC_s versus L and D_T versus C_s for the steady state data of runs 6 and 7. The resulting time lag was 129 minutes. From

equation 38, with $k^2 = 6.55$, (D_T) avg. was 12.5×10^{-5} cm²/sec. No direct experimental measurement of the time lag was made, hence no comparison between unsteady and steady state flows can be made on the basis of time lag.

Qualitative discussion of excess flow theory

The concentration profiles obtained in this study seem to indicate that for the system CH₃Br porous Vycor the basic assumptions of previously proposed theories of surface transport are not valid. The true nature of the excess flow is undoubtedly much more complicated than these simple theories can describe.

One of the questionable features of these theories is the approximation of the true density distribution within small pores as pointed out previously in this discussion. This approximation involves assuming a relatively dense layer at the surface in equilibrium with a gas phase of a radially uniform density corresponding to the equilibrium pressure. The real average density distribution is probably some relatively smooth transition from the relatively dense phase at the surface to a less dense phase near the center of the pore. In fact, it seems conceivable that the density near the center of the pore may not be the same as the density corresponding to isotherm equilibrium pressure if the pores are small enough that the molecules never effectively leave the influence of the surface. In such small pores with

heterogeneous walls, the ideas of density and pressure themselves, as normally used, become questionable. In light of these speculations, it might be better to consider the flow through very small micropores as single phase flow with a velocity profile due to the surface field.

Even if one accepts the density approximation, the assumption of the Knudsen equation to describe the gas phase transport seems questionable. As Field et al. (15) point out, the effect of the adsorbed layer on the type of molecular reflection (assumed to be cosine law reflection in the Knudsen equation) from the walls is unknown. The assumption of a linear axial density gradient in the Knudsen type derivation also seems shaky on the basis of the non-linear equilibrium pressure profiles calculated in this study. Hence if this density profile approximation is to be used, much work needs to be done on the effect of the adsorbed layer on the gas phase transport.

In line with accepting the density profile approximation, some means of describing the surface phase transport is needed. In order to describe this transport, much more information concerning the mobility of the adsorbed phase is required. All physically adsorbed molecules are probably mobile to some degree. It would be expected that the mobility would increase non-linearly as the surface concentration increased due to the heterogeneity of the surface,

the non-linear variation of surface forces with distance, and the adsorbed molecule interactions.

The other factor in describing the transport by a two phase scheme is the net flux interchange indicated by the non-linear surface concentration and equilibrium pressure profiles. However, this factor cannot be understood until the individual phase transports are more clearly understood.

CHAPTER VII

CONCLUSIONS

The following conclusions can be drawn from this study.

1. A system capable of measuring the steady and unsteady state flow rates of gases through and adsorbed gas concentration profiles within a porous solid plug has been built and its usefulness has been demonstrated by investigating the system CH_3Br and porous Vycor glass.

2. The adsorbed phase concentration profile as well as the pressure profile, calculated assuming adsorption equilibrium, are both non-linear for the system CH_3Br -porous Vycor.

3. If the system CH_3Br -porous Vycor is typical of adsorbable gas-microporous solid flow systems, the present theories presented in the literature do not describe the measured internal concentration profiles even though they do correlate flow data for limited ranges and systems.

4. Some kind of an end effect, which acts as a barrier to flow, can exist at the exit end of a porous media through which an adsorbable gas is flowing if the exit pressure is essentially zero.

5. The non-linear adsorbed phase concentration and gas phase equilibrium pressure profiles indicate gas phase-

surface phase net flux interchange for the system CH_3Br -Vycor when a two phase transport theory is employed.

6. Steady state flow of methyl bromide through porous Vycor is 2 to 4 times as large as predicted from the Knudsen flow mechanism.

7. The use of unsteady state concentration profiles to estimate the steady state concentration profile and flow rate indicates a minor effect of dead end or blind pores in porous Vycor.

CHAPTER VIII

RECOMMENDATIONS

It is recommended that the following information be obtained in order to gain a better understanding of the results of this study and more generally a better understanding of the transport of adsorbable gases through porous materials.

1. Measure the adsorption and desorption isotherms for the CH_3Br -porous Vycor system at several temperatures.

2. Determine the heat of adsorption as a function of surface coverage for the CH_3Br -porous Vycor system.

3. Measure the pore size distribution of the porous Vycor used in this study.

4. Study the mobility of CH_3Br on porous Vycor possibly by using a dynamic desorption system similar to that used by Lacksonen (11).

5. Study the reflection of molecules from a surface contaminated with an adsorbed layer, using a molecular beam approach.

6. Study more closely the end effect observed in this investigation.

7. Determine the effect of a non-adsorbable gas, such as helium, on the CH_3Br concentration profile in both co-current and countercurrent flow through porous Vycor.

8. Determine if there is an effect of a non-adsorbable gas, such as helium, on the CH_3Br transport.

9. Study other systems with uniform pore sizes such as saran carbon with halogenated hydrocarbons.

10. Improve the accuracy of the x-ray concentration profile measurements by installing suitable voltage stabilizers on the x-ray power line and replacing the variable capacitance x-ray scanner position indicator by a variable inductance coil type indicator.

11. Study the effect of pore size on adsorbable gas flow through porous Vycor glass of various average pore sizes.

APPENDIXES

APPENDIX A

NOMENCLATURE

A_m	molecular area, cm^2
A_p	cross-sectional area of porous plug, cm^2
A_R	cross-sectional area of reference detector pin hole, cm^2
A_s	cross-sectional area of sample detector pin hole, cm^2
B	blockage factor, ratio of Knudsen permeabilities with and without adsorbed phase
cc.	cubic centimeters
c.f.m.	cubic feet per minute
CPM	counts per minute
cm^2	square centimeters
C_m	monomolecular layer concentration, $\text{cc. (S.T.P.)}/\text{gm.}$
C_o	inlet surface phase concentration, $\text{cc. (S.T.P.)}/\text{gm.}$
C_R	coefficient of resistance, $\text{gm.}/\text{sec.}-\text{cm}^2$
C_s	concentration of adsorbed gas, $\text{cc. (S.T.P.)}/\text{gm.}$
C'_s	concentration of adsorbed gas, $\text{cc. (S.T.P.)}/\text{cc.}$
D_K	Knudsen mechanism diffusion coefficient, $\text{cm}^2/\text{sec.}$
D_p	diameter of porous plug, cm.
D_s	surface phase diffusion coefficient, $\text{cm}^2/\text{sec.}$

D_T^0	total diffusion coefficient at $C_S=0$, cm^2/sec .
D_T	total diffusion coefficient, cm^2/sec .
$(D_T)_{ss}$	steady state total diffusion coefficient, cm^2/sec .
\bar{d}	average pore diameter, cm.
F	attenuation factor defined by equation 9
f	fraction of molecules diffusely reflected
gm.	gram
gm.-mole	gram molecular weight
hr.	hour
I	x-ray intensity, CPM
I_0	incident x-ray intensity, CPM
I_R	reference x-ray beam intensity, CPM
I_S	sample x-ray beam intensity, CPM
I_{R0}	incident reference x-ray beam intensity, CPM
I_{S0}	incident sample x-ray beam intensity, CPM
I'_S	sample detector x-ray intensity reading with no methyl bromide present, CPM
$(I_R)_B$	same as I_R except at base conditions, CPM
$(I'_S)_B$	same as I'_S except at base conditions, CPM
ΔI	difference in x-ray beam intensities, CPM
$(\Delta I)_B$	same as ΔI except at base conditions, CPM
ΔI_R	difference in reference detector intensity readings, CPM
ΔI_S	difference in sample detector intensity readings, CPM

$\Delta(\Delta I)$	difference of difference in x-ray beam intensities, CPM
J_g	gas phase flux, cc.(S.T.P.)/cm ² -sec.
J_K	flux by Knudsen mechanism, cc.(S.T.P.)/cm ² -sec.
J'_K	flux by Knudsen mechanism, mg.-mole/cm ² -sec.
J_s	surface phase flux, cc.(S.T.P.)/cm ² -sec.
J_T	total flux, cc.(S.T.P.)/cm ² -sec.
K	a constant in x-ray data correlating equation, cc.(S.T.P.)/gm.
k	tortuosity factor
^o K	degrees Kelvin
K_M	empirical dimensional constant, cm./hr.-mm.Hg- (cc.(S.T.P.)) ²
K_1	a constant
KV	kilovolts
L	length, cm.
L_p	plug length, cm.
M	molecular weight
m ²	square meters
ma	milliampores
mg.-mole	milligram molecular weight
mm.Hg	millimeters of mercury
mv.	millivolts
N	Avogadro's constant
N_K	flow rate by Knudsen mechanism, cc.(S.T.P.)/hr.

N_K^i	molar flow rate by Knudsen mechanism, gm.-mole/sec.
N_S	surface flow rate, cc.(S.T.P.)/hr.
N_T	total flow rate, cc.(S.T.P.)/hr.
N_T^i	molar total flow rate, gm.-mole/sec.
P	gas phase pressure, mm.Hg
\bar{P}	arithmetic average pressure, mm.Hg
P^o	vapor pressure of pure material, mm.Hg.
P_e	gas phase pressure in equilibrium with given C_S , mm.Hg
p_g^i	permeability through porous media, $\frac{\text{mg.-mole-cm.}}{\text{cm}^2\text{-hr.-mm.Hg}} \left(\frac{\text{gm.-}^\circ\text{K}}{\text{gm.-mole}} \right)^{1/2}$
P_i	plug inlet pressure, mm.Hg
P_o	plug exit pressure, mm.Hg.
$Q(L)$	flux interchange, cc.(S.T.P.)/sec.-cm ²
R	gas constant
R^i	ratemeter count rate, CPM
\bar{r}	average pore radius, cm.
S_S	specific surface area, cm ² /gm.
S.T.P.	standard temperature and pressure
T	absolute temperature, ^o K
t	time, sec.
t^i	temperature, ^o C
V_o	volume of gm.-mole at S.T.P., cc.(S.T.P.)/gm.-mole
W_p	weight of the porous plug, gm.

y	thickness, cm.
α	a constant
ϵ	porosity, cc./cc.
θ	ratemeter time constant, sec.
μ	linear x-ray absorption coefficient, cm. ⁻¹
ρ	density, gm./cc.
ρ_{app}	apparent or bulk density, gm./cc.
ρ_s	true density of solid, gm./cc.
σ_i	standard deviation of a single count rate reading, %
σ_t	standard deviation of a time averaged count rate reading, %

APPENDIX B

EQUIPMENT DETAILS

Porous plug imbedding

As stated in the Experimental Equipment section, the sides of the porous plug had to be sealed and gas inlet and exit tubes attached. The epoxy resin which was used was a casting type resin and hence flowed freely. This presented problems in terms of keeping the end faces of the plug open and of keeping the epoxy in place while it cured. Consequently a special clamp was made to hold the pieces together while the epoxy was applied and cured. This clamp assembly is shown in Figure 37.

The apparatus was assembled by first cutting two 3 inch long pieces of 10 mm. pyrex glass tubing. Three layers of Kel-F ribbon pipe sealant were wound around the 10 mm. tubing so that the glass would fit snugly into the split brass holders. The Vycor plug was cut, measured, dried at 105°C with full vacuum, weighed, and then used to find the correct position of the 10 mm. glass tubing in the brass holders. The ends of the 10 mm. tubing were ground flat and discs of 1/8 inch thick porous teflon having 55% voids and 5 micron pore size were cut to fit snugly into the

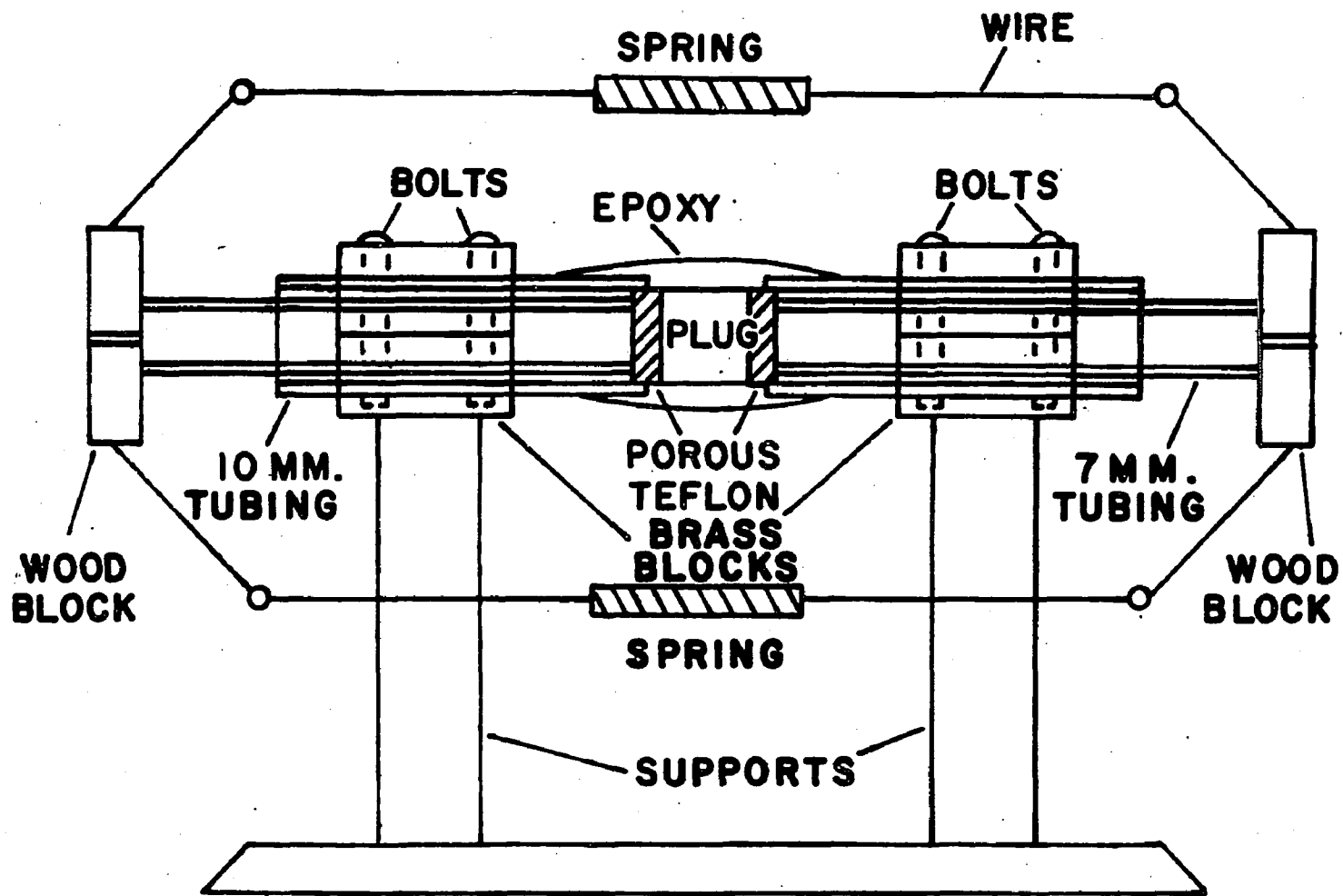


Fig. 37. Plug clamping assembly.

10 mm. glass tubing. The discs were inserted into the tubing so that they extended about 1 mm. out of the tubing end. The 10 mm. glass tubings were clamped in the brass clamp. Then, 4 inch long 7 mm. glass tubes, with both ends ground flat, were inserted into the 10 mm. tubing. The porous plug was placed between the Teflon discs and spring tension put on the 7 mm. glass tubing to press the Teflon discs tightly against the faces of the Vycor plug. These Teflon discs prevented epoxy from coating the plug faces.

The Epocast 31A resin and hardner 9216-1 were weighed out in the proportion of 100 to 19 respectively. After thorough mixing in a crucible, the epoxy was left to polymerize for about one hour. If one waits too long, the epoxy will gel and be useless. The epoxy was smeared on to cover the plug and well out onto the 10 mm. glass tubing with a spatula. The whole plug assembly was then rotated by hand to keep the plug coated as uniformly as possible. After about 20-40 minutes, the epoxy set enough that it was no longer necessary to maintain the rotation. The assembly was allowed to room temperature cure for about 8 hours. This was followed by an oven cure at about 105°C for another 12 hours to complete the cure. Care must be used so that the heating and cooling rates are no greater than 50°C per hour in order not to cause cracks in the Vycor glass.

After the plug assembly was cool and had been removed from the holder, the Teflon discs were carefully cut out

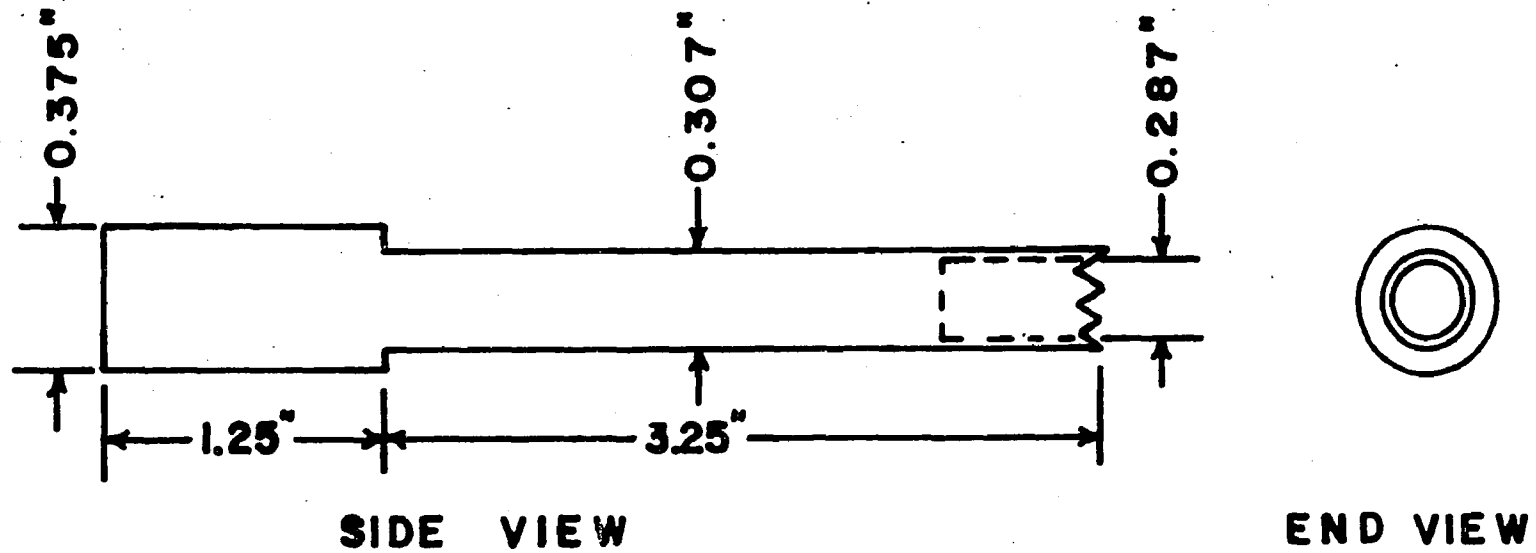
using the specially made tool shown in Figure 38. The excess epoxy was removed by sanding to a uniform diameter. To facilitate the use of a belt sander, Teflon rings of the desired thickness were placed on the 10 mm. glass tubes to hold the assembly the desired distance above the sanding belt.

The plug assembly was completed by polishing the epoxy with Buehler Limited 1552AB Gamma Polishing Alumina No. 2 and No. 3. The final assembly had a diameter of about 0.425 inches.

Extreme care must be used in handling porous Vycor during and after imbedding as it is very sensitive to both thermal and mechanical shock.

Pin hole window for scintillation counter

In order to avoid smearing out the concentration profile by the analytical system, it was desirable to obtain point x-ray absorption measurements. As a compromise, a pin hole with a diameter of about 1% of the plug length was chosen. This pin hole had to be made in 1/8 inch thick lead with a diameter of 0.1 mm. Since drilling did not seem practical, the apparatus shown in Figure 39 was built to allow casting lead around a #40 gauge (.0031" diam.) wire. The wire was very lightly coated with Type N Apeizon grease to facilitate removal of the wire after the lead hardened. The wire was installed in the apparatus as vertically as



NOTE: MAT'L- 304 S.S.

Fig. 38. Teflon disc removal tool.

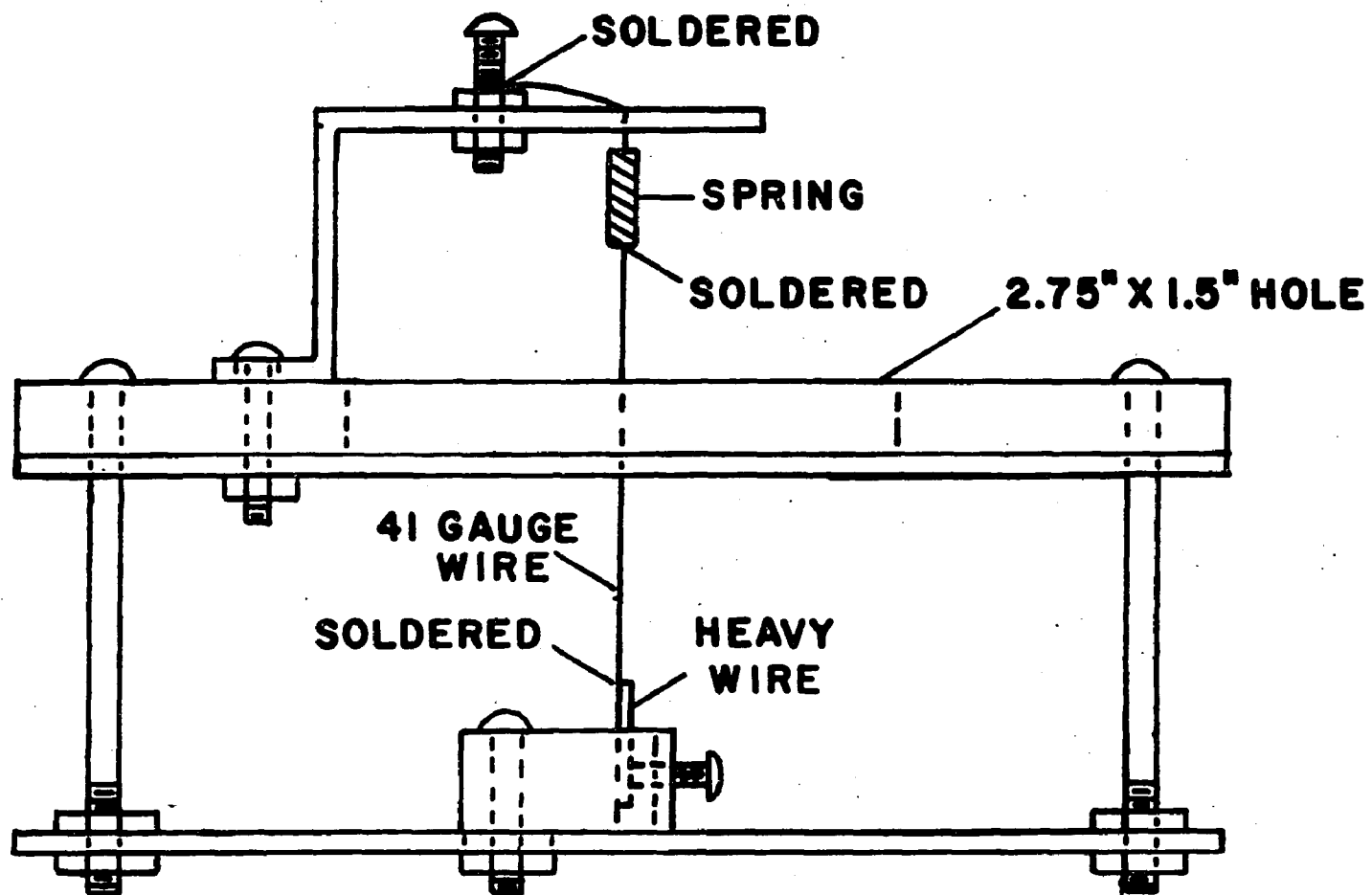


Fig. 39. Pin hole mold.

possible and soldered in place. Then molten lead was poured quickly into the mold. After the lead cooled, the wire was carefully pulled out of the lead.

The resulting pin hole was approximately round. The diameter was measured with a 10X microscope using a micrometer eyepiece. Two diameters were measured on each side and found to have an average diameter of 0.00321 inches or 0.0816 mm.

Before installing the pin hole window in the scanning device, thin pieces of polyethylene film were taped over each side of the pin hole to prevent any dust from clogging the hole.

Electrical circuits

The main electrical circuit for the x-ray analytical system is shown in Figure 40. The circuits were designed to give as much flexibility in the method of operation as possible. The relays associated with turning the x-ray beam on were necessary in order to maintain the safety features incorporated in the original x-ray power equipment, i.e., automatic shut down of the equipment due to power or water failure.

The electrical circuit for the x-ray scan position recorder is shown in Figure 41. The 10 meg-ohm potentiometer was necessary in order to minimize the current drawn from the Decker Delta Unit. For details, consult the Decker Delta Unit instruction manual (60).

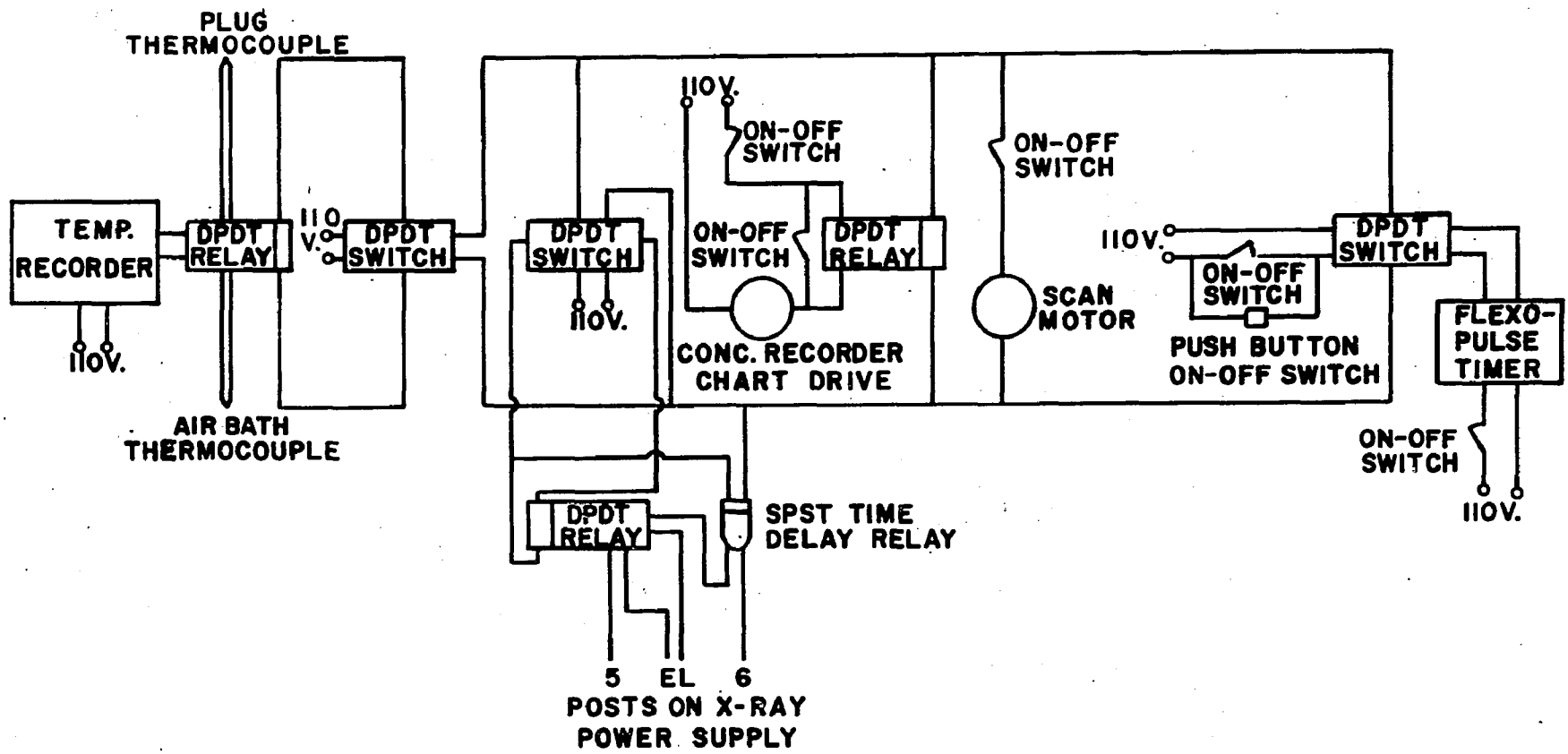


Fig. 40. Main electrical circuit.

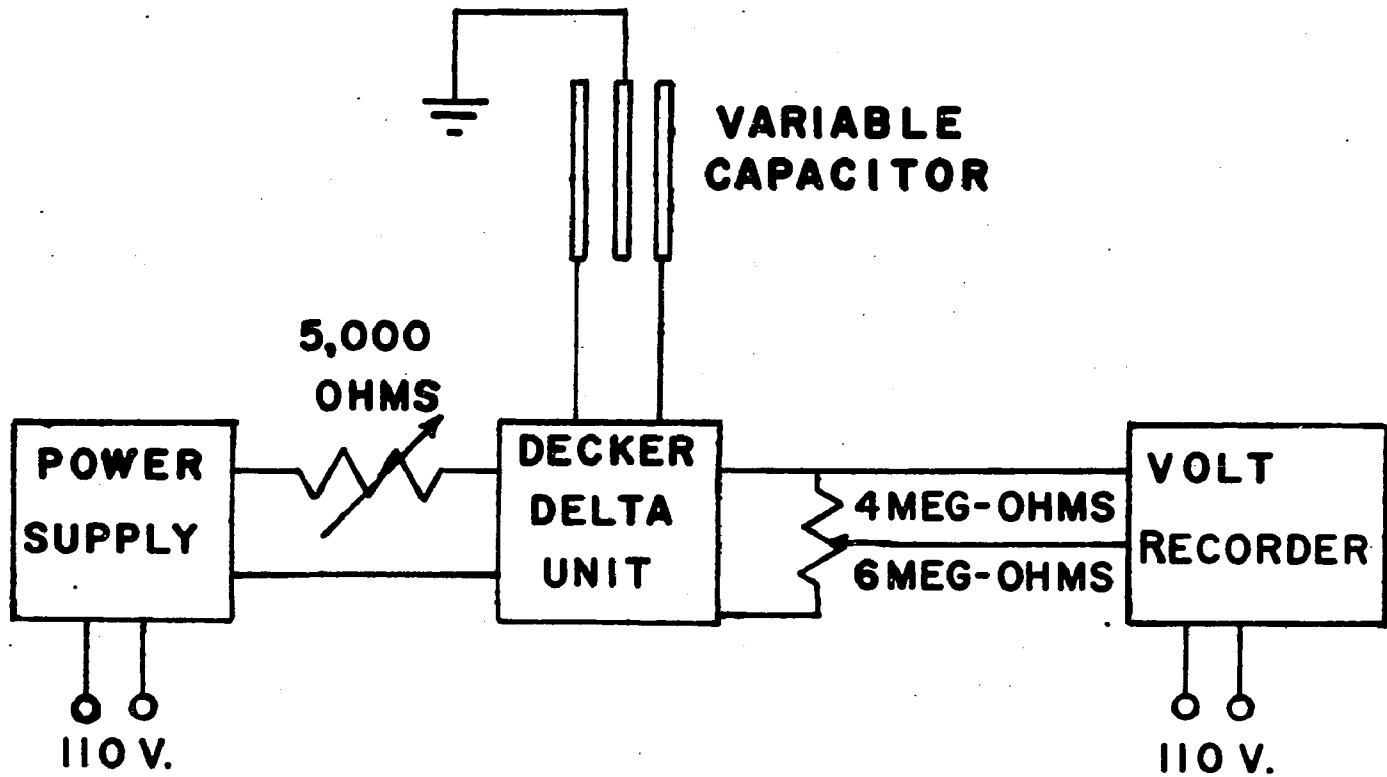


Fig. 41. Scanner position indicator circuit.

APPENDIX C

X-RAY SYSTEM VARIABLES AND EQUATIONS

Discussion and equations

Many variables effect the sensitivity, accuracy, and response of the x-ray absorption measurements. Among these are the x-ray source KV and ma, the quantity of the sample and reference beams reaching the detectors (size of pin holes), and the rate meter time constant and count rate scale. The x-ray kilovoltage determines both the quality (penetrating power) and the quantity of the x-rays while the x-ray load current ma effects only the quantity of x-rays. In general, for maximum sensitivity, it is desirable to operate at the lowest possible KV and maximum ma. This general scheme must be compromised so that an acceptable quantity of x-rays reaches the scintillation detectors. This acceptable quantity is determined by the largest pin hole of x-rays permissible without too much smearing of the concentration profile, by the statistical error in count rate, and the dynamic response (characterized by the ratemeter time constant) required.

The Picker Manual (61) shows that the statistical error due to the randomness of the radiation process has a

standard deviation in per cent given by

$$\sigma_i = 100/(2\Theta R')^{1/2} \quad (40)$$

Hence the higher the count rate, R' and the time constant, Θ , the smaller the statistical error due to the random nature of the x-radiation. This error can be reduced by recording the signal for a longer time and using the time average of this recording. The standard deviation of this time averaged signal has been given by Burgess (52) as

$$\frac{\sigma_t}{\sigma_i} = \left\{ \frac{2\Theta}{t} \left(1 - \frac{\Theta}{t} + \frac{\Theta}{t} e^{-t/\Theta} \right) \right\}^{1/2} \quad (41)$$

Hence step scanning permits use of a lower count rate and time constant without losing too much accuracy due to the statistical nature of the system.

Another variable which contributes to the accuracy of the measurements is the maximum count rate range between a completely evacuated plug and one which is equilibrated with the adsorbable gas. The larger the range, the less the measurement error. The effect of the system variables on the range can best be shown by deriving the equations for the x-ray intensity as seen by the scintillation detectors.

The following derivations lean heavily on the excellent books on x-ray technology by McMaster (63), Price (64), and Liebhafsky (65).

Beer's law, which is applicable to the absorption of x-rays, is

$$I = I_0 e^{-y\mu} \quad (42)$$

where I is the x-ray intensity after absorption

I_0 is the incident x-ray intensity

y is the thickness of the absorbing material

μ is the linear x-ray absorption coefficient

This is strictly applicable only to monochromatic (single wavelength) x-rays, but may also be applied to polychromatic x-ray beams by using an effective wavelength characteristic of the polychromatic beam.

For a composite absorber (more than one material), the x-ray absorption of the components of the composite are additive. Similarly, the absorption by each element in a compound is the same as if the element were in a pure state. Hence the x-ray mass absorption coefficients for the elements may be combined on a weight fraction basis to give the mass absorption coefficient of a compound.

Hence for the reference beam:

$$I_R = I_{R0} e^{-\sum y_R \mu_R} \quad (43)$$

where $\sum y_R \mu_R$ refers to the x-ray absorption by the air, Vycor, epoxy, Aluminum foil and teflon in the path between the x-ray tube and the reference detector.

Similarly, for the sample beam

$$I_S = I_{SO} e^{-(\sum \gamma_S \mu_S - (\gamma \mu)_{CH_3Br})} \quad (44)$$

The difference between the two intensities is then

$$\Delta I = I_R - I_S = I_{RO} e^{-\sum \gamma_R \mu_R} - I_{SO} e^{-(\sum \gamma_S \mu_S - (\gamma \mu)_{CH_3Br})} \quad (45)$$

In order to show more clearly the effect of the system variables on the quantity ΔI , which is what was recorded in this study, we will assume that

$$\sum \gamma_R \mu_R = \sum \gamma_S \mu_S \quad (46)$$

When this is substituted into equation 45, and we employ equation 43, equation 47 is obtained.

$$\Delta I = I_R - I_S = I_R \left(1 - \frac{I_{SO}}{I_{RO}} e^{-(\gamma \mu)_{CH_3Br}} \right) \quad (47)$$

Since the same incident x-ray beam is used for both reference and sample,

$$\frac{I_{SO}}{I_{RO}} = \frac{A_S}{A_R} \quad (48)$$

where A_S and A_R are the areas of the pin holes passing the x-ray beams respectively. Substitution of equation 48 into equation 47 gives

$$\Delta I = I_R \left(1 - \frac{A_S}{A_R} e^{-(\gamma \mu)_{CH_3Br}} \right) \quad (49)$$

When the plug is completely evacuated, γ_{CH_3Br} is zero and hence

$$\Delta I = I_R (1 - A_S/A_R) \quad (50)$$

Then the range of x-ray intensity from an empty plug to one containing methyl bromide is obtained by subtracting equations 49 and 50

$$\Delta(\Delta I) = I_R \frac{A_S}{A_R} (e^{-(y\mu)_{\text{CH}_3\text{Br}}} - 1) \quad (51)$$

From equation 50, it can be seen that A_S/A_R should be as close to one as possible while equation 51 indicates that for a maximum range, I_R must be as large as possible. Since A_S is limited by previously given considerations, A_R is fairly well specified. Equation 51 also indicates that the longest allowable x-ray wavelength should be used since $\mu_{\text{CH}_3\text{Br}}$ is strongly dependent on wavelength. Thus to obtain a maximum I_R , the highest x-ray tube load current, ma, should be used in conjunction with the lowest possible excitation voltage (KV).

For the x-ray system used the assumption of Equation 46 did not hold. Consequently, use of a semi-empirical equation for correlating the concentration of methyl bromide in the Vycor plug with the x-ray intensity or count rate was necessary. In addition, the x-ray source beam varied somewhat throughout each experimental run and it was necessary to correct all data to some base condition. This base condition was determined arbitrarily, and all data referred to this base.

The derivation of this equation is as follows.

$$\Delta I = I_R - I'_S e^{-(\gamma\mu)} \quad (52)$$

where

$$I_R = (I_R)_B + \Delta I_R \quad (53)$$

$$I'_S = (I'_S)_B + \Delta I_S \quad (54)$$

$(I_R)_B$ is the reference beam intensity at the base conditions

ΔI_R is the difference between the reference beam intensity at the measuring and base conditions

$$I'_S = I_{S0} e^{-\sum \gamma_s \mu_s}$$

$(I'_S)_B$ is I'_S at the base conditions

$\Delta I'_S$ is the difference between I'_S at the measuring and base conditions

$(\gamma\mu)$ refers to methyl bromide

$$\Delta I = I_R - ((I'_S)_B + \Delta I'_S) e^{-(\gamma\mu)} \quad (55)$$

or

$$e^{-(\gamma\mu)} = \frac{I_R - \Delta I}{(I'_S)_B + \Delta I_S} \quad (56)$$

However, since the base condition selected was with the plug evacuated

$$(I'_S)_B = (I_R)_B - (\Delta I)_B \quad (57)$$

It was shown experimentally, by varying the KV from 28 to 30, that the relative effect on the sample and reference

detectors was essentially constant over the plug length. The experimental data are given in the Appendix on Original Data Tabulations, Table 27. Hence for small KV changes

$$\Delta I_S = 0.9 \Delta I_R \quad (58)$$

within $\pm 4\%$. For changes in the x-ray load current, ΔI_S and ΔI_R would be the same. Substituting equations 53, 57, and 58 into equation 56

$$e^{-(y\mu)} = \frac{I_R - \Delta I}{0.9 I_R + 0.1 (I_R)_B - (\Delta I)_B} \quad (59)$$

or

$$y = -\frac{1}{\mu} \ln \left(\frac{I_R - \Delta I}{0.9 I_R + 0.1 (I_R)_B - (\Delta I)_B} \right) \quad (60)$$

If we neglect the small amount of methyl bromide in the gas phase compared to that on the surface (reported in Appendix on Calculated Data), the relationship between y and C_S is

$$C_S = \frac{22,400 \rho y}{\rho_{app} DM} = K_1 \rho y \quad (61)$$

where

ρ = density of adsorbed material

ρ_{app} = plug density

D = plug diameter

M = molecular weight of adsorbed material

K_1 = constant

Substitution of equation 61 and since μ/p is essentially constant for small changes in x-ray source voltage gives the final correlation equation for converting the x-ray data to concentration data on a common base at each position along the plug.

$$C_s = -K \ln \left(\frac{I_R - \Delta I}{0.9 I_R + 0.1 (I_R)_B - (\Delta I)_B} \right) = -K \ln F \quad (10)$$

where

$K = \text{constant}$

$F = \text{x-ray attenuation factor (defined in equation 9)}$

I_R and ΔI are measured quantities for each scan during each experimental run and $(I_R)_B$ and $(\Delta I)_B$ were the initial base conditions.

The estimated variation of μ/p with KV for CH_3Br is shown in Figure 42. A sample calculation of μ/p is shown in the Appendix on Calculated Quantities. The straight line portion is given by $\mu/p = (\text{KV})^{0.282}$. Hence for a KV variation from 28.5 to 29.5, the change in μ/p is just over 1%.

Estimation of composite system
absorbitivity

A computer program for estimating the x-ray absorptivity maximum change, and brightness contrast in absorbitivity of a porous plug assembly at various wavelengths and plug thicknesses was prepared. The results from this program were used to help specify the x-ray equipment and may be helpful if use of a different gas-solid system is considered

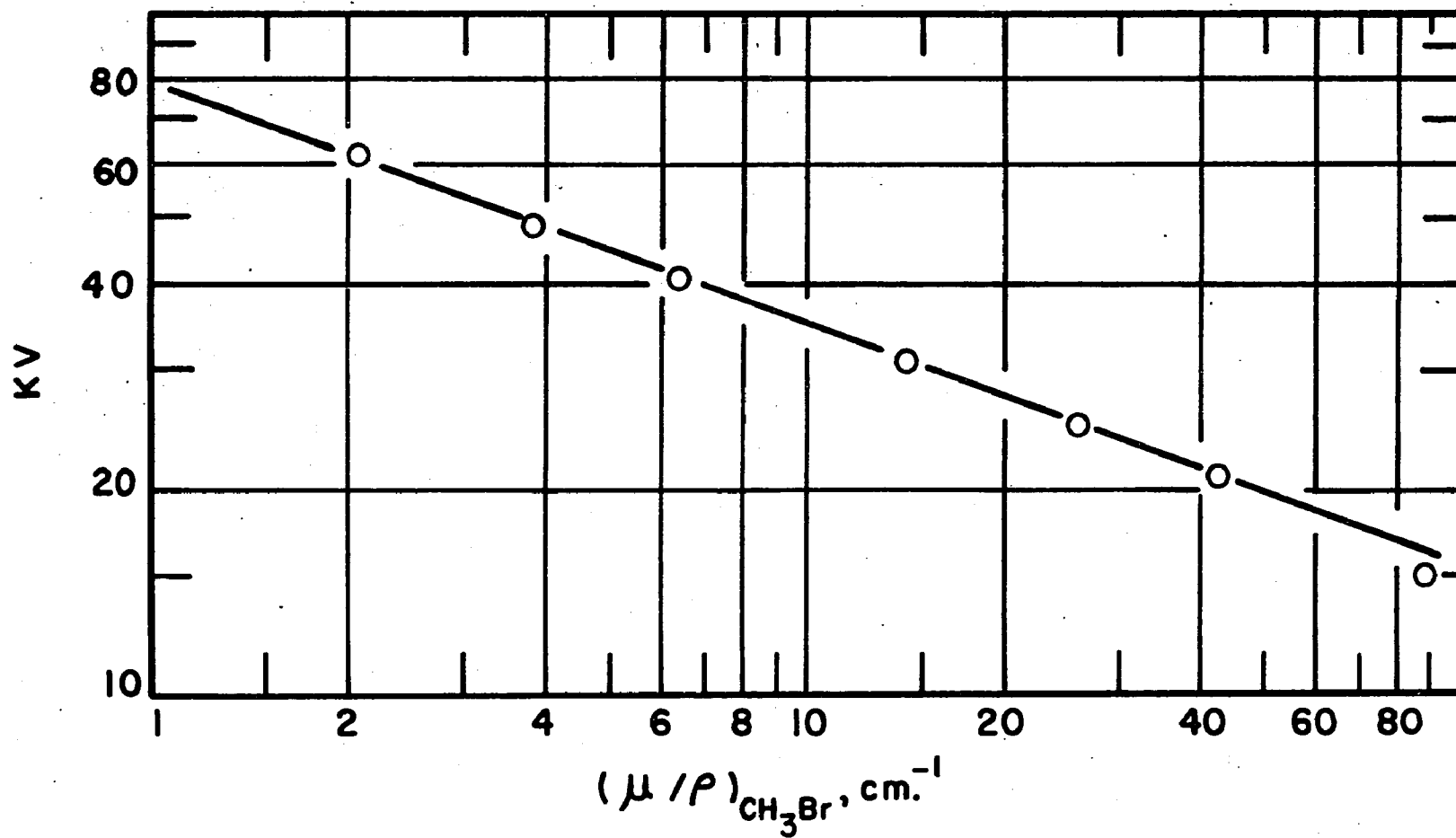


Fig. 42. Variation of $(\mu/\rho)_{\text{CH}_3\text{Br}}$ with KV.

in the future. The symbols used in this computer section are defined for this section only as they are introduced.

The computer program solves the equations:

$$Y = U + V + W$$

$$E = XY + T$$

$$S = e^E$$

$$A = 100 (1 - (1/S))$$

$$Y = W$$

$$F = XY + T$$

$$S = e^F$$

$$B = 100 (1 - (1/S))$$

$$C = A - B$$

$$R = E - F$$

$$S = e^R$$

$$D = 100 (1 - (1/S))$$

where $U =$ x-ray absorptivity per unit of plug diameter
for the absorbed gas at one wavelength.

$V =$ x-ray absorptivity per unit of plug diameter
for the nonadsorbed gas at one wavelength.

$W =$ x-ray absorptivity per unit of plug diameter
for the porous plug at one wavelength.

$T =$ x-ray absorptivity of the material coating the
the porous plug at one wavelength.

$X =$ plug diameter

E = total x-ray attenuation with plug saturated at a given pressure.

F = total x-ray attenuation with plug evacuated.

A = x-ray absorptivity with plug saturated at a given pressure.

B = x-ray absorptivity with plug evacuated.

C = maximum difference in absorptivity for a plug saturated at a given pressure and an evacuated plug.

D = brightness contrast.

Hence, a set of U, V, W, and T for the wavelengths in Angstroms of .1, .15, .2, .25, .3, .4, .5, .6, and .8 is the data required for the computer to find A, B, C, and D for each wavelength for the plug diameters .3, .5, .7, .9, 1.1, 1.3, 1.5, 1.7, 1.9, and 2.1 cm.

The computer program was written in SCATLAN language for the I.B.M. 7090 computer at the Ohio State Numerical Computations Laboratory and was as follows.

```

HAZLEBECK, DAVID E.      JOB 122.57      03/11/63      915027      PAGE  *
SOURCE LANGUAGE STATEMENTS
1  DIMENSION (A(400,M),B(400,M),C(400,M),D(400,M),U(50),V(50),W(50),Y(50))
2  START      READ INPUT ,DATA,(K,M,(U(J),V(J),W(J),T(J),J=1,7),J,LE,K))
3  F DATA    (213/(4F10.5))
4  WRITE OUTPUT ,ALPHA
5  F ALPHA    (1H,4X,62HESTIMATION OF X-RAY ABSORPTION FOR VYCOR-METHYL BROMIDE SYSTEM)
6  WRITE OUTPUT ,BETA
7  F BETA     (4X,28HLINEAR ABSORPTION INPUT DATA//6X,15HU-ADSORBED MEBR,4X,16HV-GAS PHASE MEBR,5X,12HW-VYCOR PLUG,
              7X,16HT-TEFLON COATING)
8  WRITE OUTPUT ,LIST,(K,(U(J),V(J),W(J),T(J),J=1,7),J,LE,K))
9  F LIST     (2X,12/(4F19.8))
10 WRITE OUTPUT ,HEAD
11 F HEAD     (1H,1X,14J,2X,1H1,2X,29HA-SATURATED PLUG ABSORPTIVITY,2X,25HB-EMPTY PLUG ABSORPTIVITY,2X,23HC-ABSORPT
              IVITY DIFFERENCE,2X,21HD-BRIGHTNESS CONTRAST)
12 I=1
13 DO THROUGH (TWO),X=0.2,0.2, PROVIDED (X,LE,2,1)-
14 DO THROUGH (ONE),J=1,1, PROVIDED (J,LE,K)-
15 Y=U(J)+V(J)+W(J)-
16 F=X*Y+I(J)-
17 A(J,1)=100.*(1.-I./EXPE.(F)))
18 Y=W(J)-
19 F=X*Y+I(J)-
20 H(J,1)=100.*(1.-I./EXPE.(F)))
21 C(J,1)=A(J,1)-B(J,1)-
22 I=E-F-
24 ONE       D(J,1)=100.*(1.-I./EXPE.(R)))
24 TWO       I=I+1-
25 WRITE OUTPUT ,RESULT,((J,(A(J,1),B(J,1),C(J,1),D(J,1),J=1,7),J,LE,K),I=1,1,(L,C,10))-
26 F RESULT  (1X,12,1X,12,14X,F,3,23G,F,3,21X,F,3,19X,F,3)
27 END PROGRAM (START)-

```

APPENDIX D

OPERATING PROCEDURES

The following operating procedures have been based on experience and the equipment manufactures' detailed operating manuals (60, 61, 66-72).

McLeod gauge operating procedure

The initial evacuation of the McLeod gauge should be done very carefully to avoid violent bumping of the mercury. This is done by setting the air leak, three-way valve so that the mechanical vacuum pump can slowly evacuate the mercury reservoir while at the same time the gauge itself is slowly evacuated by the system mechanical vacuum pump. These rates must be balanced so that the pressure in the mercury reservoir and in the gauge remain approximately equal. When the gauge and the reservoir are both evacuated, the gauge is ready for normal operation. The gauge and reservoir should always be left evacuated after the initial evacuation.

The normal procedure for taking a pressure reading is itemized in the following.

1. Turn the stopcock to connect the air leak to the mercury reservoir. This allows the mercury to rise into the gauge.

2. As the mercury reaches the zero line, close the stopcock slightly to stop the mercury.

3. To read a 0-100 microns, raise the mercury in the open capillary tube to the top zero line and read the pressure indicated by the mercury level in the closed capillary.

4. To read 0-1.0 mm., raise the mercury in the closed capillary tube to the middle zero line and read the pressure indicated by the mercury level in the open capillary.

5. To read 0-10 mm., raise the mercury in the closed capillary tube to the bottom zero line and read the pressure indicated by the mercury level in the closed capillary.

6. To lower the mercury, turn the stopcock so that the mechanical vacuum pump can evacuate the mercury reservoir.

Operating procedure for the dual
count rate meter and recording
system

1. Adjust the meter mechanical zeros by means of the zero adjusting screws on the lower plastic meter fronts to zero.

2. Turn the power switch in the back of the Speedomax recorder to the On position (chart drive switch off) and allow the instrument to warm up at least one hour for stable operation.

3. Turn the rate meter Range switches to the 1,000,000 count per minute (CPM) range and the Time Constant switches to the 0.03 Second Time constant.

4. Turn the Control switch to the On position and allow the instrument a few minutes to stabilize.

5. Adjust the small screw driver adjusting screws beneath the respective meters until the meter pointers lie exactly on zero.

6. Check the ratemeter circuits by turning the Control switch to Test, the Range switches to 10K, and the Time Constant switches to 1 second. The meters should now indicate 3600 CPM.

7. Check the recorder by switching each meter to indicate on the recorder using the Recorder Variable Selector switch on the main panel. If the recorder does not indicate 36 on the 0 to 100 mv. scale, adjust the appropriate potentiometer accordingly.

8. Turn the Range and Time Constant switches to the desired operating conditions.

9. Turn the Control switch to the On position.

10. Turn the High Voltage switch on.

11. To shut down, merely turn off the High Voltage switch, the Control switch, and the power switch in the Speedomax recorder.

Selection of high voltage level for the scintillation detectors

1. Turn on and adjust the ratemeter as given in the preceding section.

2. Set the Range Selector switches on a low scale such as 1K and the Time Constant switches to 0.3 seconds.

3. Turn on the x-ray unit at some low level such that with the detector high voltage set at 500 volts, no indication is showing on the ratemeter.

4. Turn the Detector B Voltage to the extreme counter clockwise position and slowly raise the high voltage until detector A begins to count.

5. Turn the Detector B voltage dial slowly clockwise until it also just begins to count. This should approximately balance the two detectors.

6. Determine the curve of the counting rate versus detector high voltage over the range 500 to 1400 volts for each detector.

7. Proceeding from low to high voltage, the counting rate will increase rapidly at first, then level out in a plateau, and finally will increase again very rapidly as the electronic noise of the phototube becomes large enough to be counted.

8. Set the high voltage at about the center of the plateau.

System and plug degassing procedure

All valve numbers refer to Figure 1.

1. Fill the thermocouple cold junction dewar with ice.
2. Turn on the water for the mercury diffusion pump.

3. Turn on the hood exhaust fan.
4. Set the air bath temperature controller to 2.75 on the fine control and the Powerstats to 37.5.
5. Set the plug air bath temperature controller to 3.7 on the fine control and the Powerstats to 25.
6. Open the air valve on the air bath air driven blower to a pressure of 20 psig.
7. Turn on the plug air bath blower motor.
8. Set the air bath and plug air bath switches on Auto.
9. Valves, 1, 2, 3, 6, 7, 26, and 27 should be closed. The rest of the valves or stopcocks should be open.
10. Turn on the system mechanical vacuum pump.
11. Set the Variac on the mercury diffusion pump heater to 82 and turn the heater on.
12. Follow the procedure for initial evacuation of the McLeod gauge given in the McLeod gauge operating procedure.
13. Evacuate all the stopcocks in the system.
14. Allow the system to evacuate for 8 hours. The air baths should be stable at 40°C by the end of this period.
15. Slowly raise the plug air bath temperature to 100-105°C by setting the plug air bath heater Powerstats at 40 and the controller coarse control at 1.75.
16. When the temperature reaches 55°C, raise the plug air bath heater Powerstats to 50.

17. When the temperature reaches 75°C , raise the plug air bath heater Powerstats to 60. The plug air bath temperature should then level out between 100 and 105°C .

18. Evacuate the plug and system under this condition for at least 24 hours or until the system pressure is below 10^{-5} mm.Hg.

19. Isolate the plug by closing stopcocks 11 and 12.

20. Slowly cool the plug air bath to 40°C by setting the plug air bath heater Powerstats at 25.

21. When the temperature reaches 73°C , set the plug air bath temperature coarse control at the lowest possible setting. The temperature should then level out at 40°C .

22. The system and plug are now ready for flow measurements.

Operating procedure for measurement
of helium permeabilities at zero
downstream pressure

This procedure assumes that the plug and system degassing procedure given previously has been completed.

All valve numbers refer to Figure 1.

1. Close valves 8 and 25 to make the manometers absolute.

2. Close valves 14, 16, 20, 21, 22, 23, 24, 26, and 28.

3. Close the pinch clamps in the helium tank and Hg bubbler lines.

4. Open valve 7 and evacuate the helium feed line.

5. Close valve 7 and open the helium tank valve 5.

6. Adjust the helium tank regulator to about 5 psig. and open the pinch clamp in the helium tank line.

7. Slowly open both valve 6 and the pinch clamp on the Hg bubbler line to fill the line with helium. Adjust the helium flow to give a fairly strong bubble rate through the Hg bubbler.

8. Open valve 7 slowly to fill the system to about 600 mm. with helium.

9. Close valve 7 and evacuate the system through valve 28.

10. Repeat steps 9 and 10 two more times.

11. When the system is full of helium for the last flushing, set the syringe feeder on manual operation, disengage the microswitch on the feeder by loosening one screw, and adjust the mercury level in the 25 cc. syringe to the red mark. Re-engage the microswitch and check to be sure it is set properly by manual feeding. Set the syringe feeder back on automatic.

12. After the system is evacuated, close the plug bypass valve 15 and open valve 16.

13. Fill the upstream system with helium to the desired inlet pressure as indicated by the upstream mercury manometer and close valve 9.

14. Turn on the upstream Thermocap relay but in the non-control position.

15. Close valve 13 and adjust the mercury level in the differential pressure manometer to just actuate the Thermocap relay.

16. Calculate the required overpressure to fill the 1 cc. dead space between valve 14 and the porous plug.

17. Obtain this overpressure by either adding more helium through valve 6 or if the run will be fairly short, by using the syringe feeder to feed in approximately 1 cc. If the syringe feeder is used, the electronic counter power switch must be turned on.

18. Close valve 5 and vent the helium regulator through the Hg bubbler.

19. Open valve 26 to the McLeod gauge, turn the Thermocap controller to the control position (toggle switch to the east), and set the electronic counter to zero and turn it on.

20. The system should now be ready to operate.

21. To start the run, simultaneously start the Time-it electric timer and open valve 14.

22. Record the time and counts on the electronic counter every minute for the first 10 minutes and every 10 minutes thereafter until the steady state flow rate is obtained.

23. During the operation the upstream and downstream pressures as well as the operating temperature should be recorded.

24. To end the run, turn off the electronic counter, electric timer, and the upstream Thermocap relay.

25. Open valve 13 to equalize the pressure on the differential pressure manometer.

26. Slowly open valve 15 and evacuate the system.

Operating procedure for measurement of helium permeabilities at some downstream pressure other than zero

This procedure assumes that the plug and system degassing procedure given previously has been completed.

All valve numbers refer to Figure 1.

1. Follow steps 1 through 11 of the procedure for measuring helium permeabilities with zero downstream pressure to purge the system.

2. Close valves 19, 26, and 28 and open valves 22 and 23.

3. With the leveling bulb raise the mercury level in the reservoir, to be used for downstream pressure control, to the red line. This can be done by turning the solenoid valve power switch to the manual position. Needle valve 32 should be throttled so that a very slow rate of mercury flow is obtained.

4. Fill the system with helium to the desired exit pressure as indicated on the downstream mercury manometer and close valves 14 and 15.

5. Plug in the downstream Thermocap and selector relays and set the Thermocap switch in the middle or non-controlling position.

6. Close valve 17 on the downstream differential manometer and adjust the mercury level to just actuate the solenoid valve.

7. Turn the solenoid valve power switch to the automatic position and turn the Thermocap switch to the control position.

8. The downstream system is now ready for operation.

9. Follow steps 13 through 19 of the procedure for measuring helium permeabilities with zero downstream pressure to set the upstream pressure.

10. The whole system should now be ready for operation.

11. Follow steps 21 through 23 of the procedure for measuring helium permeabilities with zero downstream pressure to make the run.

12. To end the run, turn off the electronic counter, electric timer, both Thermocap relays, and the downstream selector relay.

13. Open valve 13 to equalize the pressure in the upstream differential pressure manometer.

14. Open valve 17 to equalize the pressure in the downstream differential pressure manometer.

15. Slowly open valve 15 to equalize the pressure throughout the system.

16. Slowly open valve 19 to evacuate the system.

Operating procedure for measurement of methyl bromide permeabilities

This procedure assumes that the plug and system degassing procedure given previously has been completed. All valve numbers refer to Figure 1. The hood exhaust fans should always be running for proper operation of the air baths and mercury diffusion pump heater and because of the high toxicity of methyl bromide.

The procedure for measuring methyl bromide permeabilities is the same as that for measuring helium permeabilities with the following exceptions. Liquid N_2 must be put in the vacuum system cold trap. The system must be left to equilibrate overnight after loading since methyl bromide is somewhat soluble in stopcock grease. The loading procedure is slightly different and is itemized as follows:

1. Close valves 8 and 25 to make the manometers absolute.
2. Close valves 14, 16, 20, 21, 22, 23, 24, 26, and 28.
3. Close the methyl bromide tank valve 1 and slowly open the needle valve 2 to purge through the Hg bubbler.
4. Intermittently open the three-way valve 3 to purge the feed line to the vent.
5. Adjust the needle valve 2 to give a fairly strong bubble rate through the Hg bubbler.

6. Open the three-way valve 3 to slowly fill the system to about 600 mm. with methyl bromide.
7. Close valve 3 and evacuate the system through valve 28.
8. Repeat steps 6 and 7 two more times.
9. Follow the procedure used for helium runs to load the system through valve 3 for either zero or other downstream pressures.
10. When the system is loaded, close valves 1 and 2.

Operating procedure for measuring
quantity collected in downstream
reservoirs

All valve numbers refer to Figure 1. It is assumed that downstream reservoir B contains collected gas and that reservoir A is evacuated. When this procedure is used the downstream pressure manometer is no longer used to measure the downstream pressure.

1. Simultaneously open valve 21 and close valve 22. This switches the downstream pressure control to reservoir A.
2. Place the power switch for solenoid valve 31 in the manual position and raise the mercury in reservoir B to the red line by raising the leveling bulb. This procedure may be speeded up by opening the needle valve 32 until the mercury approaches the top of reservoir B. When the mercury level reaches the red line, shut the solenoid valve.

3. Read the pressure on the downstream mercury manometer. Also record the measuring temperature.
4. Lower the mercury level back into the reservoir by opening the solenoid valve and lowering the leveling bulb.
5. Open valve 24 to slowly exhaust the collected gas through the cold trap and vacuum pump.
6. When the McLeod gauge indicates a low pressure, close valves 23 and 24 and raise the mercury level in reservoir B back to the red line using the leveling bulb.
7. Place the solenoid power control switch in the automatic position.
8. The reservoir is now ready for collecting more material.
9. A similar procedure is used for measuring the gas collected in reservoir A.

Operating procedure for position
calibration of x-ray scanner

Due to instability of the electronic gear and variation in the atmospheric conditions, the voltage signal indication of the x-ray scanner position must be calibrated frequently. The following procedure was used for this calibration.

1. Turn on the ratemeter by turning the Control switch to the On position, the Range switches to 100,000, and the Time Constant switches to 0.3 sec. Allow a few moments to stabilize.

2. Turn the Bausch & Lomb recorder on by turning the control switch to Measure. Set the range dial to 1 volt. Allow at least 1 hour for stabilization.

3. Turn on the Decker unit by turning on the precise power supply. The power supply D.C. voltage should be set at 185 volts. Allow at least 1 hour for stabilization.

4. Set the main panel control switches as follows:

Manual Analytical System	- off
X-ray Power	- off
Program Timer	- off
Flexopulse	- off
Analytical System	- on
Recorder Variable Selector	- open
Scan Drive	- on

5. Prepare to operate the x-ray unit by turning the Start-Stop switch to start, the timer dial off of zero, and pulling out the Main switch. These are all located on the x-ray unit control panel. Check to be sure water is now flowing through the x-ray tube. Turn the Kilovolts and Milliamperes dials fully counterclockwise.

6. Turn on the x-ray beam by turning the x-ray power switch on the main control panel to the Manual On position. Slowly adjust the x-ray unit Kilovolts and Millamperes dials to obtain 29 KV and 37 ma respectively. Allow the x-ray unit at least 30 minutes to stabilize.

7. Start the scanner in operation by turning the Manual Analytical System switch to the on position. When the scanner pin hole passes from off one end of the plug to off

the other end of the plug, the A ratemeter will start at zero, increase rapidly as the pin hole approaches the end of the plug, indicate a fairly steady reading while on the plug, rise sharply as it leaves the end of the plug, and then fall sharply as the pin hole passes the end of the detector crystal. By noting the reading of the Bausch & Lomb recorder at the ends of the plug, adjust the recorder Zero Adjust to give a voltage range of about 0.15 to 0.75 volts. Be sure to record this range. Determination of the exact range was easier using the push button switch rather than the toggle switch on the Manual Analytical System control.

8. With the scanner operating, set the recorder chart speed at 5 inches per minute and record at least 3 scans in each direction by turning the recorder switch to the record position.

9. The calibration curve was constructed by assuming the scan drive was constant and hence the distance the chart had gone was proportional to the distance down the plug. A sample calculation is given in the Appendix on Calculated Quantities.

Operating procedure for making a concentration profile measurement

It is assumed that the ratemeter and recorder has been properly adjusted as given previously in this appendix. It is further assumed that the position scanner calibration as

given previously has just been completed. Hence everything is warmed up and the x-ray beam is on.

1. Set the Flexopulse schedule for 11 seconds off and 1 second on.

2. Set the scanner just off one end of the plug with the manual analytical system.

3. Set the main panel control switches as follows:

Manual Analytical System	- off
X-ray Power	- on
Program Timer	- off
Flexopulse	- off
Analytical System	- Auto
Recorder Variable Selector	- B-A
Scan Drive	- on

4. Set the Bausch & Lomb recorder chart speed to 1 inch per minute and turn the recorder control to Record.

5. Turn the Speedomax recorder chart drive on to record the base line for just a few seconds, then turn the Flexopulse switch to the on position and allow the Flexopulse to automatically step-scan the pin hole along the plug. It is helpful in data workup to mark both on the position and concentration recorder traces where the detector first indicates that the pin hole is on the plug. It is also helpful to mark on the concentration recorder trace at several points when the scanner is moving.

6. When the end of the plug is reached, turn off the Flexopulse but record the base line for a few seconds.

7. Turn off the Speedomax chart drive, turn the Bausch & Lomb recorder to Measure and turn the Recorder Variable Selector to open.

This completes one step-scan. Step-scans can be made in either direction and sometimes if the concentration profile is changing rapidly, scans in both directions may be helpful.

X-ray system shut down procedure

1. Turn off the x-ray beam by turning the x-ray power switch on the main control panel to the off position. Be sure to leave the Main power switch on the x-ray unit panel on for at least 15 minutes after turning off the x-ray beam so that the x-ray tube will be completely cooled.

2. Turn off the Bausch & Lomb recorder, the Speedomax power, the Decker unit power, and the scan drive.

3. Turn the Start-Stop switch to stop, the timer dial to zero, and push in the Main power switch on the x-ray unit panel board.

APPENDIX E

ORIGINAL DATA TABULATION

TABLE 10

THERMOCOUPLE CALIBRATION DATA

Reference junctions at 0°C in ice-water bath.
 Thermometer calibrated to 0.1°C by National Bureau of Standards

No. 5503110, Range -38 to + 2°C.
 No. 5607004, Range +28 to + 52°C.
 No. 5503107, Range +73 to ±102°C.

Thermometer °C ^a	Plug air bath thermocouple mv. ^b	Air bath thermocouple mv. ^b
0.7	0.041	0.040
30.4	1.555	1.557
33.0	1.683	1.683
36.5	1.870	1.865
38.3	1.964	1.959
40.2	2.054	2.057
41.6	2.125	2.124
44.1	2.255	2.255
46.0	2.355	2.353
48.0	2.453	2.458
48.2	2.468	2.466
82.0	4.268	4.275
82.0	4.267	4.280
86.8	---	4.535
87.0	4.555	---

^aThermocouples were taped to thermometer and immersed in a water bath.

^bMv. was measured with a Leeds & Northrup No. 8662 Portable Precision Potentiometer.

TABLE 11
MANOMETER SCALE CALIBRATION DATA

Upstream Manometer Scale	
Manometer Scale, mm.	Cathetometer Scale, ^a mm.
900	784.78
800	684.50
700	585.18
600	485.23
500	385.28
400	285.29
300	185.50
200	85.75
100	off scale

Downstream Manometer Scale	
Manometer Scale, mm.	Cathetometer Scale, mm.
980	940.03
880	840.16
780	740.25
680	640.41
580	540.42
480	440.50
380	340.37
280	240.53
180	140.46
80	40.28

^aThe cathetometer was a Griffin and George, Lmt. Cat. No. S31-950 with an accuracy of ± 0.015 mm. and calibrated at 20°C.

TABLE 12
 SYRINGE FEEDER CALIBRATION DATA

Syringe feeder drive set on speed D
 Temperature -82°C .
 Specific volume of Hg. at 82°F $-0.0739255\text{cm}^3/\text{gm}$.
 Operating head - approximately 710 mm.Hg. gauge

Syringe ml.	Counter reading counts	W-weight of reading Hg. displaced gm.	ΔW^a gm.	Δ counts ^b counts	$\frac{\text{cm}^3}{\text{count}} \times 10^{-4}$
21	0	30.4581	--	--	--
20	1,111	42.8013	12.3432	1,111	8.213
19	2,212	54.9316	12.1303	1,101	8.147
18	3,319	67.1663	12.2347	1,107	8.169
17	4,405	79.1560	11.9897	1,086	8.161
16	5,515	91.4084	12.2524	1,110	8.161
15	6,609	103.4699	12.0615	1,094	9.147
14	7,710	115.5753	12.1054	1,101	8.124
13	8,806	127.7284	12.1531	1,096	8.198
12	9,906	139.8780	12.1496	1,100	8.161
11	11,012	152.1310	12.2530	1,106	8.191
10	12,106	164.2582	12.1272	1,094	8.191
9	13,199	176.3355	12.0773	1,093	8.169
8+	14,312	188.6464	12.3109	1,113	8.176
New tare weight-30.4581			--	--	--
7.5+	15,520	43.7710	13.3129	1,208	8.147
7	16,606	55.8138	12.0428	1,086	8.198
6	17,703	67.9237	12.1099	1,097	8.161
5	18,808	80.1528	12.2291	1,105	8.184
4	19,902	92.2343	12.0815	1,094	8.161
3	21,006	104.4501	12.2158	1,104	8.176
2+	22,102	116.5626	12.1125	1,096	8.169
1.75	22,614	122.2357	5.6731	512	8.191

Syringe feed shut off automatically

^a ΔW is the amount of mercury displaced by the syringe plunger between two successive readings.

^b Δ counts is the number of counts between two successive readings.

TABLE 13
CALIBRATION DATA FOR SYSTEM VOLUME

Volume	System menometer mm. Hg.	System Temp. °C	Hg. fed counts	Barometer mm. Hg.	Barometer Temp. °C	Calculated Volume ^a c.c.
1 ^b	319.45-152.32	27.5	0	862.5-118.1	25.7	--
1	289.55-163.79	27.5	7,303	862.4-118.2	25.8	86.10
1	255.71-177.01	27.7	14,601	862.3-118.3	25.6	86.80
1	216.46-192.34	27.75	21,904	862.2-120.5	25.6	86.69
2 ^c	317.32-153.06	26.9	0	859.9-120.5	24.6	--
2	298.93-160.31	27.15	7,302	859.9-120.5	24.7	139.78
2	278.68-168.30	27.4	14,600	859.8-120.6	25.2	139.10
2	256.85-176.76	27.45	21,903	859.8-120.7	25.5	139.15
3 ^d	315.98-153.67	26.2	0	858.7-121.7	26.5	--
3	300.01-159.99	26.2	7,307	858.7-121.7	26.3	155.82
3	282.80-166.65	26.2	14,673	858.7-121.6	26.3	156.67
3	263.79-174.16	26.2	22,009	858.9-121.5	26.2	155.70
4 ^e	742.78-169.97 ^f	25.3	0	--	--	--
4	749.68-152.45	25.5	7,349	--	--	143.61
4	757.00-133.32	25.6	14,614	--	--	142.87
4	765.18-112.25	25.6	22,008	--	--	142.88

^aA sample calculation of the volume is given in the appendix on Calculated Quantities.

^bVolume 1 is the inlet system between valves 9, 14, and 15 with valves 12 and 13 closed. Valve numbers refer to Figure 1.

^cVolume 2 is the system between valves 9, 14, 16, 19, 21, and 22 with valves 12, 13, 17, and 18 closed.

TABLE 13--Continued

^dVolume 3 is the system between valves 9, 19, 21, and 22 with valves 12, 13, 17, and 18 closed.

^eVolume 4 is the system between valves 9, 10, 14, 16, 19, 22, 23, and 24 with valves 12, 13, 17, and 18 closed. Had valves 22 and 23 been open in place of valves 20 and 21, the volume difference was estimated as only 0.04 c.c.

^fVolume 4 was calibrated using the closed end manometer on the exit side and hence the barometric pressure had no effect.

TABLE 14
STEADY STATE HELIUM PERMEABILITY AT 40°C

Run	P_{in} mm.Hg	P_{out} mm.Hg	ΔP mm.Hg	$N \times 10^2$ $\frac{\text{mg.mole}}{\text{hr.}}$	$\frac{P_g}{P} \cdot \frac{MT}{X10^2}$ $\frac{\text{mg.mole-cm.}}{\text{hr.-cm}^2\text{-mm.Hg.}} \left(\frac{\text{gm.}}{\text{g.mole}} \right)^{1/2}$	\bar{P} mm.Hg
H-1	704.0	0.0	704.0	7.646	0.890	352.0
H-2	706.9	517.1	189.8	2.017	0.871	612.0
H-3	102.5	12.3	90.2	0.982	0.892	57.4
H-4	101.0	11.9	89.1	0.979	0.900	56.5
H-5	404.6	0.0	404.6	4.332	0.878	202.3
H-6	636.7	399.2	237.5	2.518	0.869	519.6

TABLE 15

HELIUM ORIGINAL FLOW DATA AT 40°C

Run H-1

Inlet manometer = 34.1 mm.Hg at 26°C
 Atmospheric pressure = 739.7 mm.Hg at 25.9°C
 Exit pressure = 0.008 mm.Hg at 26°C

Time sec.	Volume Fed c.c. at P ₁	Time sec.	Volume Fed c.c. at P ₁
0	0.00	6,600	3.348
650	0.046	7,200	3.689
810	0.169	7,500	3.892
1,200	0.428	8,100	4.419
1,920	0.802	8,700	4.691
2,520	1.147	9,300	4.983
3,000	1.387	9,900	5.318
3,600	1.722	10,500	5.718
4,200	2.055	11,100	5.992
4,805	2.384	16,200	9.270
5,400	2.701	16,800	9.443
6,000	3.031	17,400	9.787

Run H-2

Inlet manometer = 38.0 mm.Hg at 25°C
 Atmospheric pressure = 746.2 mm.Hg at 24.7°C
 Exit pressure = 521.0 mm. Hg at 25°C

Time sec.	Volume Fed c.c. at P ₁	Time sec.	Volume Fed c.c. at P ₁
0	0.000	20,400	2.408
60	0.158	21,600	2.588
240	0.257	22,800	2.857
1,400	0.364	24,000	3.003
2,800	0.612	25,200	3.196
3,600	0.705	26,400	3.380
4,800	0.863	30,400	3.934
6,000	1.066	31,800	4.163
9,600	1.213	33,000	4.354
11,275	1.231	34,200	4.528
11,800	1.252	35,400	4.740
12,600	1.350	36,600	4.903
14,200	1.554	37,800	5.084
15,600	1.736	39,000	5.258
17,400	1.977	40,200	5.457
19,200	2.265		

TABLE 15--continued

Run H-3			
Inlet manometer	=	638.9 mm.Hg	at 24.5°C
Atmospheric pressure	=	739.9 mm.Hg	at 24.5°C
Exit pressure	=	13.9 mm.Hg	at 24.5°C
Time sec.	Volume Fed c.c. at P _i	Time sec.	Volume Fed c.c. at P _i
0	0.000	7,200	5.834
2,300	3.854	12,600	8.835
2,700	3.555	13,200	8.907
3,000	3.694	13,800	9.246
4,300	4.394	14,500	9.495
5,400	4.992	15,630	10.200
6,000	5.323	16,800	10.886
6,600	5.531	18,060	11.491
Run H-4			
Inlet pressure	=	103.0 mm.Hg	at 25°C
Exit pressure	=	13.9 mm.Hg	at 25°C
Time sec.	Volume Fed c.c. at P _i	Time sec.	Volume Fed c.c. at P _i
0	0.000	7,200	4.612
200	0.356	8,400	5.252
600	1.068	9,600	5.893
1,200	1.420	10,800	6.530
1,810	1.770	12,040	7.186
3,010	2.390	13,280	7.794
3,610	2.718	14,400	8.386
4,800	3.354	15,600	9.012
6,000	3.982	16,200	9.317

TABLE 15--Continued

Run H-5			
Inlet pressure = 408.0 mm.Hg at 26°C			
Exit pressure = 0.004 mm.Hg at 26°C			
Time sec.	Volume Fed c.c. at P ₁	Time sec.	Volume Fed c.c. at P ₁
0	0.000	3,000	2.603
30	0.210	4,200	3.306
60	0.413	5,450	4.005
90	0.618	9,600	6.384
120	0.739	10,800	7.088
180	0.824	12,000	7.788
240	0.863	13,200	8.472
300	0.909	14,400	9.178
600	1.138	15,600	9.877
1,200	1.530	16,800	10.587
1,800	1.905	18,120	11.346
2,400	2.257	19,250	11.997
Run H-6			
Inlet pressure = 641.0 mm.Hg at 24.3°C			
Exit pressure = 502.5 mm.Hg at 24.3°C			
Time Sec.	Volume Fed c.c. at P ₁	Time sec.	Volume Fed c.c. at P ₁
0	0.000	6,030	2.115
60	0.372	10,000	2.965
90	0.572	11,500	3.250
120	0.242	12,600	3.483
300	0.902	13,800	3.752
600	0.965	15,000	4.016
1,200	1.083	16,200	4.276
2,400	1.342	17,420	4.527
3,000	1.489	18,600	4.785
3,600	1.617	20,000	5.081
4,200	1.747	21,600	5.414

TABLE 16

STEADY STATE CH₃Br PERMEABILITY AT 40°C

Run	P _{in} mm.Hg	P _{out} mm.Hg	ΔP mm.Hg	\bar{P} mm.Hg	(C _B) _{in} cc.(STP) gm.	(C _B) _{out} cc.(STP) gm.	ΔC _B cc.(STP) gm.	\bar{C}_B cc.(STP) gm.	N cc.(STP) gm.	$\frac{p_g}{\text{cm}^2\text{-hr-mm.Hg}}$ MI X10 ² $\frac{\text{mg.mole-cm}}{(\text{g.mole}^{-\text{OK}})^{1/2}}$
1	50.2	10.9	39.3	30.6	5.3	2.8	2.5	4.05	0.0796	3.66
2	147.8	50.2	97.6	94.0	8.6	5.3	3.3	6.92	0.166	3.06
3	295.6	147.8	147.8	221.7	10.8	8.7	2.1	9.75	0.247	3.01
4	449.5	305.0	144.5	377.3	13.0	10.9	2.1	11.95	0.258	3.21
5	604.4	457.9	146.5	531.2	16.7	13.2	3.5	14.95	0.259	3.19
6	602.5	0.0	602.6	301.3	16.6	0 ^a	16.6	8.30	1.081	3.24
7	599.2	0.0	599.2	299.6	16.5	0 ^a	16.5	8.25	1.079	3.24
8	613.8	588.4	25.4	601.1	17.0	16.2	0.8	16.60	0.0286	2.04
9	613.8	564.0	49.8	588.9	17.0	15.5	1.5	16.25	0.102	3.70
10	613.8	513.3	100.5	563.6	17.0	14.2	2.8	15.60	0.163	2.92
11	613.8	214.8	398.9	414.5	17.0	9.8	7.2	13.40	0.689	2.99
13	598.2	0.0	598.2	299.1	16.5	0 ^a	16.5	8.25	1.075	3.24

^aX-ray data indicate that C_{out} should be about 3.0 c.c.(S.T.P.)/gm.

TABLE 17

METHYL BROMIDE ORIGINAL FLOW DATA AT 40°C

Run 1			
Inlet pressure = 52.0 mm.Hg at 27.3°C			
Exit pressure = 12.5 mm.Hg at 26°C			
Time sec.	Volume Fed cc. at P ₁	Time sec.	Volume Fed cc. at P ₁
0	0.000	11,400	11.869
770 ^a	3.326	12,640	12.512
900	3.750	13,800	13.082
1,100	4.209	15,000	13.641
1,220	4.367	16,200	14.178
1,810	5.019	17,400	14.700
2,400	5.658	18,600	15.211
3,000	6.219	19,800	15.701
3,600	6.775	21,200	16.247
4,800	7.762	22,200	16.630
6,000	8.647	23,400	17.099
7,350	9.538	24,600	17.556
7,800	9.823	25,800	17.995
9,120	10.612	26,400	18.245
10,230	11.245	26,682	18.303

^aInlet pressure controller start to control at this time.

Run 2			
Inlet pressure = 150.0 mm.Hg at 26°C			
Exit pressure = 52.0 mm.Hg at 27.3°C			
Time sec.	Volume Fed cc at P ₁	Time sec.	Volume Fed cc. at P ₁
0	0.000	18,060	10.577
360 ^b	2.351	19,800	11.072
630	3.383	21,800	11.629
1,200	3.923	23,400	12.054
1,800	4.389	25,200	12.535
2,400	4.777	27,000	13.030
3,600	5.450	28,800	13.511
4,800	6.069	30,600	14.003
6,000	6.595	32,400	14.476
7,290	7.121	34,200	14.958
8,400	7.554	36,000	15.439
9,600	7.976	40,820	16.809
12,800	9.040	42,200	17.177
14,400	9.546	43,050	17.411
16,200	10.082	43,800	17.597

^bInlet pressure controller had just started to control at this time.

TABLE 17--continued

Run 3

Inlet pressure = 298.5 mm.Hg at 26.5°C

Exit pressure = 150.0 mm.Hg at 26°C

Time sec.	Volume Fed cc at P ₁	Time sec.	Volume Fed cc. at P ₁
0	0.000	12,020	5.318
170 ^c	1.077	13,430	5.617
360	1.706	15,010	5.960
630	1.930	16,800	6.317
950	2.137	18,600	6.690
1,510	2.427	20,400	7.050
1,840	2.553	22,280	7.434
3,000	2.989	23,540	7.689
4,470	3.458	28,960	8.707
5,360	3.692	30,040	8.962
6,000	3.869	31,200	9.195
8,400	4.485	33,940	9.729
9,600	4.759	37,000	10.368
10,800	5.059		

^cInlet pressure controller started to control at 160 seconds.

Run 4

Inlet pressure = 453.0 mm.Hg at 24.5°C

Exit pressure = 308.0 mm.Hg at 26.5°C

Time sec.	Volume Fed cc at P ₁	Time sec.	Volume Fed cc. at P ₁
0	0.000	12,600	2.962
180 ^d	0.529	13,800	3.147
450	0.745	15,000	3.308
600	0.830	16,200	3.459
1,440	1.111	17,400	3.620
1,860	1.241	19,080	3.853
3,000	1.561	20,400	4.005
4,200	1.838	22,600	4.328
5,520	2.045	27,040	4.988
8,010	2.358	28,860	5.150
9,040	2.491	29,400	5.320
10,860	2.758		

^dInlet pressure controller started to control at about 30 seconds.

TABLE 17--continued

Run 5			
Inlet pressure = 608.5 mm.Hg at 25.5°C			
Exit pressure = 461.5 mm.Hg at 24.5°C			
Time sec.	Volume Fed cc. at P ₁	Time sec.	Volume Fed cc. at P ₁
0	0.000	9,000	2.291
120 ^e	0.755	10,800	2.485
180	0.852	12,600	2.634
240	0.919	14,490	2.839
360	1.016	16,200	3.009
480	1.060	18,000	3.202
600	1.131	19,850	3.400
900	1.221	21,760	3.580
1,800	1.406	22,200	3.629
3,000	1.599	28,130	4.244
4,200	1.780	30,010	4.483
5,400	1.935	32,850	4.765

^eInlet pressure controller started to control at 102 seconds.

Run 6			
Inlet pressure = 607 mm.Hg at 26°C			
Exit pressure = 0.008 mm.Hg			
Time sec.	Volume Fed cc. at P ₁	Time sec.	Volume Fed cc. at P ₁
0	0.000	7,800	9.133
360 ^f	2.433	9,000	9.710
480	2.891	10,800	10.565
600	3.187	12,600	11.359
720	3.429	14,400	12.149
900	3.750	16,200	12.911
1,200	4.209	18,010	13.723
1,800	4.953	20,090	14.612
3,000	6.069	21,600	15.232
4,200	6.987	22,800	15.736
5,400	7.762	24,100	16.285
6,600	8.489	25,200	16.753

^fInlet pressure controller started to control at 350 seconds.

TABLE 17--continued

Run 7			
Inlet pressure = 603.5 mm.Hg at 25.2°C			
Exit pressure = 0.008 mm.Hg			
Time sec.	Volume Fed cc. at P ₁	Time sec.	Volume Fed cc. at P ₁
0	0.000	7,200	8.707
300 ^g	2.026	8,400	9.349
420	2.490	9,650	9.930
480	2.665	10,930	10.503
600	2.995	12,000	11.002
900	3.566	13,200	11.519
1,200	3.996	14,400	12.036
1,800	4.754	15,600	12.545
2,400	5.425	16,800	13.083
3,600	6.475	18,000	13.592
4,800	7.337	19,260	14.134
6,600	8.359	20,400	14.581

^gInlet pressure controller started to control at 280 seconds.

Run 8			
Inlet pressure = 618.5 mm.Hg at 28.9°C			
Exit pressure = 593.0 mm.Hg at 28.9°C			
Time sec.	Volume Fed cc. at P ₁	Time sec.	Volume Fed cc. at P ₁
0	0.000	3,600	0.205
60	0.057	4,950	0.222
180	0.105	6,800	0.279
240	0.116	7,800	0.304
300	0.116	9,000	0.312
600	0.136	9,600	0.317
1,200	0.155	10,800	0.327
1,800	0.176	13,450	0.368
2,400	0.180	14,370	0.379
3,060	0.198	16,370	0.388

TABLE 17--continued

Run 9			
Inlet pressure = 618.5 mm.Hg at 28.9°C			
Exit pressure = 568.5 mm.Hg at 29.5°C			
Time sec.	Volume Fed cc. at P ₁	Time sec.	Volume Fed cc. at P ₁
0	0.392	14,970	0.873
600	0.428	15,600	0.909
1,390	0.473	16,400	0.945
1,800	0.480	16,870	0.961
2,400	0.480	17,570	0.988
3,000	0.480	18,086	1.002
3,600	0.490	18,800	1.043
4,250	0.507	19,800	1.078
4,950	0.526	20,650	1.114
6,490	0.566	21,420	1.144
7,950	0.620		

Run 10			
Inlet pressure = 618.5 mm.Hg at 28.9°C			
Exit pressure = 517.5 mm.Hg at 28.8°C			
Time sec.	Volume Fed cc. at P ₁	Time sec.	Volume Fed cc. at P ₁
0	1.183	37,800	3.848
600	1.248	38,480	3.885
1,240	1.280	39,300	3.925
1,800	1.325	40,200	4.004
2,700	1.380	40,930	4.048
3,200	1.414	41,500	4.086
3,600	1.443	42,310	4.159
36,400	3.761	43,270	4.218
37,520	3.834	44,160	4.267

TABLE 17--continued

Run 11			
Inlet pressure = 618.5 mm. Hg at 28.9°C			
Exit pressure = 217.5 mm. Hg at 30.0°C			
Time sec.	Volume Fed cc. at P ₁	Time sec.	Volume Fed cc. at P ₁
0	0.000	10,860	2.502
5,400	1.029	11,520	2.674
6,000	1.190	12,060	2.825
7,000	1.468	12,620	2.984
7,200	1.517	14,540	3.498
8,000	1.694	15,000	3.627
8,400	1.824	15,620	3.788
9,000	2.004	17,880	4.394
9,600	2.167	18,530	4.569
10,200	2.319	19,060	4.711
Run 13			
Inlet Pressure = 602.5 mm.Hg at 25.6°C			
Exit Pressure = 0.008 mm.Hg			
Time sec.	Volume Fed cc. at P ₁	Time sec.	Volume Fed cc. at P ₁
0	0	6,540	8.021
220	1.512	7,140	8.319
350	2.206	7,780	8.660
540	2.638	8,340	8.950
840	3.224	8,940	9.225
1,140	3.683	9,540	9.540
1,740	4.436	10,140	9.824
2,340	5.084	10,740	10.085
2,940	5.612	11,340	10.373
3,540	6.127	11,940	10.629
4,140	6.556	17,940	13.298
4,740	6.961	18,540	13.539
5,340	7.316	19,140	13.783
5,940	7.663	19,740	14.017

TABLE 18
EXIT PRESSURE DATA FOR RUNS 6, 7, AND 13

Run	6	7	13
Time sec.	Exit Pressure, microns		
2,600	--	--	0.01
3,040	--	0.01	--
3,600	0.01	--	0.01
3,630	--	0.01	--
4,800	--	--	0.25
4,830	--	0.3	--
5,400	--	--	0.73
5,470	--	1.1	--
5,880	--	1.5	--
6,000	--	--	1.9
6,600	3.5	--	3.3
6,630	--	3.8	--
7,200	--	--	4.3
7,250	--	4.9	--
7,800	--	5.7	5.4
8,400	--	--	5.9
8,740	--	6.5	--
9,000	--	--	6.5
9,145	--	6.6	--
9,600	--	--	6.9
9,620	6.8	--	--
10,200	7.3	--	7.1
10,226	--	7.3	--
10,800	--	--	7.4
11,400	--	--	7.7
12,000	7.8	7.8	--
13,200	8.0	--	--
13,400	--	8.3	--
16,200	8.2	--	--
16,240	--	8.4	--
18,000	--	--	8.3
20,400	8.3	--	--

TABLE 19

ADSORPTION ISOTHERM DATA AT 40°C

$P = 839.5 - 230.0 = 609.5$ mm.Hg at 25.6°C
 Hence $P = 605.2$ mm.Hg at 0°C

Time	System Pressure mm.Hg	Plug Tempera- ture °C	Collected Gas	
			Pressure mm.Hg	Temperature °C
3:10 PM	0.043	40	0.043	26.6
3:15 PM	678.5-647.0 = 31.5	40	--	--
3:30 PM	686.0-627.0 = 59.0	40	--	--
3:45 PM	687.0-623.0 = 64.0	40	--	--
3:50 PM	690.0-617.0 = 73.0	40	--	--
4:30 PM	693.5-608.5 = 85.0	40	--	--
7:00 PM	695.5-604.0 = 91.5	40	--	--
7:35 PM	695.5-604.0 = 91.5	40	--	--
8:10 PM	687.5-623.5 = 64.0	40	845.0-359.0 = 486.0	25.6
9:15 PM	approx. 39.0	40	837.0-379.0 = 458.0	25.0
10:00 PM	675.5-654.5 = 21.0	40	818.5-425.5 = 393.0	25.2
10:50 PM	670.5-666.5 = 4.0	40	--	--
8:30 AM	671.0-666.5 = 4.5	40	--	--
9:30 AM	671.0-666.0 = 5.0	40	779.5-526.5 = 253.0	26.0
--	--	40	784.0-513.0 = 271.0	25.8
4:00 PM	670.0-668.5 = 1.5	100	763.0-567.0 = 196.0	26.6
9:35 PM	670.0-668.5 = 1.5	100	731.5-646.5 = 85.0	25.7
10:15 PM	670.0-668.5 = 1.5	100	711.5-697.5 = 14.0	25.3

TABLE 19--continued

P = 730.5 - 513.5 = 217.0 mm.Hg at 27.4°C
Hence P = 213.5 mm.Hg at 0°C

Time	System Pressure mm.Hg	Plug Tempera- ture °C	Collected Gas Pressure mm.Hg	Temperature °C
1:20 PM	0.05	40	0.05	--
2:15 PM	670.0-666.5 = 3.5	40	859.0-321.5 = 537.5	24.7
2:50 PM	--	40	--	--
5:00 PM	670.5-666.5 = 4.0	75	779.0-525.0 = 254.0	24.7
8:30 PM	--	103.2	727.0-658.0 = 69.0	23.7
9:00 PM	--	103.2	720.0-674.5 = 45.5	23.5
10:00 PM	--	103.2	712.0-696.0 = 16.0	23.5
10:15 PM	--	103.2	707.5-706.0 = 1.5	22.8
8:45 AM	--	103.2	714.0-689.0 = 25.0	22.7
9:30 AM	--	103.2	710.0-700.5 = 9.5	23.3
11:20 AM	--	103.2	709.0-702.5 = 6.5	24.1
1:20 PM	--	103.2	709.0-702.5 = 6.5	23.8
2:45 PM	--	103.2	708.5-704.0 = 4.5	23.7

P = 14.5 mm.Hg at 27°C
Hence P = 13.0 mm.Hg at 0°C

Time	System Approx. Pressure mm.Hg	Plug Tempera- ture °C	Collected Gas Pressure mm.Hg	Temperature °C
2:35 PM	0.0005	40	0.0005	--
3:45 PM	2	40	729.5-651.5 = 78.0	27.0
7:15 PM	2	102.4	731.0-647.5 = 83.5	25.9
9:45 PM	2	102.4	717.0-683.5 = 33.5	25.9
11:00 AM	1.5	102.4	713.5-692.5 = 21.0	25.9
4:45 PM	1.5	102.4	710.0-700.5 = 9.5	25.6
7:30 AM	1.5	102.4	707.5-705.3 = 2.0	22.0

TABLE 20
SUMMARIZED EXPERIMENTAL ADSORPTION ISOTHERM DATA^a

Temperature °C	Pressure mm.Hg	Amount Adsorbed cc.(S.T.P.)/gm.
40	605.2	16.60
40	213.5	9.62
40	13.0	2.57

^aThe appendix on Calculated Quantities contains a sample calculation of the isotherm points from the data given in Table 19.

TABLE 21
CALCULATED ADSORPTION ISOTHERM DATA^a

P_e , mm.Hg	C_s , cc.(S.T.P.)/gm.	F
10	2.65	0.760
50	5.27	0.583
100	7.36	0.471
150	8.73	0.410
200	9.48	0.380
300	10.73	0.334
400	12.15	0.288
500	13.89	0.242
600	16.51	0.185

^aThis isotherm data was obtained by reading P_e and C_s values from Figures 8 and 9 at the given values of F.

TABLE 22

X-RAY DETECTOR POSITION CALIBRATION FOR X-RAY CALIBRATION PROFILES

Pressure, mm.Hg	0	0 ^a	10.9	50.2	147.8						
Span, in.	0.680	0.620	0.660	0.665	0.650	0.630	0.640	0.655	0.610	0.580	
Volts	% of L _p										
0.08	--	--	--	--	--	--	--	--	--	--	--
0.12	0.0	0.0	--	--	0.0	0.0	--	--	--	--	--
0.14	--	--	--	--	--	--	--	--	0.0	0.0	--
0.17	--	--	0.0	0.0	--	--	--	--	--	--	--
0.19	--	--	--	--	--	--	0.0	0.0	--	--	--
0.20	13.2	11.3	--	--	10.8	13.5	--	--	13.1	12.1	--
0.30	31.6	26.6	24.3	22.6	23.9	25.4	20.3	19.9	31.1	29.3	--
0.40	45.6	43.6	40.9	41.4	34.6	26.5	39.0	38.2	50.8	50.0	--
0.50	58.8	57.3	57.6	58.6	50.0	49.2	55.5	51.9	67.2	63.8	--
0.60	71.3	69.5	71.2	70.7	63.1	68.3	70.3	68.7	83.6	79.3	--
0.70	83.8	84.0	83.4	86.5	80.8	82.5	84.4	84.8	95.9	91.4	--
0.74	--	--	--	--	--	--	--	--	100.0	100.0	--
0.77	91.9	93.6	--	--	92.3	92.1	--	--	--	--	--
0.79	--	--	100.0	100.0	--	--	--	--	--	--	--
0.81	--	--	--	--	--	--	100.0	100.0	--	--	--
0.82	100.0	100.0	--	--	100.0	100.0	--	--	--	--	--
0.83	--	--	--	--	--	--	--	--	--	--	--

^aCalibration after Run 5.

TABLE 22--continued

Pressure, mm.Hg	305		457.9		605.2		609.6	
Span, in.	0.580	0.615	0.620	0.595	0.650	0.610	0.605	0.590
Volts	% of L _p							
0.16	--	--	--	--	0.0	0.0	--	--
0.17	--	--	--	--	--	--	0.0	0.0
0.20	--	--	--	--	8.5	3.3	--	--
0.21	0.0	0.0	--	--	--	--	--	--
0.24	--	--	0.0	0.0	--	--	--	--
0.30	13.8	13.8	12.1	10.9	25.4	24.6	24.8	23.8
0.40	34.5	33.3	29.0	27.7	41.6	39.4	39.6	37.3
0.50	50.0	50.4	48.4	46.2	56.2	58.2	56.2	57.6
0.60	66.4	65.0	62.9	61.3	71.6	69.7	71.9	71.2
0.70	79.3	78.9	81.4	75.6	87.7	86.1	89.2	89.9
0.78	--	--	--	--	--	--	100.0	100.0
0.80	--	--	93.5	93.3	100.0	100.0	--	--
0.83	100.0	100.0	--	--	--	--	--	--
0.86	--	--	100.0	100.0	--	--	--	--

TABLE 23

X-RAY CALIBRATION PROFILES

P = 0 (Initial Scan)			
$I_R = 99,000$ (I_R) _B = 97,500			
L %	$\Delta I \times 10^{-3}$ counts/min.	$(\Delta I)_B \times 10^{-3}$ counts/min.	F
11.0	17.5	16.9	0.996
20.2	17.5	13.0	0.951
30.6	13.8	10.0	0.964
37.5	10.5	8.4	0.979
43.7	7.0	7.5	1.008
48.7	8.0	7.0	0.992
57.7	7.5	7.7	1.003
65.0	11.0	9.0	0.980
72.8	13.0	11.8	0.989
84.7	13.0	16.1	1.040
89.5	18.0	17.3	0.994
97.0	18.5	18.0	0.990
			Avg. = 0.990
P = 0 (After Run 5)			
$I_R = 97,500$, (I_R) _B = 97,500			
L %	$\Delta I \times 10^{-3}$ counts/min.	$(\Delta I)_B \times 10^{-3}$ counts/min.	F
1.7	18.0	18.0	1.000
9.5	18.0	17.3	0.992
17.7	11.0	14.2	1.039
22.8	10.5	12.0	1.017
31.8	9.5	9.7	1.002
42.5	8.0	7.7	0.997
56.0	6.5	7.3	1.008
61.0	9.5	8.1	0.985
66.7	8.0	9.6	1.018
73.5	11.0	12.0	1.012
78.0	14.0	13.8	0.998
86.1	18.5	16.7	0.979
96.0	17.5	18.0	1.006
			Avg. = 1.004

TABLE 23--continued

P = 10.9 mm.Hg
 $I_R = 97,000$, $(I_R)_B = 97,500$

L %	$\Delta I \times 10^{-3}$ counts/min.	$(\Delta I)_B \times 10^{-3}$ counts/min.	F
2.9	38.0	18.0	0.747
10.5	38.0	17.0	0.738
21.0	35.0	12.7	0.736
27.8	31.8	10.7	0.756
35.3	31.5	8.9	0.743
41.6	31.5	7.8	0.735
48.8	30.0	7.9	0.744
55.0	30.5	7.1	0.740
65.2	32.0	9.1	0.752
77.6	35.0	13.7	0.745
86.5	33.0	16.7	0.797
94.2	37.0	18.0	0.759
			Avg. = 0.749

P = 50.2 mm.Hg
 $I_R = 93,000$ $(I_R)_B = 97,500$

L %	$\Delta I \times 10^{-3}$ counts/min.	$(\Delta I)_B \times 10^{-3}$ counts/min.	F
4.3	49.5	18.0	0.578
11.0	48.5	16.9	0.582
19.0	46.0	13.7	0.590
22.4	45.0	12.2	0.591
32.0	42.5	9.7	0.603
44.9	43.0	7.3	0.593
54.8	41.0	7.0	0.613
57.7	43.0	7.7	0.595
66.3	45.5	9.5	0.578
73.8	45.5	12.0	0.596
80.0	45.0	14.8	0.610
88.3	47.0	17.0	0.602
96.6	47.5	18.0	0.604
			Avg. = 0.595

TABLE 23--continued

P = 147.8 mm.Hg
 $I_R = 94,500, (I_R)_B = 97,500$

L %	$\Delta I \times 10^{-3}$ counts/min.	$((\Delta I)_B \times 10^{-3})$ counts/min.	F
3.1	64.5	18.0	0.401
13.0	62.5	16.2	0.411
18.3	63.0	14.0	0.406
24.2	62.0	11.7	0.406
34.0	62.0	9.2	0.395
39.0	60.5	8.1	0.407
48.8	60.0	7.0	0.408
56.3	60.5	7.3	0.404
59.6	62.5	8.4	0.386
70.0	61.5	10.7	0.396
79.2	63.0	14.3	0.395
83.8	63.0	16.0	0.404
89.0	64.0	17.3	0.425
			Avg. = 0.403

P = 305 mm.Hg
 $I_R = 92,000, (I_R)_B = 97,500$

L %	$\Delta I \times 10^{-3}$ counts/min.	$(\Delta I)_B \times 10^{-3}$ counts/min.	F
5.3	67.0	17.9	0.335
12.6	68.0	16.4	0.315
21.3	67.0	12.6	0.313
27.7	66.0	10.7	0.318
37.3	66.5	8.4	0.303
46.5	65.0	7.1	0.316
51.6	63.5	7.0	0.333
59.2	64.0	7.9	0.331
67.2	65.0	9.8	0.326
73.0	65.0	11.8	0.334
80.2	65.0	14.9	0.348
86.5	66.0	16.7	0.343
96.5	65.5	18.0	0.355
			Avg. = 0.328

TABLE 23--continued

P = 457.9 mm.Hg
 $I_R = 93,500$, $(I_R)_B = 97,500$

L %	$\Delta I \times 10^{-3}$ counts/min.	$(\Delta I)_B \times 10^{-3}$ counts/min.	F
4.7	73.0	18.0	0.270
13.2	73.0	16.0	0.263
21.6	74.0	12.4	0.240
26.7	72.0	10.9	0.259
35.0	70.5	9.0	0.271
43.1	70.5	7.6	0.267
48.0	70.0	7.0	0.270
56.2	71.0	7.3	0.260
66.4	71.5	9.5	0.249
72.1	71.5	11.4	0.255
79.9	71.5	14.9	0.266
85.3	72.0	16.3	0.277
90.0	72.5	17.3	0.274
			Avg. = 0.263

P = 605.2 mm.Hg
 $I_R = 95,500$, $(I_R)_B = 97,500$

L %	$\Delta I \times 10^{-3}$ counts/min.	$(\Delta I)_B \times 10^{-3}$ counts/min.	F
3.3	81.0	18.0	0.187
10.3	81.0	17.0	0.184
16.7	81.0	14.9	0.180
25.2	80.0	11.3	0.184
32.7	80.5	9.4	0.174
39.3	80.0	8.0	0.177
47.2	80.0	7.1	0.175
55.0	80.0	7.1	0.175
61.2	80.0	8.2	0.177
71.0	79.0	11.0	0.202
78.3	79.5	14.0	0.196
86.8	80.0	16.5	0.196
92.7	78.0	17.8	0.174
			Avg. = 0.183

TABLE 23--continued

P = 609.6 mm.Hg			
$I_R = 97,000, (I_R)_B = 97,500$			
L %	$\Delta I \times 10^{-3}$ counts/min.	$(\Delta I)_B \times 10^{-3}$ counts/min.	F
0.0	82.0	18.0	0.190
10.5	84.0	17.0	0.163
22.5	81.3	12.2	0.185
30.7	82.0	10.0	0.172
41.0	82.0	7.8	0.168
57.2	81.5	7.4	0.173
65.0	82.0	9.0	0.171
76.5	83.0	13.1	0.167
85.7	83.0	16.4	0.174
93.0	83.0	17.9	0.176
98.2	82.0	18.0	0.190
			Avg. = <u>0.175</u>

TABLE 24

X-RAY DETECTOR POSITION CALIBRATION FOR CH₃Br PROFILES

Run	1		2		3		4		5	
Scan	Steady State		Steady State		Steady State		Steady State		Steady State	
Span, in.	0.630	0.620	0.610	0.590	0.580	0.615	0.595	0.640	0.615	0.620
Volts	% of L _p									
0.18	0.0	0.0	0.0	0.0	--	--	--	--	0.0	0.0
0.21	0.0	0.0	--	--	0.0	0.0	0.0	0.0	--	--
0.30	14.3	16.1	24.6	25.4	13.8	13.8	16.0	15.0	19.5	21.8
0.40	33.4	34.7	42.6	40.7	34.5	33.3	35.4	32.5	39.8	38.7
0.50	47.7	48.4	59.8	59.3	50.0	50.4	48.8	48.4	52.8	54.8
0.60	65.2	67.8	73.8	72.9	66.4	65.0	64.8	63.4	72.4	71.8
0.70	80.2	79.9	95.1	91.5	79.3	78.9	82.4	78.4	88.6	85.5
0.78	--	--	100.0	100.0	--	--	--	--	--	--
0.80	87.4	90.4	--	--	--	--	94.1	94.2	--	--
0.81	--	--	--	--	--	--	--	--	100.0	100.0
0.83	--	--	--	--	100.0	100.0	--	--	--	--
0.85	--	--	--	--	--	--	100.0	100.0	--	--
0.86	100.0	100.0	--	--	--	--	--	--	--	--

TABLE 24--continued

Run	6		6		7		7		11	
Scan	Inlet to Exit		Exit to Inlet		Inlet to Exit		Exit to Inlet		Steady State	
Span, in.	0.600	0.615	0.615	0.655	0.590	0.625	0.650	0.630	0.585	0.605
Volts	% of L_p									
0.15	--	--	--	--	0.0	0.0	0.0	0.0	--	--
0.16	0.0	0.0	0.0	0.0	--	--	--	--	--	--
0.17	--	--	--	--	--	--	--	--	0.0	0.0
0.20	5.8	7.3	8.9	9.2	8.5	10.4	10.8	11.1	--	--
0.30	24.2	27.6	25.2	24.4	26.3	28.8	26.9	26.2	19.7	21.5
0.40	40.0	43.0	44.7	42.8	44.1	43.2	44.6	45.2	39.4	38.8
0.50	58.4	61.0	64.2	62.6	61.9	62.4	64.6	65.1	55.6	57.0
0.60	71.7	74.0	77.2	77.9	80.5	76.8	80.0	82.5	71.9	73.5
0.70	90.0	95.2	89.5	91.6	93.2	93.6	95.4	95.2	88.1	90.9
0.75	--	--	--	--	100.0	100.0	100.0	100.0	--	--
0.77	100.0	100.0	100.0	100.0	--	--	--	--	100.0	100.0

TABLE 24--continued

Run	12		12		12		12	
Scan	Scans 1-6 Inlet to Exit		Scans 1-6 Exit to Inlet		Scans 7-9 Inlet to Exit		Scan 10 Inlet to Exit	
Span, in.	0.555	0.590	0.615	0.645	0.585	0.610	0.585	0.545
Volts	% of L _p							
0.15	0.0	0.0	0.0	0.0	0.0	0.0	--	--
0.16	--	--	--	--	--	--	0.0	0.0
0.20	10.8	7.6	9.0	10.9	8.5	9.0	9.4	5.5
0.30	28.0	28.0	23.6	27.2	23.1	23.0	29.1	27.5
0.40	46.9	48.3	44.8	46.5	36.0	36.1	45.3	44.0
0.50	63.1	66.1	64.3	67.5	47.9	49.2	65.0	64.3
0.60	80.3	83.9	76.5	84.5	64.2	65.6	79.5	81.6
0.70	--	--	--	--	82.1	80.4	100.0	100.0
0.71	100.0	100.0	100.0	100.0	--	--	--	--
0.80	--	--	--	--	100.0	100.0	--	--

TABLE 25

STEADY STATE CONCENTRATION PROFILES FOR CH₃Br RUNS

Run 1						
IR = 96,000						
L cm.	$\Delta I \times 10^{-3}$ counts/mm.	Cs cc. (S.T.P.)/gm.	Cs	Pe mm.Hg		
0.038	50.5	5.27		50		
0.073	50.0	5.24		47		
0.170	49.5	5.555		53		
0.213	46.5	5.02		42		
0.279	43.0	4.68		36		
0.367	43.0	4.888		39		
0.405	42.0	4.78		38		
0.475	42.0	4.88		39		
0.553	39.5	4.47		33		
0.632	39.5	4.28		30		
0.693	38.0	3.70		21		
0.771	40.0	4.02		25		
0.876	39.5	3.14		14		
0.910	37.5	2.83		11		
Run 2						
IR = 92,000						
L cm.	$\Delta I \times 10^{-3}$ counts/min.	Cs cc. (S.T.P.)/gm.	Cs	Pe mm.Hg		
0.014	62.0	8.60		147		
0.121	61.0	8.51		142		
0.189	59.0	8.33		134		
0.216	55.0	7.39		102		
0.328	56.0	7.97		121		
0.404	54.0	7.63		110		
0.452	52.0	7.23		97		
0.546	52.0	7.13		93		
0.607	52.0	7.02		90		
0.678	50.0	6.27		70		
0.737	49.0	5.75		62		
0.798	50.0	5.65		58		
0.860	50.5	5.58		57		

TABLE 25--continued

Run 3			
I _R = 92,500			
L cm.	$\Delta I \times 10^{-3}$ counts/min.	C _s cc. (S.T.P.)/gm.	P _e mm.Hg
0.024	67.5	10.80	298
0.088	67.0	10.62	286
0.142	65.0	10.11	237
0.223	64.5	10.92	266
0.312	64.0	10.52	273
0.37	60.5	9.57	198
0.456	61.5	9.95	225
0.527	59.0	9.20	177
0.582	60.0	9.38	185
0.635	59.0	8.98	165
0.708	59.0	8.60	147
0.730	58.0	8.20	130
0.803	58.0	7.84	117
0.911	59.0	7.60	108
Run 4			
I _R = 95,000			
L cm.	$\Delta I \times 10^{-3}$ counts/min.	C _s cc. (S.T.P.)/gm.	P _e mm.Hg
0.01	74.5	12.95	447.5
0.066	74.0	12.76	435
0.113	73.5	12.65	430
0.214	73.5	13.20	460
0.281	72.0	12.80	438
0.314	72.0	12.87	442
0.411	70.5	12.49	426
0.488	70.0	12.31	408
0.501	70.0	12.31	408
0.586	70.0	12.17	400
0.674	68.0	11.10	323
0.701	70.0	11.73	367
0.784	68.0	10.56	276
0.860	69.0	10.66	285

TABLE 25---continued

Run 5					
IR = 92,000					
L cm.	$\Delta I \times 10^{-3}$ counts/min.	Cs cc. (S.T.P.)/gm.	Cs	Pa mm.Hg	
0.071	78.0	15.84		578	
0.121	79.0	16.67		605	
0.205	78.0	16.50		600	
0.285	76.0	14.30		517	
0.355	80.0	16.67		605	
0.427	77.0	15.07		550	
0.505	76.5	14.85		541	
0.614	75.5	14.17		510	
0.680	78.0	15.16		552	
0.761	75.0	13.20		460	
0.831	75.0	12.95		448	
0.888	75.0	12.83		442	
Run 6					
IR = 96,000					
L cm.	$\Delta I \times 10^{-3}$ Counts/min.	Cs cc. (S.T.P.)/gm.	Cs	Pe mm.Hg	
0.012	82.0	16.80		611	
0.104	81.0	16.27		597	
0.185	80.0	16.10		590	
0.222	78.0	15.08		555	
0.314	77.0	14.84		546	
0.407	74.5	13.83		498	
0.478	70.5	12.25		405	
0.534	69.5	11.85		378	
0.607	65.5	10.30		234	
0.683	63.0	9.22		164	
0.749	60.0	8.04		122.5	
0.821	53.5	6.10		74	
0.931	93.5	3.86		25	

TABLE 25--continued

Run 7 I _R = 95,000					
L cm.	$\Delta I \times 10^{-3}$ counts/min.	Cs cc. (S.T.P.) / gm.	Pe mm.Hg		
0.093	80.0	16.16	590.5		
0.153	80.0	16.40	597.5		
0.213	78.0	15.60	572.0		
0.295	78.0	15.75	577.0		
0.370	75.0	14.38	522.5		
0.935	73.0	13.57	482.0		
0.506	68.0	11.59	363.0		
0.549	68.0	11.50	356.5		
0.648	65.0	10.20	255.0		
0.726	60.0	8.30	133.0		
0.745	55.0	6.90	88.5		
0.825	51.0	5.62	58.0		
0.904	41.0	3.50	21.0		
Run 11 I _R = 98,000					
L cm.	$\Delta I \times 10^{-3}$ counts/min.	Cs cc. (S.T.P.) / gm.	Pe mm.Hg		
0.062	82.0 ^a	16.87	610		
0.139	84.0	17.22	619		
0.202	83.0	17.00	614		
0.280	82.5	16.95	613		
0.347	80.0	15.67	572		
0.425	78.0	14.81	540		
0.507	76.0	13.88	496		
0.579	76.0	13.75	489		
0.643	75.0	13.10	455		
0.706	73.0	12.05	390		
0.768	73.0	11.73	367		
0.811	72.0	11.20	330		
0.914	70.0	10.30	245		

^aI_R = 96,000.

TABLE 26

UNSTEADY STATE CONCENTRATION PROFILES FOR CH₃Br RUNS

Run 6 - Scan 1		t = 0.88 - 3.54 minutes	
I _R = 95,500		Exit to inlet	
L cm.	$\Delta I \times 10^{-3}$ counts/min.	C _s cc. (S.T.P.)/gm.	P _e mm.Hg
0.016	73.5	12.33	411.0
0.085	59.0	7.47	104.0
0.154	35.5	2.85	13.0
0.222	14.0	0.25	0.5
0.321	14.0	0.53	1.0
0.389	7.0	0.000	0.0
0.449	9.0	0.21	0.5
0.500	6.5	0.00	0.0
0.567	10.5	0.38	1.0
0.636	11.0	0.12	0.5
0.696	12.0	0.00	0.0
0.781	13.0	0.00	0.0
0.834	18.5	0.15	0.5
0.877	18.0	0.03	0.0
Run 6 - Scan 2		t = 4.73 - 7.30 minutes	
I _R = 96,000		Inlet to exit	
L cm.	$\Delta I \times 10^{-3}$ counts/min.	C _s cc. (S.T.P.)/gm	P _e mm.Hg
0.016	74.0	12.38	414.0
0.107	60.0	7.75	113.0
0.178	37.5	3.33	18.0
0.211	16.0	0.43	1.0
0.292	13.0	0.32	1.0
0.364	7.0	0.00	0.0
0.409	8.5	0.10	0.5
0.497	8.0	0.10	0.5
0.555	15.0	0.82	1.0
0.612	13.0	0.43	1.0
0.683	14.0	0.29	1.0
0.752	15.5	0.12	0.5
0.803	19.0	0.32	1.0
0.922	16.0	0.00	0.0

TABLE 26--continued

Run 6 - Scan 3		t = 13.1 - 15.7 minutes	
I _R = 92,500		Exit to inlet	
L cm.	$\Delta I \times 10^{-3}$ counts/min.	C _a cc. (S.T.P.)/gm.	P _e mm.Hg
0.043	79.5	14.55	530.0
0.107	74.5	12.28	407.5
0.190	62.0	8.46	140.0
0.286	46.0	5.18	48.5
0.348	23.5	1.75	5.0
0.415	12.0	0.45	1.0
0.499	7.0	0.00	0.0
0.576	9.5	0.12	0.5
0.648	10.5	0.00	0.0
0.705	13.5	0.12	0.5
0.781	15.5	0.00	0.0
0.840	19.5	0.22	0.5
0.885	18.0	0.00	0.0
Run 6 - Scan 4		t = 16.7 - 19.3 minutes	
I _R = 98,000		Inlet to exit	
L cm.	$\Delta I \times 10^{-3}$ counts/min.	C _s cc. (S.T.P.)/gm.	P _e mm.Hg
0.005	81.5	15.44	566.0
0.099	75.5	12.53	423.0
0.177	67.0	9.80	222.5
0.233	56.0	7.05	92.5
0.314	44.0	4.85	42.0
0.393	24.0	1.88	6.0
0.485	7.0	0.00	0.0
0.527	8.5	0.10	0.5
0.599	13.0	0.43	1.0
0.691	13.5	0.15	0.5
0.759	13.0	0.00	0.0
0.822	15.5	0.00	0.0
0.920	19	0.10	0.5

TABLE 26--continued

Run 6 - Scan 5		t = 25.9 - 28.7 minutes	
IR = 94,500		Exit to inlet	
L cm.	$\Delta I \times 10^{-3}$ counts/min.	C_s cc.(S.T.P.)/gm.	P_e mm.Hg
0.036	80.5	16.68	605.0
0.119	77.0	14.66	535.0
0.172	71.5	12.34	411.0
0.260	62.0	9.27	183.5
0.335	52.0	6.88	87.5
0.349	43.0	5.07	46.5
0.449	25.5	2.33	8.5
0.508	14.5	0.90	2.0
0.567	11.0	0.33	1.0
0.668	12.0	0.12	0.5
0.734	12.5	0.00	0.0
0.771	15.5	0.03	0.0
0.851	15.0	0.00	0.0
0.900	18.5	0.03	0.0
Run 6 - Scan 6		t = 29.1 - 32.1 minutes	
IR = 95,000		Inlet to exit	
L cm.	$\Delta I \times 10^{-3}$ counts/min.	C_s cc.(S.T.P.)/gm	P_e mm.Hg
0.024	80.0	16.03	586.5
0.095	80.0	16.16	590.0
0.189	73.5	13.10	457.0
0.245	67.5	10.93	313.5
0.324	60.5	8.98	167.5
0.402	48.5	6.20	71.0
0.456	35.0	3.67	23.0
0.539	22.0	1.75	5.0
0.623	13.0	0.43	1.0
0.684	14.0	0.30	1.0
0.745	12.0	0.00	0.0
0.828	12.0	0.00	0.0
0.868	18.0	0.02	0.0
0.931	19.0	0.12	0.5

TABLE 26--continued

Run 6 - Scan 7		t = 40.5 - 43.1 minutes	
I _R = 97,000		Exit to inlet	
L cm.	$\Delta I \times 10^{-3}$ counts/min.	Cs cc.(S.T.P.)/gm	Pe mm.Hg
0.093	82.0	16.34	596.5
0.134	78.0	14.20	557.0
0.236	73.0	13.56	482.0
0.301	69.5	11.30	342.5
0.388	60.0	8.62	148.0
0.441	52.0	6.77	85.0
0.500	37.5	4.03	28.5
0.576	29.5	2.65	11.5
0.647	17.5	0.85	1.5
0.697	12.0	0.00	0.0
0.775	15.0	0.00	0.0
0.829	18.0	0.10	0.5
0.884	19.0	0.10	0.5
Run 6 - Scan 8		t = 44 - 46.6 minutes	
I _R = 99,000		Inlet to exit	
L cm.	$\Delta I \times 10^{-3}$ counts/min.	Cs cc.(S.T.P.)/gm	Pe mm.Hg
0.024	83.5	16.17	590.0
0.121	84.0	16.67	605.0
0.198	78.0	13.80	494.5
0.244	73.5	12.10	397.0
0.333	69.5	10.89	310.0
0.394	62.0	8.81	158.0
0.485	53.0	6.75	84.0
0.539	36.5	3.70	23.0
0.631	24.5	1.75	5.0
0.714	16.0	0.30	1.0
0.730	14.0	0.000	0.0
0.808	17.0	0.00	0.0
0.896	20.0	0.00	0.0

TABLE 26--continued

Run 6 - Scan 9		t = 60.5 - 65.5 minutes	
IR = 95,500		Exit to inlet	
L cm.	$\Delta I \times 10^{-3}$ counts/min.	Cs cc.(S.T.P.)/gm.	Pe mm.Hg
0.066	82.0	17.10	615.5
0.128	80.5	16.28	594.0
0.221	76.0	14.24	516.5
0.320	70.0	11.93	386.5
0.397	67.0	11.02	321.0
0.466	63.0	9.83	222.0
0.525	58.0	8.40	137.5
0.607	48.0	5.90	64.0
0.705	36.0	3.27	17.5
0.772	23.0	0.98	2.0
0.815	20.0	0.43	1.0
0.884	18.0	0.00	0.0
Run 6 - Scan 10		t = 66.7 - 69.5 minutes	
IR = 91,00		Inlet to Exit	
L cm.	$\Delta I \times 10^{-3}$ counts/min.	Cs cc.(S.T.P.)/gm	Pe mm.Hg
0.004	77.0	16.25	593.5
0.077	78.0	17.00	613.0
0.118	75.0	15.13	559.0
0.206	73.5	14.87	544.0
0.276	71.0	13.70	489.0
0.323	68.0	9.44	196.5
0.416	63.0	9.12	175.0
0.496	56.0	7.43	103.0
0.560	51.5	6.33	74.0
0.635	43.5	4.60	37.5
0.711	34.0	2.74	12.0
0.764	29.0	1.73	5.0
0.825	22.0	0.53	1.0
0.909	19.5	0.12	0.5

TABLE 26--continued

Run 7 - Scan 1		t = 60.6 - 63.0 minutes	
I _R = 98,000		Exit to inlet	
L cm.	$\Delta I \times 10^{-3}$ counts/min.	C _s cc.(S.T.P.)/gm.	P _e mm.Hg
0.866	15.0	0.00	0.0
0.804	19.0	0.33	0.5
0.737	20.0	0.73	1.0
0.661	32.0	2.73	12.0
0.574	45.0	5.18	48.0
0.491	54.5	7.20	96.5
0.442	61.5	8.93	164.0
0.381	63.5	9.70	215.0
0.300	70.0	11.25	338.0
0.236	73.0	12.14	400.0
0.146	78.0	13.90	500.0
0.076	82.0	15.78	578.0
Run 7 - Scan 2		t = 65 = 67.4 minutes	
I _R = 96,000		Inlet to exit	
L cm.	$\Delta I \times 10^{-3}$ counts/min.	C _s cc.(S.T.P.)/gm	P _e mm.Hg
0.101	79.0	15.60	572.0
0.178	77.0	14.34	521.0
0.220	71.0	13.80	495.0
0.312	67.0	11.87	282.0
0.425	61.0	9.90	230.0
0.506	55.5	8.35	136.0
0.582	48.0	6.33	74.0
0.645	41.0	4.73	39.5
0.730	29.0	2.20	7.5
0.803	21.0	0.68	1.0
0.900	15.0	0.00	0.0

TABLE 26--continued

Run 7 - Scan 3 $I_R = 95,000$		$t = 98.2 = 100.6$ minutes Exit to inlet	
L cm.	$\Delta I \times 10^{-3}$ counts/min.	C_s cc.(S.T.P.)/gm.	P_e mm.Hg
0.852	30.5	1.93	6.5
0.767	41.5	3.93	27.0
0.693	47.0	5.36	52.0
0.630	52.0	6.80	86.0
0.545	57.0	8.18	128.0
0.456	61.0	9.34	188.0
0.410	66.0	11.78	375.0
0.350	70.5	12.74	437.0
0.262	75.0	14.60	532.5
0.196	77.0	15.47	567.0
0.128	78.5	15.80	578.5
0.055	79.0	16.02	589.0
Run 7 - Scan 4 $I_R = 94,000$		$t = 102.2 - 105$ minutes Inlet to exit	
L cm.	$\Delta I \times 10^{-3}$ counts/min.	C_s cc.(S.T.P.)/gm.	P_e mm.Hg
0.093	79.0	16.02	589.0
0.170	78.0	15.80	578.5
0.253	72.0	13.07	455.0
0.336	72.0	13.30	468.0
0.410	68.0	11.83	380.0
0.507	63.0	10.15	251.0
0.565	59.5	9.00	168.5
0.647	57.0	8.07	125.0
0.723	52.0	6.45	77.0
0.789	46.0	4.77	42.5
0.872	40.5	3.52	21.5
0.928	28.0	1.38	3.0

TABLE 26--continued

Run 7 - Scan 5		t = 156 - 158.2 minutes		
I _R = 96,000		Inlet to exit		
L cm.	$\Delta I \times 10^{-3}$ counts/min.	C _S cc.(S.T.P.)/gm.	P _e mm.Hg	
0.056	82.0	16.83	609.0	
0.110	80	15.70	576.0	
0.197	79.0	15.54	570.0	
0.270	78.0	15.26	559.0	
0.370	73.0	13.13	458.5	
0.451	69.5	11.88	382.5	
0.532	67.0	10.97	317.0	
0.616	65.0	10.10	247.0	
0.693	61.0	8.62	148.0	
0.745	57.0	7.25	98.0	
0.825	51.0	5.54	57.0	
0.898	43.0	3.80	24.5	
0.945	27.5	1.27	3.0	

Run 7 - Scan 6		t = 196 - 198 minutes		
I _R = 100,000		Inlet to exit		
L cm.	$\Delta I \times 10^{-3}$ counts/min.	C _S cc.(S.T.P.)/gm.	P _e mm.Hg	
0.109	82.0	16.52	601.0	
0.201	81.0	15.78	578.0	
0.278	80.0	15.50	568.0	
0.345	73.0	13.04	453.5	
0.435	72.0	12.64	431.0	
0.507	70.0	11.88	382.5	
0.598	67.0	10.33	266.0	
0.661	62.0	8.95	165.5	
0.745	56.5	7.36	100.5	
0.803	53.0	6.05	67.5	
0.863	49.0	4.80	41.0	
0.945	38.0	2.80	12.5	

TABLE 26--continued

Run 12 - Scan 1		t = .55 - 3.1 minutes	
I _R = 99,000		Inlet to exit	
L cm.	$\Delta I \times 10^{-3}$ counts/min.	C _s cc.(S.T.P.)/gm.	P _e mm.Hg
0.921	77.0	12.73	436.0
0.858	79.5	13.97	502.5
0.803	81.0	14.90	545.0
0.701	82.0	15.94	584.0
0.649	82.0	16.18	591.5
0.568	82.0	16.42	598.0
0.479	82.0	16.53	602.0
0.419	82.0	16.47	599.0
0.345	82.0	16.30	594.5
0.264	82.0	16.19	591.5
0.168	84.5	17.23	618.0
0.119	80.5	14.60	532.5
0.035	74.0	11.50	356.5
Run 12 - Scan 2		t = 3.8 - 6.2 minutes	
I _R = 99,000		Exit to inlet	
L cm.	$\Delta I \times 10^{-3}$ counts/min.	C _s cc.(S.T.P.)/gm.	P _e mm.Hg
0.063	71.0	10.42	273.0
0.120	78.0	13.40	474.0
0.211	80.5	15.10	519.5
0.284	82.5	16.51	600.0
0.356	83.0	17.00	613.0
0.441	83.0	17.08	615.0
0.536	81.0	15.93	583.0
0.594	83.0	17.00	613.0
0.668	83.0	16.70	606.0
0.747	80.5	15.00	549.0
0.808	77.0	12.97	450.0
0.879	71.0	10.42	273.0

TABLE 26--continued

Run 12 - Scan 3		t = 12.7 - 15.3 minutes	
I _R = 96,000		Inlet to exit	
L cm.	$\Delta I \times 10^{-3}$ counts/min.	C _S cc.(S.T.P.)/gm	P _e mm.Hg
0.025	59.0	7.30	99.0
0.111	69.0	10.57	272.5
0.192	74.0	13.00	451.5
0.248	76.0	14.16	512.0
0.337	79.5	16.30	594.5
0.418	80.0	16.67	604.5
0.474	80.0	16.67	604.5
0.519	80.0	16.58	602.5
0.642	79.0	15.90	582.5
0.699	77.0	14.56	530.0
0.777	74.5	12.93	447.5
0.846	69.0	10.50	280.0
0.908	61.0	7.88	117.5
Run 12 - Scan 4		t = 24.6 - 27. minutes	
I _R = 100,000		Inlet to exit	
L cm.	$\Delta I \times 10^{-3}$ counts/min.	C _S cc.(S.T.P.)/gm.	P _e mm.Hg
0.000	55.0	5.84	63.0
0.082	66.0	8.65	149.5
0.165	68.0	9.61	207.5
0.220	70.5	10.67	292.5
0.312	73.0	11.83	380.0
0.399	73.0	12.00	391.5
0.457	73.0	12.07	395.0
0.551	73.5	12.17	401.0
0.635	73.0	11.78	375.0
0.699	73.0	11.53	358.5
0.785	69.0	9.77	220.0
0.848	67.0	8.97	166.5
0.924	58.0	6.50	78.0

TABLE 26--continued

Run 12 - Scan 5		t = 42.5 - 45.1 minutes	
I _R = 100,500		Inlet to exit	
L cm.	$\Delta I \times 10^{-3}$ counts/min.	C _S cc.(S.T.P.)/gm	P _e mm.Hg
0.006	50.0	4.75	40.0
0.101	58.0	6.54	79.0
0.184	62.0	7.95	120.0
0.232	66.0	9.22	181.5
0.310	68.0	10.07	245.0
0.399	68.0	10.23	257.5
0.482	69.0	10.60	285.0
0.578	68.0	10.23	257.5
0.627	66.5	9.60	207.5
0.716	65.0	8.80	157.5
0.769	63.0	8.00	122.0
0.870	58.0	6.50	78.0
0.939	49.0	4.60	37.5
Run 12 - Scan 6		t = 90.4 - 92.8 minutes	
I _R = 102,000		Inlet to exit	
L cm.	$\Delta I \times 10^{-3}$ counts/min.	C _S cc.(S.T.P.)/gm.	P _e mm.Hg
0.026	48.0	4.25	32.0
0.110	49.0	4.60	37.5
0.192	51.0	5.39	52.5
0.257	54.5	6.32	73.5
0.337	56.0	6.84	87.0
0.425	58.5	7.57	107.5
0.517	59.0	7.71	111.5
0.602	57.5	7.18	96.0
0.682	55.5	6.47	77.5
0.755	55.0	5.96	65.0
0.786	51.5	5.18	48.5
0.877	48.0	4.27	32.0
0.945	42.5	3.15	16.5

TABLE 26--continued

Run 12 - Scan 7		t - 113.6 - 118 minutes	
I _R = 94,500		Inlet to exit	
L	$\Delta I \times 10^{-3}$	C _S	P _e
cm.	counts/min.	cc.(S.T.P.)/gm.	mm.Hg
0.036	44.0	4.10	29.0
0.130	44.0	4.36	33.5
0.204	47.0	5.40	53.0
0.277	52.0	6.71	83.0
0.375	53.0	7.22	97.0
0.454	53.0	7.35	101.5
0.523	53.0	7.35	101.5
0.602	52.0	6.90	88.5
0.670	50.0	6.17	70.0
0.763	48.0	5.27	50.0
0.811	46.0	4.64	38.5
0.891	44.0	4.10	29.0

Run 12 - Scan 8		t = 150.2 - 153 minutes	
I _R = 92,000		Inlet to exit	
L	$\Delta I \times 10^{-3}$	C _S	P _e
cm.	counts/min.	cc.(S.T.P.)/gm.	mm.Hg
0.061	40.0	3.54	21.5
0.152	40.5	3.97	27.0
0.229	43.0	4.91	43.0
0.289	45.0	5.52	56.0
0.369	45.0	5.74	61.5
0.461	46.0	6.08	68.0
0.516	45.0	5.82	62.5
0.594	45.0	5.67	59.0
0.662	43.0	5.03	46.0
0.724	43.0	4.75	40.0
0.787	42.0	4.17	30.0
0.864	41.0	3.73	23.5
0.945	38.0	3.15	16.5

TABLE 26--continued

Run 12 - Scan 9		t = 180.5 = 182.9 minutes	
I _R = 98,000		Inlet to exit	
L cm.	$\Delta I \times 10^{-3}$ counts/min.	C _s cc.(S.T.P.)/gm	P _e mm.Hg
0.078	38.0	2.85	12.5
0.173	42.0	3.97	27.0
0.241	43.0	4.44	34.5
0.295	43.5	4.70	39.0
0.376	44.0	5.00	45.0
0.461	44.0	5.11	47.0
0.515	44.0	5.11	47.0
0.594	43.0	4.76	40.0
0.661	43.0	4.52	36.0
0.702	43.0	4.33	33.0
0.796	42.0	3.72	23.5
0.864	41.0	3.33	18.0
0.945	36.5	2.55	10.0
Run 12 - Scan 10		t = 262 - 264 minutes	
I _R = 99,000		Inlet to exit	
L cm.	$\Delta I \times 10^{-3}$ counts/min.	C _s cc.(S.T.P.)/gm.	P _e mm.Hg
0.088	35.5	2.40	8.5
0.155	40.0	3.55	21.5
0.216	39.0	3.60	22.0
0.300	38.0	3.70	23.0
0.378	37.0	3.72	23.5
0.450	36.5	3.74	24.0
0.541	36.5	3.68	22.5
0.611	38.0	3.75	24.0
0.681	38.0	3.50	20.5
0.759	37.0	2.92	13.5
0.801	37.0	2.77	12.0
0.886	35.0	2.24	8.0

TABLE 27

X-RAY INTENSITY VARIATION WITH KV. CHANGES

Load current - 37 ma.						
L % of L_p	KV.	$I_s \times 10^{-3}$ counts/min.	$I_R \times 10^{-3}$ counts/min.	$\Delta I_s \times 10^{-3}$ counts/min.	$\Delta I_R \times 10^{-3}$ counts/min.	$\frac{\Delta I_s}{\Delta I_R}$
0.5	28	44.5	54.0	--	--	--
0.5	29	59.5	71.5	15.0	17.5	0.857
0.5	30	76.5	91.5	17.0	19.5	0.872
21.3	28	48.0	54.5	--	--	--
21.3	29	64.0	71.5	16.0	17.0	0.942
21.3	30	82.5	91.5	18.5	20.0	0.925
42.5	28	52.0	56.0	--	--	--
42.5	29	69.5	75.0	17.5	19.0	0.922
42.5	30	87.5	94.5	18.0	19.5	0.923
61.6	28	50.0	54.0	--	--	--
61.6	29	67.0	72.0	17.0	18.0	0.944
61.6	30	86.0	94.0	19.0	22.0	0.865
73.5	28	47.5	53.5	--	--	--
73.5	29	62.5	70.5	15.0	17.0	0.883
73.5	30	81.5	92.5	19.0	22.0	0.864
84.2	28	47.5	55.5	--	--	--
84.2	29	63.5	73.5	16.0	18.0	0.889
84.2	30	78.0	90.5	14.5	17.0	0.853
97.2	28	45.0	55.0	--	--	--
97.2	29	61.5	73.5	16.5	18.5	0.892
97.2	30	78.0	91.5	16.5	18.0	0.917
						Avg. = 0.897

APPENDIX F

CALCULATED QUANTITIES

Sample calculation of system
volumes of Table 13

Sample calculation of volume 1

The volume was obtained by measuring the change in pressure when a known volume of mercury was added through the syringe feeder. The equation for the original volume, V_1 , is then obtained as follows.

Volume of Hg fed = V_F : 7,303 counts $\times 8.171 \times 10^{-4}$ cc./count

$$V_F = 5.9673 \text{ cc.}$$

Volume correction, V_c , due to movement of Hg below the red reference mark on the manometer leg, Δh , is given by:

$$V_c = \pi D^2 \Delta h / 4$$

$$V_c = \frac{\pi \times 0.1008}{4} (31.945 - 28.955)$$

$$V = 0.2367 \text{ cc.}$$

Temperature correction of the barometric pressure was made by using the tables, given in the "Handbook of Chemistry and Physics," 35th ed., Chem. Rubber Pub. Co., as follows.

$$\text{At } 25.7^\circ\text{C, } p = 862.5 - 118.1 - 3.1 = 741.3 \text{ mm.Hg}$$

$$\text{At } 25.8^\circ\text{C, } p = 862.4 - 118.2 - 3.1 = 741.1 \text{ mm.Hg}$$

Temperature correction of the manometer reading was made for

the expansion of mercury and cathetometer scale as follows:

$$\begin{aligned} \text{Corrected manometer reading} &= \text{M.R.} \\ &= (\text{M.R.})(1 - 17 \times 10^{-6}(t - 20)) \\ &\quad (1 - .000181792t) \end{aligned}$$

At 27.5°C,

$$\text{M.R.} = (319.45 - 152.32)(0.9948738) = 166.3 \text{ mm.Hg}$$

$$\text{M.R.} = (289.55 - 163.79)(0.9948738) = 125.1 \text{ mm.Hg}$$

The initial pressure, P_1 , and the final pressure, P_2 , was obtained by subtracting the corrected manometer readings from the corrected barometric pressure as follows:

$$P_1 = 741.3 - 166.3 = 575.0 \text{ mm.Hg}$$

$$P_2 = 741.1 - 125.1 = 616.0 \text{ mm.Hg}$$

The original volume was then obtained from the following equation which is based on the ideal gas law.

$$V_1 = (V_F - V_c) / (1 - (P_1 T_2 / P_2 T_1))$$

$$V_1 = (5.9673 - 0.2367) / \left(1 - \frac{(575)(300.7)}{(616)(300.7)} \right)$$

$$V_1 = 86.10 \text{ cc.}$$

Calculation of surface to gas phase concentration ratio

For $P = 615 \text{ mm.Hg}$, the quantity of gas phase CH_3Br per gm. is given by:

$$V_g = \frac{22,400 V_p \epsilon P}{RT \rho_{\text{app}}}$$

$$V_g = \frac{(22,400)(0.408 \times 0.945)(0.301)(615)}{(62,361)(313)(1.441)} = 0.0569 \frac{\text{cc. (S.T.P.)}}{\text{gm.}}$$

The quantity of CH_3Br in the adsorbed phase per gm. is obtained directly from the adsorption isotherm of Figure 10:

$$C_s = 17.08 \text{ cc. (S.T.P.) / gm.}$$

Hence the minimum ratio of surface to gas phase concentrations was:

$$C_s/V_g = (17.08)/(0.0569) = 305$$

Sample calculation of CH_3Br mass absorption coefficients

The x-ray mass absorption coefficient of a compound can be estimated by adding the mass absorption coefficients of the elements making up the compound on a weight fraction basis. For example for CH_3Br , the coefficient can be obtained for an x-ray wavelength of 0.5 \AA as follows:

$$\text{Carbon: weight fraction} = y_c = 12.01/94.95 = 0.1264$$

$$\text{mass absorption coefficient} = (\mu/\rho)_c = 0.3357 \text{ cm.}^{-1}$$

$$\text{Hydrogen: weight fraction} = y_H = 3.02/94.95 = 0.0318$$

$$\text{mass absorption coefficient} = (\mu/\rho)_H = 0.3660 \text{ cm.}^{-1}$$

$$\text{Bromine: weight fraction} = y_{\text{Br}} = 79.92/94.95 = 0.842$$

$$\text{mass absorption coefficient} = (\mu/\rho)_{\text{Br}} = 30.78 \text{ cm.}^{-1}$$

$$(\mu/\rho)_{\text{CH}_3\text{Br}} = y_c (\mu/\rho)_c + y_H (\mu/\rho)_H + y_{\text{Br}} (\mu/\rho)_{\text{Br}}$$

$$\begin{aligned} (\mu/\rho)_{\text{CH}_3\text{Br}} &= (0.1264)(0.3357) + (0.0318)(0.3660) \\ &\quad + (0.842)(30.78) = 26.05 \text{ cm.}^{-1} \end{aligned}$$

Sample calculation of scanner position calibration curve

The scanner position was calibrated by measuring the distance the position recorder chart had moved during the voltage span from one end of the plug to the other. Assuming that the scan rate was constant and the recorder chart drive was constant, the distance the chart had moved was proportional to the axial distance along the plug. Hence if the first calibration point for run 1 in Table 24 is taken as an example, the total chart distance was 0.630 inches and the voltage span was 0.86 volts. The distance the chart has moved while the voltage at the plug inlet, 0.21 volts, has changed to any other voltage can be measured with a scale having 0.01 inch divisions. The ratio of the measured distance, i.e., 0.09 inches to the total distance, 0.630 inches, is the same as the fraction of the axial distance down the plug. Hence $(0.09/0.63) = 0.143$ or 14.3% of the distance down the plug corresponds to a voltage of 0.3 volts. Similar calculations give the scanner position calibration.

Sample calculation of reduction of x-ray data

As an example, the first concentration measured in the steady state concentration profile for run 1 (given in Table 24) will be calculated.

$$\Delta I = 50,500 \text{ counts/min.}$$

$$I_R = 96,00 \text{ counts/min.}$$

For % of $L_p = (0.038/0.945)100 = 4.02\%$, $(\Delta I)_B$ can be obtained from Figure 6, $(\Delta I)_B = 18,000$ counts/min. $(I_R)_B$ is 97,500 counts/min. for all scans. Then using equation 7, the attenuation factor can be obtained:

$$F = (I_R - \Delta I) / (0.9I_R + 0.1(I_R)_B - (\Delta I)_B)$$

$$F = (96,000 - 18,000) / (0.9(96,000) + 0.1(97,500) - 18,000)$$

$$F = 0.582$$

Using $F = 0.582$, C_s can be obtained from Figure 9 and P_e can be obtained from the isotherm, Figure 10.

$$C_s = 5.27 \text{ cc. (S.T.P.) / gm.}$$

$$P_e = 50 \text{ mm.Hg}$$

Calculation of λ / d ratios

Calculation of minimum mean free paths

The mean free path, λ , can be calculated from the equation given by Kennard (73).

$$\lambda = \frac{3\mu}{2P} \sqrt{\frac{\pi RT}{2M}}$$

For helium:

$$T = 313^\circ\text{K}$$

$$P = \frac{(615 \text{ mm.Hg})(1.013 \times 10^6 \text{ dynes/atm.-cm}^2)}{(760 \text{ mm.Hg/atm.)}}$$

$$P = 0.82 \times 10^6 \text{ dynes/cm}^2$$

$$\mu = 194 \times 10^{-6} \text{ poises (from reference (74))}$$

$$M = 4 \text{ gm./g-mole}$$

$$\lambda = \frac{(3)(194 \times 10^{-6})}{2(0.82 \times 10^6)} \sqrt{\frac{\pi(8.314 \times 10^7)(313)}{(2)(4)}} = 3.58 \times 10^{-5} \text{ cm.}$$

Similarly for CH_3Br , with $\mu = 143.8 \times 10^{-6}$ poises
(reference (75)): $\lambda = 5.41 \times 10^{-6}$ cm.

Calculation of minimum λ/d ratios

For helium: $\lambda/d = 3580/43.6 = 82.0$

For methyl bromide: $\lambda/d = 541/43.6 = 12.4$

Sample calculation of helium permeability

As an example, the helium permeability for run H-6 was calculated as follows. First the measured pressures had to be corrected to 0°C and for the meniscus error due to use of different size tubing in the arms of the manometer. The meniscus error was a constant 1.5 mm.Hg too high.

$$P \text{ at } 0^\circ\text{C} = P_t (P_t / P_o)$$

$$\rho_{\text{Hg}} = 13.5955 \text{ gm./cc. at } 0^\circ\text{C}$$

$$\rho_{\text{Hg}} = 13.5340 \text{ gm./cc. at } 25^\circ\text{C}$$

$$P_{\text{in}} = 103.0 \frac{13.5340}{13.5955} - 1.5 = 101.0 \text{ mm.Hg}$$

$$P_{\text{out}} = 13.5 \frac{13.5340}{13.5955} - 1.5 = 11.9 \text{ mm.Hg}$$

$$\Delta P = P_{\text{in}} - P_{\text{out}} = 101.0 - 11.9 = 89.1 \text{ mm.Hg}$$

The quantity of helium fed was plotted against time elapsed. After steady state was reached, the slope of the plot was calculated.

$$N = (\text{slope}) \frac{(P_{\text{in}})(273)(1)}{(760)(313)(22.4)}$$

$$N = \frac{(8.2-1.8)}{(3.875-0.5)} \frac{(101.0)}{(760)} \frac{(273)}{(313)} \frac{(1)}{(22.4)} = 9.796 \times 10^{-3} \text{ mg.-mole/hr.}$$

$$p'_g \sqrt{MT} = \frac{N L_p}{A_P \Delta P} \sqrt{MT}$$

$$p'_g \sqrt{MT} = \frac{(9.796 \times 10^{-3})(0.945)}{(0.408)(89.1)} (4 \times 313)^{1/2} =$$

$$9.00 \times 10^{-3} \frac{\text{mg.}-\text{mole}-\text{cm.}}{\text{cm}^2-\text{hr.}-\text{mm. Hg}} \left(\frac{\text{gm.}-^\circ\text{K}}{\text{gm.}-\text{mole}} \right)^{1/2}$$

Sample calculation of CH_3Br
steady state permeability

As an example, the CH_3Br permeability for run 1 was calculated as follows. First the measured pressures had to be corrected to 0°C and for the meniscus error of 1.5 mm.Hg too high due to use of different size tubing in the arms of the manometer.

$$P \text{ at } 0^\circ\text{C} = P_t \left(\rho_t / \rho_o \right)$$

$$\rho_{\text{Hg}} = 13.5955 \text{ gm./cc. at } 0^\circ\text{C}$$

$$\rho_{\text{Hg}} = 13.5274 \text{ gm./cc. at } 27.3^\circ\text{C}$$

$$\rho_{\text{Hg}} = 13.5315 \text{ gm./cc. at } 26^\circ\text{C.}$$

$$P_{\text{in}} = 52.0 \frac{(13.5274)}{(13.5955)} - 1.5 = 50.2 \text{ mm.Hg}$$

$$P_{\text{out}} = 12.5 \frac{(13.5315)}{(13.5955)} - 1.5 = 10.9 \text{ mm.Hg}$$

$$\Delta P = P_{\text{in}} - P_{\text{out}} = 50.2 - 10.9 = 39.3 \text{ mm.Hg}$$

The quantity of CH_3Br fed was plotted against time elapsed.

After steady state was reached, the slope of the plot was calculated.

$$N = (\text{slope}) \frac{(P_{\text{in}})(273)(1)}{(760)(313)(22.4)}$$

$$N = \frac{(18.1-14.3)}{(7.25-4.5)} \frac{(50.2)}{(760)} \frac{(273)}{(313)} \frac{(1)}{(22.4)} = 3.554 \times 10^{-3} \text{ mg.}-\text{mole/hr.}$$

$$p_g' \sqrt{MT} = \frac{N L_p}{A_p \Delta P} \sqrt{MT}$$

$$p_g' \sqrt{MT} = \frac{(3.554 \times 10^{-3})(0.945)}{(0.408)(89.1)} (94.95 \times 313)^{1/2}$$

$$p_g' \sqrt{MT} = 0.0366 \frac{\text{mg.-mole-cm.}}{\text{cm}^2\text{-hr.-mm.Hg}} \left(\frac{\text{gm.-}^\circ\text{K}}{\text{gm.-mole}} \right)^{1/2}$$

Sample calculation of adsorption isotherm point

The isotherm point at $P = 605.2$ mm.Hg is given as an example of these calculations. All measured pressures had to be corrected to 0°C in the following way:

$$P \text{ at } 0^\circ\text{C} = P_t \left(\rho_t / \rho_0 \right)$$

the CH_3Br removed from the equilibrated plug was collected in the 500 cc. reservoirs and compressed into a known volume. Only one of these 8 collections will be calculated here.

$$\text{Equilibrium Pressure} = 609.5 \frac{(13.5325)}{(13.5955)} - 1.5 = 605.2 \text{ mm.Hg}$$

$$\text{Collecting Temperature} = 25.6^\circ\text{C}$$

$$\text{Collecting Pressure} = 486.0 \frac{(13.5325)}{(13.5955)} - 1.5 = 482.2 \text{ mm.Hg}$$

The collecting volume included one leg of the measuring manometer and hence the collecting volume had to be corrected for the distance of the Hg level above the calibration mark as follows:

$$V = 10 - \frac{\pi D^2}{40} (P_{\text{man.}} - 207.5)$$

$$V = 10 - 0.007917(359.0 - 207.5) = 8.800 \text{ cc.}$$

This volume collected was reduced to S.T.P. as follows:

$$V = (8.800) \left(\frac{482.2}{760} \right) \left(\frac{273}{298.6} \right) = 5.105 \text{ cc. (S.T.P.)}$$

The eight collections yielded a total of 20.823 cc. (S.T.P.). There was a dead space on both sides of the plug between the inlet and outlet side valves. This dead space was originally filled with CH_3Br at the equilibrating pressure and temperature. Hence this quantity of CH_3Br must be subtracted from the total quantity collected to obtain the true amount of CH_3Br removed from the plug.

$$V \text{ in dead space} = (16.7) \left(\frac{605.2}{760} \right) \left(\frac{273}{313} \right) = 11.599 \text{ cc. (S.T.P.)}$$

$$V \text{ adsorbed} = 20.823 - 11.599 = 9.224 \text{ cc. (S.T.P.)}$$

$$w_p = 0.5557 \text{ gm.}$$

$$C_s = 9.224 / 0.5557 = 16.60 \text{ cc. (S.T.P.) / gm. at } 602.5 \text{ mm.Hg}$$

Material balance for run 2 steady state

Volume fed over a period of 5 hours of steady state operation was:

$$V_{in} = (22,280 - 16,304) \text{ counts} \times (8.171 \times 10^{-4}) \text{ cc./count}$$

$$V_{in} = 4.88 \text{ cc. at } 147.8 \text{ mm.Hg and } 40^\circ\text{C}$$

$$V_{in} = 4.88 \left(\frac{147.8}{760} \right) \left(\frac{273}{313} \right) = 0.826 \text{ cc. (S.T.P.)}$$

Volume collected at exit was calculated the same way as the volume collected in measuring the adsorption isotherm point given in this Appendix.

$$V_{out} = 10 - (0.007917)(432) = 6.60 \text{ cc. at } 94.0 \text{ mm. Hg and } 26.0^\circ\text{C}$$

$$V_{\text{out}} = 6.6 \left(\frac{94}{760} \right) \left(\frac{273}{299} \right) = 0.746$$

There was one slight correction due to a capillary tee which was evacuated before the collection and hence was filled during the collection. This volume was estimated as 0.942 cc. at 50.2 mm.Hg and $t = 26.0^{\circ}\text{C}$.

$$V_{\text{Tee}} = 0.942 \left(\frac{50.2}{760} \right) \left(\frac{273}{279} \right) = 0.058 \text{ cc. (S.T.P.)}$$

$$V_{\text{out}} = 0.746 + 0.058 = 0.804 \text{ cc. (S.T.P.)}$$

$$\text{Net difference} = V_{\text{in}} - V_{\text{out}} = 0.826 - 0.804 = 0.022 \text{ cc. (S.T.P.)}$$

$$\% \text{ less} = 0.022 \times 100 / 0.826 = 2.66\%$$

Estimation of CH_3Br molecular area

Emmett and Brunauer (53) gave the following equation for calculating the molecular area based on close packing (12 nearest neighbors) and the normal solid or liquid density.

$$A = 1.091 (M/\rho_L N)^{2/3}$$

The density was obtained by extrapolating to 40°C the following data given by Dreisbach (56).

$T, ^{\circ}\text{C}$	$\frac{\text{gm./cc.}}{\text{---}}$
0	1.732
20	1.676
25	1.662

From this data $\rho_L = 1.618 \text{ gm./cc. at } 40^{\circ}\text{C}$

$$A = 1.091 (94.95 / 1.618 \times 6.023 \times 10^{23})^{2/3} = 23.1 \text{ \AA}^2$$

Estimation of average pore radius
and surface area from helium
permeability

Wheeler (76) gives the equation

$$\bar{r} = 2V_g/S_s$$

where $V_g = \epsilon / \rho_{app} =$ pore volume per gm.

$S_s =$ specific surface area

$\bar{r} =$ average pore radius

$$S_s = 2 \epsilon / \bar{r} \rho_{app}$$

\bar{r} can be obtained from the experimental helium permeability
by using equation (15) with certain assumptions. Equation
(15) is:

$$N'_K = \frac{8}{3} \frac{n \pi \bar{r}^3}{\sqrt{2\pi RTM}} \left(\frac{2-f}{f} \right) \frac{dP}{k^2 dL}$$

For parallel pore model $n \pi \bar{r}^2 = \epsilon A_p$

Substituting for $n \pi \bar{r}^2$ and solving for \bar{r} :

$$\bar{r} = N'_K / \left(\frac{8}{3} \frac{\epsilon A_p}{\sqrt{2\pi RTM}} \left(\frac{2-f}{f} \right) \frac{dP}{k^2 dL} \right)$$

N'_K is related to the modified permeability $p'_g \sqrt{MT}$ by the
equation:

$$N'_K / A_p \frac{dP}{dL} = p'_g \sqrt{MT} / \sqrt{MT}$$

with appropriate units.

Substitution yields

$$\bar{r} = p'_g \sqrt{MT} / \left(\frac{8 \epsilon}{3k^2 \sqrt{2\pi R}} \right) \left(\frac{2-f}{f} \right)$$

$$p'_g \sqrt{MT} = 0.883 \times 10^{-5} \frac{\text{gm.-mole-cm.}}{\text{hr.-cm}^2\text{-mm.Hg}} \left(\frac{\text{gm.-}^\circ\text{K}}{\text{gm.-mole}} \right)^{1/2}$$

$$\epsilon = 0.301$$

Assume $f = 1$ and $k^2 = 6.55$ as given by Barrer and Barrie (9).

$$\bar{r} = (0.883 \times 10^{-5}) / \left[\frac{(8)(1333)(3600)(0.301)}{(3)(6.55)(2 \times 8.314 \times 10^7)^{1/2}} \right]$$

$$\bar{r} = 34.2 \times 10^{-8} \text{ cm.}$$

Since $\rho_{\text{app}} = 1.441 \text{ gm./cc.}$

$$S_s = 2\epsilon / \bar{r} \rho_{\text{app}} = \frac{(2)(0.301)}{(34.2 \times 10^{-8})(1.441)} = 122 \text{ m}^2/\text{gm.}$$

Estimation of average pore radius
from measured surface areas

As stated previously Wheeler (76) gives the equation

$$\bar{r} = 2V_g/S_s$$

$$V_g = \epsilon / \rho_{\text{app}} = (0.301)/1.441 = 0.209 \text{ cc./gm.}$$

From the N_2 - B.E.T. measurement, $S_s = 192 \text{ m}^2/\text{gm.}$

$$\bar{r} = 2 (0.209) 10^8 / (192 \times 10^4) = 21.8 \text{ \AA}$$

Estimation of tortuosity factor

As shown previously in this Appendix on Calculated Quantities, the following equation can be obtained from equation 15.

$$\bar{r} = p'_g \sqrt{MT} / \left(\frac{8}{3k^2} \frac{\epsilon}{\sqrt{2\pi R}} \left(\frac{2-f}{f} \right) \right)$$

Dividing both sides of this equation by $k^2 \bar{r}$ and inverting

$$k^2 = \frac{8}{3} \frac{\bar{r} \epsilon}{\sqrt{2\pi R}} \left(\frac{2-f}{f} \right) / p'_g \sqrt{MT}$$

$$\bar{r} = 21.8 \times 10 \text{ cm.}$$

$$f = 1$$

$$p'_g \sqrt{MT} = 0.883 \times 10^{-5} \frac{\text{gm.-mole-cm.}}{\text{hr.-cm}^2\text{-mm.Hg}} \left(\frac{\text{gm.-}^\circ\text{K}}{\text{gm.-mole}} \right)^{1/2}$$

$$\epsilon = 0.301$$

$$k^2 = \frac{(8)(21.8 \times 10^{-8})(0.301)(3600)(1333)}{(3)(2\pi \times 8.314 \times 10^7)^{1/2}(0.883 \times 10^{-5})}$$

$$k^2 = 4.18$$

$$k = 2.04$$

Sample calculation of B and Ds
for Table 6

For run 6, $\Delta C_s = 16.6 - 0 = 16.6 \text{ cc. (S.T.P.) / gm.}$

Hence $\bar{C}_s = 16.6 / 2 = 8.3 \text{ cc. (S.T.P.) / gm.}$

$$\rho_{app} = 1.441 \text{ gm./cc.}$$

$$M = 94.95 \text{ gm./gm.-mole}$$

$$\rho_L = 1.618 \text{ gm./cc.}$$

$$\epsilon = 0.301$$

From equation 4:

$$B = \left[1 - \left(\frac{\rho_{app} M C_s}{22,400 \rho_L \epsilon} \right) \right]^{3/2}$$

$$B = \left[1 - \frac{(1.441)(94.95)(8.3)}{(22,400)(1.618)(0.301)} \right]^{3/2}$$

$$B = 0.848$$

The average permeability, $p_g \sqrt{MT}$ was 0.883×10^{-2}

$$N_K = \left[\left(\frac{0.883 \times 10^{-2}}{\sqrt{MT}} \right) (22.4 A_p) \frac{\Delta P}{L_p} \right] \text{cc. (S.T.P.)/hr.}$$

$$\sqrt{MT} = (94.95 \times 313)^{1/2} = 172.44$$

$$A_p = 0.408 \text{ cm}^2$$

$$\Delta P = 602.6 - 0 = 602.6 \text{ mm.Hg}$$

$$L_p = 0.945 \text{ cm.}$$

$$N_K = \frac{(0.883 \times 10^{-2})(22.4)(0.408)(602.6)}{(172.44)(0.945)}$$

$$N_K = 0.301 \text{ cc. (S.T.P.)/hr.}$$

$$BN_K = (0.848)(0.301) = 0.255 \text{ cc. (S.T.P.)/hr.}$$

$$N_T = 1.081 \text{ cc. (S.T.P.)/hr.}$$

$$N_S = N_T = BN_K$$

$$N_S = 1.081 - 0.255 = 0.826 \text{ cc. (S.T.P.)/hr.}$$

$$D_S = N_S \rho_{app} / 3600 A_p (\Delta C / L_p)$$

$$D_S = \frac{(0.826)(1.441)}{(3600)(0.408)(16.6/0.945)}$$

$$D_S = 4.62 \times 10^{-5} \text{ cm}^2/\text{sec.}$$

Calculation of C_R

From Figure 28

$$\text{slope} = 0.86/260 = \frac{3600 RT \rho_{app} A_p}{22,400 k^2 C_R S_S L_p}$$

$$C_R = 48.6 RT \rho_{app} A_p / k^2 S_S L_p$$

$$R = 8.314 \times 10^7 \text{ dyne-cm./mole-}^\circ\text{K}$$

$$T = 313^\circ\text{K}$$

$$\rho_{app} = 1.441 \text{ gm./cc.}$$

$$A_p = 0.408 \text{ cm.}$$

$$k^2 = 6.55$$

$$S_s = 192 \times 10^4 \text{ cm./gm.}$$

$$L_p = 0.945 \text{ cm.}$$

$$C_R = \frac{(48.6)(8.314 \times 10^7)(313)(0.408)}{(6.55)(192 \times 10^4)}$$

$$C_R = 0.6 \times 10^5 \text{ gm./sec.-cm}^2$$

Sample calculation for Tables 8 and 9

For runs 6 and 7

$$J_T = \frac{N_T}{3600A_p} = 1.08/(3600)(0.408)$$

$$J_T = 7.35 \times 10^{-4} \text{ cc.(S.T.P.)}/\text{sec.-cm}^2$$

$$\text{At } L = 0.1 \text{ cm., } C_s = 16.3 \text{ cc. (S.T.P.)}/\text{gm.}$$

$$P_e = 594.5 \text{ mm.Hg}$$

$$\frac{dC_s}{dL} = -3.0 \text{ cc.(S.T.P.)}/\text{gm.-cm.}$$

$$\frac{dP_e}{dL} = -111 \text{ mm.Hg/cm.}$$

$$\frac{dC_s}{dP_e} = 0.0357 \text{ cc.(S.T.P.)}/\text{gm.-mm.Hg}$$

From equation 4:

$$B = \left[1 - \frac{(1.441)(94.95)(16.3)}{(22,400)(1.618)(0.301)} \right]^{3/2}$$

$$B = 0.709$$

From equation 24:

$$J_g = - \frac{(22.4)(0.709)(0.887 \times 10^{-2})(-111)}{(3600)(94.95 \times 313)^{1/2}}$$

$$J_g = 0.252 \times 10^{-4}$$

From equation 26:

$$k^2 C_R S_S = - \frac{(8.314 \times 10^7)(313)(1.441)(16.3)^2(-111)}{(22,400)(594.5)(7.35 - 0.252)10^{-4}}$$

$$k^2 C_R S_S = 1.17 \times 10^{11} \text{ sec.}^{-1}$$

From equation 27:

$$K_M = - \frac{(7.35 - 0.252) 10^{-4}}{[1.637(16.3)(594.5)(0.00357) + (16.3)^2(-111)}$$

$$K_M = 7.68 \times 10^{-7} \text{ gm}^2/\text{cc. (S.T.P.)-cm.-sec.-mm.Hg}$$

From equation 25:

$$D_S = (7.35 - 0.252)10^{-4} / -(1.441)(-3.0)$$

$$D_S = 1.64 \times 10^{-4} \text{ cm}^2/\text{sec.}$$

Estimation of minimum flow in exit tube

From Loeb (33)

$$N_K^1 = \frac{8\pi \bar{r}^3}{3 \sqrt{2\pi RTM}} \frac{\Delta P}{L}$$

$$\bar{r} = 0.2 \text{ cm.}$$

$$R = 8.314 \times 10^7 \text{ gm.-cm}^2/\text{gm.-mole-}^\circ\text{K-sec.}$$

$$T = 313^\circ\text{K}$$

$$M = 94.95 \text{ gm./gm.-mole}$$

$$\Delta P = (15 - 0.008)(1333) = 20,000 \text{ gm./cm.-sec}^2$$

$$L = 250 \text{ cm.}$$

$$N_K^i = \frac{(8\pi)(0.008)(20,000)}{(3)(2 \times 8.314 \times 10^7 \times 313 \times 94.95)^{1/2}(250)}$$

$$N_K^i = 1.31 \times 10^{-6} \text{ gm.-mole/sec.}$$

The measured flow was

$$N_T = 1.08 \text{ cc. (S.T.P.) / hr.}$$

$$N_T^i = (1.08) / (22,400)(3600) = 1.36 \times 10^{-8} \text{ gm.-mole/sec.}$$

therefore $N_K^i / N_T^i \approx 100$

Solutions of equation 33

Equation 33 is

$$\frac{d[D_T(dC_S/dL)]}{dL} = 0 \quad (33)$$

The boundary conditions are

$$C_S = C_0, \quad L = 0$$

$$C_S = C_L, \quad L = L_p$$

Integration of equation 33 twice gives

$$\int D_T dC_S = AL + B$$

where A and B are constants

Substitution of equation 29 for D_T and integration gives

$$\frac{-D_T^0 C_0}{\alpha} \ln(1 - \alpha C_S / C_0) = AL + B$$

From the two boundary conditions

$$B = -\frac{D_T^0 C_0}{\alpha L_p} \ln(1 - \alpha)$$

$$A = \frac{D_T^0 C_0}{\alpha L_p} \ln\left(\frac{1 - \alpha}{1 - \alpha C_L / C_0}\right)$$

Substitution for A and B followed by algebraic manipulation gives equation 34

$$\frac{C_s}{C_o} = 1 - (1 - \alpha) \left(\frac{1 - \alpha}{1 - \alpha C_L/C_o} \right)^{-L/L_p} \quad (34)$$

Similarly substitution of equation 31 for D_T into the doubly integrated equation 33 and subsequent integration gives

$$\frac{D_T^o \alpha}{C_o} e^{\alpha C_s/C_o} = AL + B$$

From the two boundary conditions

$$B = \frac{D_T^o \alpha}{C_o} e^{\alpha}$$

$$A = \frac{D_T^o \alpha}{C_o L_p} \left(e^{\alpha C_L/C_o} - e^{\alpha} \right)$$

Substitution for A and B followed by algebraic manipulation gives equation 35

$$\frac{C_s}{C_o} = \frac{1}{\alpha} \ln \left\{ \frac{L}{D_p} \left(e^{\alpha C_L/C_o} - e^{\alpha} \right) + e^{\alpha} \right\} \quad (35)$$

Solution of equation 36

Equation 36 is:

$$N_T = \frac{36000 P_{app} A_p}{L_p} \int_{C_L}^{C_o} D_t dC_s \quad (36)$$

Substitution of equation 30 with $C_o = 16.6$ and $C_L = 3.0$

$$N_T = \frac{(3600)(1.441)(0.408)}{(0.945)} \int_3^{16.6} \left(\frac{1.6 \times 10^{-5}}{1 - 0.0535 C_s} \right) dC_s$$

Integration gives

$$N_T = \frac{(3600)(1.441)(0.408)(1.6 \times 10^{-5})}{(0.945)(-0.0535)} [\ln(1-0.0535C_s)]_3^{16.6}$$

Substitution of limits gives

$$N = 1.357 \text{ cc. (S.T.P.) / hr.}$$

Similarly, substitution of equation 32 into equation 36 with the same limits gives

$$N_T = \frac{(3600)(1.441)(0.408)}{(0.945)} \int_3^{16.6} 0.8 \times 10^{-5} e^{0.1385C_s} dC_s$$

Integration gives

$$N_T = \frac{(3600)(1.441)(0.408)(0.8 \times 10^{-5})}{(0.945)(0.1385)} [e^{0.1385C_s}]_3^{16.6}$$

Substitution of limits gives

$$N_T = 1.096 \text{ cc. (S.T.P.) / hr.}$$

REFERENCES

REFERENCES

1. Volmer, M. and Estermann, I., Z. Physik., 7, 1 (1921).
2. Becker, J. A., Trans. of the Am. Electrochem. Soc., 55, 153 (1929).
3. Clancey, V. J., Nature, 166, 275 (1950).
4. Lord Rayleigh, Proc. Roy. Soc. (London), A156, 350 (1936).
5. Volmer, M. and Adhikari, G., Z. Phys. Chem., 119, 46 (1926).
6. Timofeev, D. P. and Voskresenskii, A. A., Doklady Akad. Nauk. S. S. S. R., 121, 434 (1958).
7. Nordberg, M. E., J. Amer. Ceramic Soc., 27, 299 (1944).
8. Lyon, L. L., Crocker, G. R., Heldman, M. J., and Fisher, J., "Surface Areas of Finely Divided Materials," Report # C00-142, A.E.C. Contract A T(11-1)-203, Sept. 1, 1953.
9. Barrer, R. M. and Barrie, J. A., Proc. Roy. Soc. (London), A213, 250 (1952).
10. Sheppard, N., Mathieu, M. -V., Yates, D. J. C., Z. Elektro. Chem., 64, 734 (1960).
11. Lacksonen, J. W., Ph.D. dissertation, Ohio State University (1964).
12. Carmen, P. C., "Flow of Gases Through Porous Media," Academic Press, New York (1956).
13. Russell, J. L., Sc. D. thesis, Mass. Inst. Technology (1955).
14. Timofeev, D. P., Russian Chemical Reviews, 3, 180 (1960).
15. Field, G. J., Watts, H., and Weller, K. R., Rev. Pure Appl. Chem., 13, 2, March (1963).
16. Barrer, R. M. and Gabor, T., Proc. Roy. Soc. (London), A256, 267 (1960).

17. Barrer, R. M. and Gabor, T., Proc. Roy. Soc. (London), A251, 353 (1959).
18. Barrer, R. M. and Strachan, E., Proc. Roy. Soc. (London), A231, 52 (1955).
19. Carmen, P. C. and Raal, F. A., Proc. Roy. Soc. (London), A203, 165 (1950).
20. Carmen, P. C. and Malherbe, P. Le R., Proc. Roy. Soc. (London), A203, 165 (1950).
21. Damkohler, G., Z. Phys, Chem., A174, 222 (1935).
22. Grove, D. M. and Ash, R., Trans. Faraday Soc., 56, 1357 (1960).
23. Haul, R. A. W., Z. Phys. Chem., N.S.1, 153 (1954).
24. Haul, R. A. W., and Peerbooms, R., Naturewissenschaften, 45, 109 (1958).
25. Ross, J. W. and Good, R. J., J. Phys. Chem., 60, 1167 (1956).
26. Wicke, E., Kolloid Zschr., 86, 167 (1939).
27. Wicke, E. and Kallenbach, R., Kolloid Zschr., 97, 135 (1941).
28. Dacey, J. R. and Fendly, J. A. in "The Structure and Properties of Porous Materials," edited by Everett, D. H. and Stone, F. S., Academic Press Inc., New York (1958).
29. Clausing, P., Ann. Physik, 7, 489 (1930).
30. Kruyer, S., Koninkl. Ned. Akad. an Wetenschap., 56B, 274 (1953).
31. de Boer, J. H., "The Dynamical Character of Adsorption," Clarendon Press, Oxford, England (1953).
32. Metzner, A. B. and Smith, R. K., Preprint of Papers, J. Phys. Chem., Presented at 38th National Colloid Symposium, Austin, Texas (1964).
33. Loeb, L. B., "The Kinetic Theory of Gases," McGraw-Hill, New York, 2nd ed. (1934).
34. Lacksonen, J. W., Private Communication.

35. Babbitt, J. D., Can. J. Res., 28A, 449 (1950).
36. Babbitt, J. D., Can. J. Phys., 29, 437 (1951).
37. Gilliland, E. R., Baddour, R. F., and Russell, J. L.,
A. I. Ch. E. Journal, 4, 90 (1958).
38. Gilliland, E. R., Baddour, R. F., and Engel, H. H., A. I.
Ch. E. Journal, 8, 530 (1962).
39. Rothfeld, L. B., Ph.D. dissertation, University of
Wisconsin (1961).
40. Flood, E. A., Tomlinson, R. H., and Leger, A. E., Can. J.
Chem., 30, 348 (1952).
41. Barrer, R. M., Can. J. Chem., 41, 1768 (1963).
42. Barrer, R. M. and Ash, R., Trans. Faraday Soc., 59, 2261
(1963).
43. Ash, R., Barrer, R. M., and Pope, C. G., Proc. Roy. Soc.
(London), A271, 1, 19 (1963).
44. Frisch, H. L., J. Phys. Chem., 61, 93 (1957).
45. Barrer, R. M., J. Phys. Chem., 57, 35 (1953).
46. Barrer, R. M., Brit. J. App. Phys. Suppl. No. 3, 5, S49
(1954).
47. Jones, W. M., Trans. Faraday Soc., 47, 381 (1951).
48. Tomlinson, R. H. and Flood, E. A., Can. J. Res., 26B, 38
(1948).
49. Macarus, D. P., Ph.D. dissertation, Ohio State University
(1959).
50. Everett, D. H. and Stone, F. S., "The Structure and
Properties of Porous Materials," Academic Press
Inc., New York (1958).
51. Brunauer, S., Emmett, P. H., and Teller, E., J. Am. Chem.
Soc., 60, 309 (1938).
52. Rutz, L. O., Ph.D. dissertation, State University of Iowa
(1958).
53. Emmett, P. H. and Brunauer, S., J. Am. Chem. Soc., 59,
1553 (1937).

54. Knudsen, M., Ann. Physik, 28, 75 (1909).
55. Engel, H. H., Sc.D. thesis, Mass. Inst. Technology (1959).
56. Dreisbach, R. R., "Advances in Chemistry Series," 29, Am. Chem. Soc., Washington, D.C. (1961).
57. Crank, J., "The Mathematics of Diffusion," Clarendon Press, Oxford, England (1956).
58. Smith, E. S., Salkover, M., and Justice, H. K., "Analytical Geometry," John Wiley & Sons, New York (1943).
59. Daynes, H. A., Proc. Roy. Soc., 97A, 286 (1920).
60. "Instruction Manual for Decker Delta Unit Model 901-1," Decker Aviation Corporation.
61. Picker X-ray Corporation instruction manual for Dual Ratemeter 600-046, Oct. 1962.
62. Burgess, R. E., Rev. Sci. Instr., 20, 964 (1949).
63. McMaster, R. C., "Non-destructive Testing Handbook," Vol. I, Ronald Press, New York (1959).
64. Price, W. J., "Nuclear Radiation Detection," McGraw-Hill Book Company, New York (1958).
65. Liebhafsky, H. A., "X-ray Absorption and Emission in Analytical Chemistry," John Wiley & Sons, New York (1960).
66. Consolidated Vacuum Corporation Instruction Bulletin No. 9-10-B, "McLeod Gauge GM-100A."
67. Picker X-ray Corporation Manual T-55-172, "Scintillation Probe," Feb. 1962.
68. Machlett Laboratories, Inc., Bulletin OEG-60, OEG-60S, April 1962.
69. Picker X-ray Corporation, Diffraction Unit Manual T-55-295, July 1963.
70. Leeds and Northrup, "Speedomax H Continuously-adjustable AZAR Recorder," Directions no. 177181, Issue 1.
71. Leeds and Northrup, "Supplementary Directions for Speedomax H Compact AZAR Recorder," Directions no. 177224, Issue 1.

72. Bausch & Lomb, Inc., Operator's Manual, Laboratory Recorder V. O. M. - 5.
73. Kennard, E. H., "Kinetic Theory of Gases," 1st ed., p. 140, McGraw-Hill, New York (1938).
74. Perry, J. H., "Chemical Engineer's Handbook," 3rd ed. p. 371, McGraw-Hill, New York (1950).
75. Titani, T., Bull. Chem. Soc. Japan, 5, 105 (1930).
76. Emmett, P. H. (ed.), "Catalysis," Vol. I, Chap 2, Reinhold Publishing, New York (1954).